Doctoral Thesis

On Adomian Based Numerical Schemes for Euler and Navier-Stokes Equations, and Application to Aeroacoustic Propagation

Author:
Imanol García de Beristain

Supervisors:
Prof. Lakdar Remaki
Prof. Luis Vega Gonzalez

A thesis submitted in fulfillment of the requirements for the degree of Doctor of Philosophy

eman ta zabal zazu

Universidad del País Vasco
Euskal Herriko Unibertsitatea

2017

Doctoral Thesis

On Adomian Based Numerical Schemes for Euler and Navier-Stokes Equations, and Application to Aeroacoustic Propagation

Tesis Doctoral

Métodos Numéricos Basados en Adomian para las ecuaciones de Euler y de Navier-Stokes, con Aplicaciones en Aeroacústica

Doktorego Tesia

Euler eta Navier-Stokes ekuazioak ebazteko Adomian Oinarrituriko Zenbakizko Metodoak, eta haien erabilera Aeroakustikan

Egilea | Autor | Author: Imanol García de Beristain

Zuzendaria | Director | Supervisor: Prof. Lakdar Remaki

Prof. Luis Vega Gonzalez

2017

Doctor of Philosophy

On Adomian Based Numerical Schemes for Euler and Navier-Stokes Equations, and Application to Aeroacoustic Propagation

by Imanol García de Beristain

Abstract

In this thesis, an *Adomian Based Scheme* (ABS) for the compressible Navier-Stokes equations is constructed, resulting in a new multiderivative type scheme not found in the context of fluid dynamics. Moreover, this scheme is developed as a means to reduce the computational cost associated with aeroacoustic simulations, which are unsteady in nature with high-order requirements for the acoustic wave propagation. We start by constructing a set of governing equations for the hybrid computational aeroacoustics method, splitting the problem into two steps: acoustic source computation and wave propagation.

The first step solves the incompressible Navier-Stokes equation using Chorin's projection method, which can be understood as a prediction-correction method. First, the velocity prediction is obtained solving the viscous Burgers' equation. Then, its divergence-free correction is performed using a pressure Poisson type projection. In the velocity prediction substep, Burgers' equation is solved using two ABS variants: a MAC type implementation, and a "modern" ADER method. The second step in the hybrid method, related to wave propagation, is solved combining ABS with the discontinuous Galerkin high-order approach. Described solvers are validated against several test cases: vortex shedding and Taylor-Green vortex problems for the first step, and a Gaussian wave propagation in the second case.

Although ABS is a multiderivative type scheme, it is easily programmed with an elegant recursive formulation, even for the general Navier-Stokes equations. Results show that its simplicity combined with excellent adaptivity capabilities allows for a successful extension to very high-order accuracy at relatively low cost, obtaining considerable time savings in all test cases considered.

Acknowledgements

I would like to give my gratitude to everyone who contributed to this thesis, making these years memorable.

The Basque Government for the Doctoral Thesis financial support (PRE-DOC program 2013-2017) and the BERC financial program. This research was also supported by the grant BFA/DFB-6/12/TK/2012/0020 (Diputación Foral de Bizkaia) by financing the BBIPED-CFD platform development. And the Spanish Ministry of Economy and Competitiveness MINECO: BCAM Severo Ochoa excellence accreditation SEV-2013-0323.

My supervisors Lakhdar Remaki and Luis Vega, without them I could have never made this work. Research opened to me thanks to your permanent support and motivation, from the beauty of mathematics on the first day, to communication and dissemination skills on the last one. Our Thesis.

The whole CFDMS team: Lakhdar, Ali, Goran, Carmen, Iñigo, Laura, and Alireza. We spent time as colleagues during work time, and also as friends in our private time.

All BCAM staff for your care towards my well-being, and your support with all my difficulties.

All the researchers I had the luck to come across. Stéphane Moreau and Marlene Sanjose in Sherbrooke University. Guillaume Puigt and Jean-François Boussuge in CERFACS. Many researchers in UPV/EHU, especially Jesús María Blanco Ilzarbe and Pedro Luis Arias Ergueta for guiding me into this research field. Finally, the reviewers and the Jury for their effort.

Many people and friends should be listed during these Ph.D years. Mikel, Janire, Iurdana, Pablo, Edu, Txema, Eider, Alba, Arantza, Susana, Vianney, Capuccine, Tania, Tijana, Biaggio, Arrate, Irati, and old BCAMtatoes and legends. Also my great office mates, you can turn now the air conditioning off.

Finalmente, a mi familia. Por estar incansablemente para y conmigo. Rosa, Loli, Ama, Aita y Joseba.

Imanol García de Beristain

March 5, 2018

Contents

List of Figures

List of Tables

List of Abbreviations

ADER	**A**rbitrary **DER**ivative
ABS	**A**domian **B**ased **S**cheme
APE	**A**coustic **P**erturbation **E**quations
BC	**B**oundary **C**ondition
CAA	**C**omputational **A**ero **A**coustics
CFD	**C**omputational **F**luid **D**ynamics
DG	**D**iscontinuous **G**alerkin
DRP	**D**erivative **R**iemann **P**roblem
DLM	**D**al Maso **L**eFloch and **M**urat
FE	**F**orward **E**uler or **F**inite **E**lement
FV	**F**inite **V**olume
FW-H	**F**fowcs **W**illiams and **H**awkings
GRP	**G**eneralized **R**iemann **P**roblem
HEOC	**H**arten **E**ngquist, **O**sher and **C**hakravarthy
HPC	**H**igh **P**erformance **C**omputing
LEE	**L**inearized **E**uler **E**quations
LES	**L**arge **E**ddy **S**imulation
MAC	**M**arker **A**nd **C**ell
NLAS	**N**on**L**inear **A**coustic **S**olver
NLDE	**N**on**L**inear **D**ecomposition **E**quations **A**ct
NS	**N**avier **S**tokes
ODE	**O**rdinary **D**ifferential **E**quations
PPE	**P**ressure **P**oisson **E**quation
RK	**R**unge **K**utta
RP	**R**iemann **P**roblem
SPL	**S**ound **P**ressure **L**evel
SNGR	**S**tochastic **N**oise **G**eneration and **R**adiation
TVD	**T**otal **V**ariation **D**iminishing

Para Rosa

Resumen

La aeroacústica es la ciencia que estudia el sonido generado por un fluido en movimiento (aerodinámica en el caso del aire). De esta manera, se encuentra entre la dinámica de fluidos y la acústica. A pesar de no ser una ciencia reciente, su actividad ha aumentado considerablemente durante las últimas décadas debido a un mayor interés por parte de la industria (con más de 64 proyectos financiados por la Comisión Europea con los términos "Aeroacoustic noise" en ellos [1]), y por el acceso a recursos computacionales más potentes. El estudio de la aeroacústica mediante herramientas computacionales se lleva a cabo por la *Aeroacústica Computacional* (CCA por sus siglas en ingles), que emplea métodos numéricos para simular la formación y propagación de las ondas acústicas.

Históricamente, la aeroacústica fue promovida mediante diversos informes publicados por la agencia medioambiental Norte Americana, NEPA, la cual señalaba la necesidad de proteger a la ciudadanía de la contaminación auditiva, principalmente de la aviación [46]. Hoy en día la reducción del ruido sigue siendo una de las principales utilidades de la aeroacústica, empleándose en sector automovilístico, ferroviario, ventilación, molinos eólicos, diseño de edificios, etc. Todos estos sectores operan, a diferencia de la aviación, en números de Mach bajos. Siendo de entre todos probablemente el de los molinos eólicos el más prolifero en investigación, con un máximo de 40 artículos en 2017 sobre un total 250 en la última década (de acuerdo con una búsqueda en Sciencedirect). Esto se debe, por una parte, a la madurez en los simuladores y conocimientos fluido dinámicos para aspas y geometrías alares [84, 99]. Y por otra parte, también al creciente interés que ha tenido el sector energético ante una demanda de energías renovables [120]. A pesar de ello, la aeroacústica computacional sigue siendo una herramienta relativamente novedosa, sin estar aún tan integrada en la industria como los simuladores aerodinámicos. La principal reticencia es el alto coste de simulación para la formación y propagación de las ondas acústicas, de naturaleza intrínsecamente no estacionaria y con altos requisitos de precisión. La precisión es requerida por la minúscula amplitud de las ondas, necesitando esquemas numéricos muchos más costosos que los tradicionales. Por lo tanto, la aeroacústica computacional sigue siendo un área aún en desarrollo. La reducción del coste computacional para la aeroacústica computacional es el principal interés de esta tesis.

Se distinguen dos principales métodos para realizar simulaciones en aeroacústica: los *métodos directos*, que obtienen los valores acústicos directamente

de la simulación del fluido en movimiento, sin suposiciones acústicas; y los *métodos híbridos*, que descomponen el problema en dos pasos, el cálculo aerodinámico seguido del acústico. En este último caso, la separación de la física tiene como desventaja una limitación en la capacidad de representación del problema [123]. De modo que un problema con acoplamiento acústico - aerodinámico, como es el sonido de batimiento de una ventana de coche por la autopista, no puede ser adecuadamente reproducido. Por otro lado, la ventaja radica en la modularidad y flexibilidad de poder usar sólveres independientes para cada uno de ellos, permitiendo usar el más adecuado para cada caso. En la práctica, el método híbrido es el más usado, especialmente para problemas con bajos valores de número de Mach. También lo emplearemos en esta tesis, describiendo a continuación las propiedades de cada parte.

En la parte aerodinámica es común suponer que el fluido es incompresible, de modo que no existan ondas acústicas en la simulación y no causen limitaciones en la estabilidad. Esta es una ventaja especialmente beneficiosa para los problemas con números de Mach bajos y discretizaciones explicitas, donde existe una marcada diferencia entre la velocidad de propagación de las ondas acústicas y la del fluido [132]. Por lo tanto, el problema pasa a ser matemáticamente elíptico, cuya interpretación física es que la propagación de la presión es lo suficientemente rápida como para considerarse instantánea. Esto se refleja en la desaparición de la derivada temporal en la ecuación de la energía, pasando a ser una restricción (divergencia de la velocidad nula). Es la ecuación del momento, junto con esta restricción, la que implícitamente fuerza a una relación entre la velocidad y la derivada de la presión [106]. Para desacoplar esta relación emplearemos el método de la proyección, de tipo predictor-corrector [72, 21]. En este método, una primera velocidad es estimada considerando la presión de forma explicita. En concreto, en esta tesis utilizamos la idea original de Kim y Moin en la que la presión es completamente ignorada, convirtiendo las ecuaciones de Navier-Stokes en las ecuaciones de Burgers, más simples y rápidas de resolver [87]. Al ignorar la presión, el campo de velocidades obtenido no necesariamente satisface la condición de divergencia de nula para las velocidades, de modo que se corrige en un segundo paso. Para construir la ecuación de corrección, se diferencia la divergencia de la velocidad respecto al tiempo, y se substituyen las ecuaciones del momento, obteniéndose así una ecuación escalar conocida como la ecuación de presión-Poisson (PPE). Resolver esta ecuación es la parte más costosa de todo el proceso, empleándose normalmente métodos iterativos [151]. De la solución se obtiene la presión a emplear en la corrección de los términos

de velocidad obtenidos previamente. Este mecanismo se describe mediante el teorema de Hodge. Este segundo paso es conocido como *proyección*, refiriéndose a un espacio de divergencia cero. Desgraciadamente, los métodos de proyección parecen estar limitados a segundo orden en el tiempo, como consecuencia del desacoplamiento entre velocidad y presión; aún es un problema de investigación abierto.

Por otro lado, en la parte acústica, las ondas se consideran matemáticamente como perturbaciones del fluido, obteniéndose mediante una linearización invíscida de las ecuaciones de Navier-Stokes en torno a un valor nominal [46, 11]. Es decir, obtenemos las ecuaciones de Euler linearizadas. De esta manera se pueden utilizar esquemas numéricos más simples y robustos. Independientemente del sistema a resolver, se requiere de alta precisión en el cálculo de la propagación con poca dispersión y disipación [93]. Para dicho fin se suelen emplean métodos de alto orden, que se demuestra tienen una mayor eficiencia comparado con métodos de bajo orden [92]. En concreto, utilizamos de Galerkin Discontinuo con orden elevado para preservar la calidad de la acústica durante la propagación [33, 35].

En el método híbrido descrito obtenemos derivadas temporales tanto en predicción de la velocidad aerodinámica, como en el la propagación de las ondas acústicas. La discretización de estos términos pueden clasificarse en tres grandes categorías en la terminología clásica de las ecuaciones diferenciales ordinarias: los multipaso, multietapa y de derivadas-sucesivas [22]. Los primeros utilizan la información de los pasos anteriores para estimar la solución en la nueva iteración. Los multietapa emplean cálculos intermedios, obteniendo el orden elevado de integración al combinar las variables auxiliares obtenidas de forma adecuada. Runge-Kutta es sin lugar a dudas el más conocido de esta familia. Por último, los métodos con derivadas-sucesivas expanden la solución en términos de Taylor. A causa de la aparición de derivadas espaciales de orden superior, así como un número apabullante de términos, los métodos en derivadas-sucesivas no son agradecidos y son por lo tanto evitados [131]. En el campo de las ecuaciones diferenciales parciales, este método también se conoce de tipo Lax-Wendroff, por ser Peter Lax y Burton Wendroff los que obtuvieron una expansión de segundo orden usando el teorema de Cauchy-Kowalewski [131, 95], siendo el único método de este tipo que es ampliamente utilizado. Excepcionalmente, en la última década, Toro [140] ha creado una familia de esquemas llamada ADER que está aumentando su uso. Este método se basa en resolver los problemas de Riemann generalizados (con más de dos derivadas espaciales no nulas), empleando

el mencionado procedimiento de Cauchy-Kowalewski (equivalente a las series de Taylor para derivadas parciales). Este proceso es también relativamente tedioso, existiendo publicaciones que intentan amainar este problema. Aun así, se puede decir que los métodos de derivadas-sucesivas no gozan de popularidad, quedando excluidas en favor de los predominantes métodos multietapa y los multipaso. Para órdenes de integración bajos o moderados, ambos métodos son usados indistintamente. Pero para órdenes elevados, típicamente mayores que tres, el método Runge-Kutta es el más utilizado. A pesar del triunfo de Runge-Kutta existe un potencial beneficio en la combinación de las distintas categorías, formando por ejemplo los métodos multietapa-multipaso. Seal [131] propone la combinación de Runge-Kutta con derivadas-sucesivas de segundo orden, como método para optimizar la memoria y numero de operaciones en los ordenadores con arquitectura moderna. Este análisis es valido para la aplicación de métodos explícitos, que son útiles en la propagación de ondas y la resolución de las ecuaciones incompresibles de Navier-Stokes para valores de Reynolds moderados, donde el tamaño del paso no está limitado por la rigidez de los términos viscosos (stiff) [116]. Los métodos explícitos también son utilizados cuando la viscosidad no es constante, donde el sistema es puramente no lineal.

Por otro lado, para abaratar el coste computacional en el método híbrido, deseamos que el método a desarrollar tenga propiedades adaptativas. Estos métodos permiten ajustar la precisión del cálculo en cada región del dominio, optimizando así los recursos disponibles. Las estrategias adaptativas se pueden plantear tanto en el dominio espacial como en el temporal. A pesar de ello, es en el plano espacial donde se centran la mayoría de los esquemas disponibles, dada la gran variedad de alternativas existentes: volumen finito, Galerkin discontinuo, métodos espectrales, etc. En el plano temporal hemos visto como son los métodos multipaso y multietapa los predominantes. Pero son, sin embargo, los métodos en derivadas-sucesivas los que tienen las mejores propiedades adaptativas, necesitando los otros dos el conocimiento a priori del orden de integración. Por ejemplo, existen antecedentes para ajustar el orden de métodos multietapa implícitos con formulas de diferenciación hacia atrás (BDF). Así, Nigro propone usar periódicamente un algoritmo de estimación del error, para elegir el orden a emplear que maximice el tamaño de paso para un error dado [114]. Hay también propone la adaptación de orden mediante el empleo de un indicador de inestabilidad [79]. Y es que su principal motivación es asegurar que el método BDF empleado está dentro de la región estable, ya que los ordenes altos de esta familia se vuelven inestables [79]. En ambos casos se requiere un método

de estimación del error, y se obtiene el orden adecuado mediante ensayo/error, requiriendo en algunas situaciones la eliminación de pasos ya computados. Por lo tanto, muchos programas se dedican exclusivamente a modificaciones en el tamaño del paso temporal y evitan así una programación más elaborada. Es esta otra razón por las que los métodos adaptativos suelen basarse en características espaciales. Identificamos por lo tanto una falta de investigación en los métodos adaptativos en el tiempo.

Planteamos en esta tesis el novedoso método en derivadas-sucesivas, que llamaremos ABS. Nos basaremos en el algoritmo de Adomian para conseguir un esquema de fácil implementación y programación. Adomian formuló una descomposición de los operadores no lineales en los conocidos como *polinomios de Adomian*. Las variables también son descompuestas en una suma de términos a resolver, para las que se demuestra en la aplicación "estándar" del algoritmo una expansión equivalente a la serie de Taylor. Sin embargo, en esta serie se obtendrán las variables de forma iterativa y secuencial, teniendo cada uno de los términos como dependencia todos aquellos calculados en las iteraciones anteriores. Se construye así una expresión mucho más simple y elegante que en el caso de Taylor, condicionado por el almacenamiento de todos los términos de Adomian calculados en cada paso. Utilizando el nuevo esquema ABS en el caso general de Navier-Stokes compresible, veremos que el número de operaciones a realizar es muy parecido al obtenido con Runge-Kutta.

La contribución principal de la tesis se encuentra en los capítulos tercero y cuarto, donde el esquema ABS es descrito e implementado para la parte aerodinámica y acústica.

Para la parte aerodinámica se han desarrollado dos métodos que modifican la estimación de la velocidad inicial, usando el nuevo esquema ABS. El primero de los métodos emplea una discretización de tipo volumen finito (ABS-FV), con una distribución de las variables semejantes al método MAC. El segundo método es una modificación del método HEOC [24], de la familia de métodos ADER (ABS-ADER). La modificación obtenida con ABS no solamente simplificará de forma considerable el algoritmo, sino que además se desarrolla de forma que el inicio del método coincida con el de ABS-FV, permitiendo considerarlo como una extensión del segundo. Ambos desarrollos son comparados con esquemas clásicos para problemas con derivadas continuas (curvas suaves). En el caso de ABS-FV, los resultados indicarán una reducción en el tiempo, mayor precisión

y estabilidad, permitiendo así tamaños de paso más amplios. El segundo método, ABS-ADER, no obtiene por si solo mejores resultados que los métodos clásicog. Sin embargo, cuando la ecuación de Burgers forma una onda de choque (con derivadas discontinuas), el método ABS-FV resulta inestable a diferencia del ABS-ADER. Este resultado nos anima a proponer la siguiente metodología para una optimización de los recursos computacionales: primero se resuelve la ecuación de Burgers empleando el esquema ABS-FV y, en presencia de discontinuidades (o limitadores activos), se empleará ABS-ADER con esquemas de Riemann adecuados. Se recuerda que, al poder usarse ABS-ADER como una extensión de ABS-FV, este paso adicional no requiere operaciones extra.

En la parte acústica, ABS es combinado con el método de Galerkin Discontinuo para discretizar las ecuaciones de Euler linearizadas, obteniéndose así un método de alto orden en el espacio y el tiempo. Como consecuencia de la linearización, el algoritmo de ABS se simplifica notablemente, pasando a almacenar el mismo número de variables independientemente del orden de integración deseado. El esquema obtenido es comparado con el método de integración de Runge-Kutta (RK-DG) [34] mediante la propagación de una Gaussiana. En los resultados se muestran órdenes de convergencia y precisión favorables para ABS, con costes hasta 20 veces menores comparando con RK. Al tratarse de un método adaptativo, este valor dependerá del problema en cuestión.

En resumen. En esta tesis se ha desarrollado un método en derivadas-sucesivas nuevo, llamado ABS. Sus propiedades son una formulación elegante basada en el algoritmo de Adomian, sencillez de implementación, y capacidad de adaptación de forma natural para cada una de las celdas del problema, obteniendo directamente estimaciones del error al obtener la magnitud de los términos calculados. Comparado con métodos explícitos clásicos, como Runge-Kutta o el método de Euler, ABS posibilita una mejora en robustez y precisión del cálculo, mientras se minimiza el coste computacional. Al tratarse de un método adaptativo, su mayor beneficio se encuentra ante problemas con requisitos computacionales desproporcionales en el dominio. El esquema ha sido probado con métodos de discretización espacial como Galerkin discontinuo, volumen finito y como modificación de un método de la familia ADER.

Chapter 1

Introduction

Aeroacoustics is an interdisciplinary field that lies between acoustics and fluid dynamics. It studies the noise generated via aerodynamic forces, involving turbulence and fluid-structure interaction. As we shall see, simulations are extremely expensive with high accuracy demand. However, there is still room for research.

1.1 Historical background

Although research in aeroacoustic has recently gone through a sudden increase in activity, it already has a long tradition in the fluid mechanic's community. Among the earliest efforts we find the paper by Gutin [74] who published the first contribution in Russia in 1936. However, modern aeroacoustics is based mostly on the shoulders of Sir James Lighthill's work [96, 97], who published what are certainly the most influential and therefore the most cited papers in the field. His contributions targeted the aircraft industry in the context of the first noise regulations from hands of the "National Environmental Policy Act" (NEPA). Noise regulations started to flourish in the middle of the 20th century, with the exploitation of transport technologies in the United States. Several health studies showed the need to protect citizens from noise pollution, especially aircraft transportation noise. A fact that strongly boosted the aeroacoustic field [46].

More recently, regulations for maximum noise levels have become more rigorous. Not only in aircraft transportation, but also in urban environments such as: the automotive industry, railway transportation, wind turbine, building design, ventilation and house appliances, etc. However, opposite to the aircraft

flight conditions, these new areas are usually low Mach number applications, with new difficulties not present at higher Mach numbers. Consequently, the recent interest for low Mach number aeroacoustics has increased. Among all mentioned industries, turbine and fan noise have been one of the hot topics in aeroacoustics. Especially wind turbine manufacturing in order to satisfy an ever-increasing energy demand. Environmental and social studies showed a need for their noise reduction, and consequently funding for its research and innovation was destinated. There is, therefore, a niche for research in low Mach number aeroacoustics, in particular for wind turbine industry. As an indicator of its success, we can find more than 64 projects in the "Aeroacoustic noise" area financed by the European Commission [1].

A big step in the aeroacoustic field has been the use of supercomputers. Whereas in the 20th century aeroacoustic methods were based on analytical developments, and thus limited to simple geometry and test cases, computational technologies allow today solving problems accurately in real geometries. *Computational Aeroacoustics* (CAA) is the branch of aeroacoustics that studies the application of computational methods.

Despite all the recent advances in the last decades, CAA technology has not yet been widely adopted in the industry due to the cost of its simulations. CAA is inherently unsteady with high accuracy requirements, and its use is confined mainly to research and prototype testing. There is a clear demand for reducing the cost of CAA simulations.

One of the main ways to speedup acoustic simulations is by employing hybrid methods [67], where aerodynamic and acoustic calculations are split into two consecutive steps. This has several advantages. First of all, a dimensional analysis shows low Mach number applications are better described with hybrid methods. Additionally, having a split solution step, different solvers can be used for each part. For the aerodynamic part, long-time validated numerical schemes can be used; whereas researchers can focus on developing efficient codes for the acoustic part. This methodology also helps to perform safety backups from the generated intermediate aerodynamic solutions, an important asset in time-constrained projects.

The most common assumption for the acoustic part is the linear wave propagation, potentially described by the linearized Euler equations (LEE). As a linear PDE, theoretical and numerical developments are well-established. On the numerical side spatial and frequency based methods have been widely used [5, 93, 19]. It also scales well in high performance computing environments.

Moreover, finely tuned linear solvers with accurate and excellent "dissipation relation preserving" (DRP) methods are available [136, 134]. Finally, building boundary conditions for linear conditions is easier and more efficient [82, 147]. Drawbacks for the use of linearized Euler equations are related to the worse physical representation. In this sense, when high accuracy is needed, or nonlinearities are relevant (in high amplitude waves), these are no longer valid equations [147]. Additionally, vorticity waves are nonphysically excited in shear flow problems due to the linearization process [5], causing stability problems. Several solutions have been proposed in literature [11].

Comparing the alternative methods available, using spatial and temporal high-order methods is usually the best strategy for unsteady problems with high accuracy demands [92]. And so, there is a very active research effort around high-order methods in modern computational architectures.

Many options for high-order spatial discretization exists. For example, discontinuous Galerkin (DG) is among the most popular methods [7, 133, 35]. It can be used for many problems, from elliptic to hyperbolic [9, 8], and from linear to nonlinear. Other methods such as flux reconstruction [6] or compact finite volume methods are also popular.

On the temporal side, in classical ODE methods three categories are distinguished: multistep, multistage and multiderivative. The first family combines previously computed timestep solutions with the current step to obtain a higher-order extrapolation. They are often used for second-order or lower requirements. Multistage methods are extremely popular, being Runge-Kutta (RK) the reference scheme [22]. They use multiple intermediate calculations (stages) in order to construct a higher-order approximation. They are very simple to implement and self-starting. Finally, multiderivative schemes expand variables in Taylor series using higher-order derivatives, which yields mixed spatial and temporal derivatives in the case of PDEs expansion. Multiderivative family is also called Lax-Wendroff when applied to PDEs, since it was Peter Lax and Burton Wendroff who first built a second-order scheme using this methodology [95, 131]. Its benefits are a small memory footprint and one-step calculations. Unfortunately, it requires more FLOPS, and the Cauchy-Kowalewski procedure becomes very tedious for high-order derivatives. Therefore, most of the high-order legacy codes use Runge-Kutta implementations. Mixed alternatives such as multistage-multiderivative methods have also been proposed. Seal gives the procedure to construct them, proposing the combination of second-order multiderivative and second-order Runge-Kutta scheme as the best choice [131].

Multistep-multistage methods can also be found [20, 69]. Finally, in the last decade, ADER family schemes have been developed by Toro [110, 140]. Algorithms in this family are based on the resolution of generalized Riemann problems, obtaining high-order convergence in time. As a multiderivative scheme, its application is elaborated, and efforts have been done to simplify it. ADER schemes are not yet largely used. All the previous discussion is applicable for explicit schemes, which are useful in wave propagation and medium Reynolds valued Navier-Stokes equations, where timestep is not limited by stiff viscous terms. Less frequently, explicit discretization is also employed in non-constant viscosity fluids, which turns the problem fully nonlinear [116].

The continuous improvement in simulation technology is not only due to the access to more powerful computers. Mathematical advances such as multigrid [105], iterative solvers [91], or adaptivity methods have contributed as much as hardware. Adaptive methods are very popular because of its flexibility and implementation "simplicity". This property allows adjusting accuracy, and hence cost, to the local needs of the problem, maximizing accuracy to cost ratio. Adaptivity in spatial discretization is probably the most popular choice due to the massive variety of spatial schemes available. Best known methods are refinement (or coarsening) and order adaptivity, also known as h and p adaptivity in the finite element community [145]. In finite difference and finite volume methods we find AMR or subdivision as the h type adaptivity equivalent, and stencil variations as the p type. In the temporal side, we stated multistep and multistage methods to be the predominant time discretization families. They are, nevertheless, multiderivative type schemes the ones with best adaptive properties. Multistep methods may seem a good candidate for order adaptivity since they only require storing extra history terms (only one new stage has to be computed in any case). Nigro provides an example for an adaptive "backward differentiation formula" (BDF) implicit method. He periodically runs an error estimate on the solution to adjust the order, such that the timestep is maximized for a given error tolerance [114]. Hay uses a similar approach, but his indicator is a stability estimate, on account of BDF being unstable for high-orders (and multistep methods in general). In both cases error measurements with trial and error tests are required for the order adaptation, sometimes discarding already computed steps. Given correct order adaptation is not straightforward, most codes consider only timestep size modifications to satisfy an accuracy constraint. Thus, needs for time-order adaptation methods in multiderivative schemes are detected.

From the previous discussion on CAA simulations, we conclude that there is a need for time-order adaptation methods in multiderivative schemes, with potential speedup and simulation robustness benefits.

1.2 Objectives

During the introduction of this thesis, the reader should have understood that CAA is a growing technology with a huge computational cost, were available resources should carefully be optimized. Consequently, using a hybrid strategy was decided, with two additional benefits: the convenience for efficiently solving growing low Mach number applications, and the possibility to use two separate solvers allowing higher flexible on each part. We aim at improving existing time schemes by developing a time-adaptive method that allows reducing the computational cost while staying robust against simulation failure.

The developed algorithm is an Adomian based scheme (ABS). Adomian algorithm is an existing method that easily converts any nonlinear operators into a series of the so-called Adomian polynomials [3, 4, 55]. Its application will result in an elegant and fast computation of the Taylor series, providing a tool to build simpler multiderivative type schemes.

Adomian has already been used in the computation of the convection-diffusion equation using finite differences [130, 111]. However, it never became popular in the computational fluid dynamics (CFD) community. Its main use in literature is as an analytical tool to easily obtain closed explicit expressions.

This thesis has been carried out within a group with interest in low Mach number turbomachinery applications. The following achievements were obtained:

- Study CAA hybrid methods to select the most suitable numerical schemes for the low Mach number turbomachinery applications, weighting pros and cons for each of them.
- Development of a new Adomian based scheme (ABS), with strengths such as time adaptivity, robustness, easy setup, and simple programming. ABS has been used with different spatial discretizations, including:
  - ABS-DG: discontinuous Galerkin to solve acoustic wave propagation.

  - ABS-FV and ABS-ADER: finite volume and ADER schemes to solve incompressible simulations and wave propagation.

- Development of an acoustic module, compatible with in-house "BBIPED" platform. The module contains Runge-Kutta time discretization, plus the new ABS-DG scheme.

1.3 Contents of the thesis

The thesis outline is as follows:

- **General background:** In chapter 2, the background for the ABS development is included. Starting with fluid flow and acoustic wave governing equations, then computational acoustic methods are exposed, and finally the basics for all employed numerical methods are explained.

- **Adomian based schemes (ABS):** In chapter 3, The ABS algorithm is obtained for the Navier-Stokes equations, its combination with discontinuous Galerkin is developed, and finally linearized Euler equations are solved for acoustic wave propagation.

- **ABS for low Mach number flows:** In chapter 4, ABS scheme is used altogether with finite volume and ADER numerical methods for incompressible Navier-Stokes, necessary for the acoustic sources computation in hybrid CAA methods.

- **conclusions:** In chapter 5, conclusions and future work are written.

Chapter 2

General Background

2.1 The physics

Waves are ubiquitous in nature, and are defined according to several properties. When waves are created by adiabatic compression and dilation of a medium, and they travel longitudinally at the speed of sound, they are called *acoustic waves*. These waves can be found in both fluid and solid media, although in this thesis we only study the first case. More specifically, "acoustic pressure waves" are pressure perturbations taking place over an ambient fluid $p' = p - p_\infty$, for which human audible levels (also called *noise*) are the most interesting ones for acoustic engineers. The range of pressure levels that a human can distinguish ranges $[2 \times 10^{-5}$ Pa , 200 Pa], and human audible frequency $f \in [20\text{ Hz}, 20\text{ kHz}]$. The main application is not only the well-known "acoustic pollution", but many additional fields of interest exist. For example, the improvement of audio hall acoustic quality, musical instrument design or combustion stability.

To deal with such a wide range of possible amplitude values, the Sound Pressure Level (SPL) measure is used, being its unit the "decibel" (dB) named after Alexander Graham Bell. The SPL compares the root mean square of an "acoustic pressure wave" amplitude (p'_{rms}), to a reference value (p_{ref}) in logarithmic scale:

$$SPL = 20\,\frac{p'_{rms}}{p_{ref}}.$$

Reference value $p_{ref} = 2 \times 10^{-5}$ Pa is the human hearing threshold at 1 kHz. In decibels, the range of human hearing ranges [0 dB , 140 dB].

To have an insight on the small amplitudes involved, 140 dB is the wave amplitude generated by a Formula 1 car at full throttle, which is 500 times smaller than the atmospheric pressure. Based on this estimation acoustic waves are assumed to be governed by the linearization of the fluid dynamics equations. Experience has shown this approximation to be good enough for most applications. Nevertheless, for very high intensities and high accuracy needs, the use of nonlinearity might be necessary.

Another common simplification is inviscid wave propagation. It turns out to be a reasonable assumption for short propagation distances, and medium to low-frequency waves. These approximations are supported by the following nondimensional analysis.

Consider wavelength (λ) and frequency (f) as spatial and temporal characteristic parameters. The following nondimensional variables are obtained,

$$x^* = \frac{x}{\lambda} \qquad t^* = tf \qquad u^* = \frac{u}{\lambda f}$$
$$p^* = \frac{p}{\rho_{ref}\ (\lambda f)^2} \qquad \rho^* = \frac{\rho}{\rho_{ref}} \qquad e^* = \frac{e}{(\lambda f)^2}$$
$$\mu^* = \frac{\mu}{\rho_0 \lambda^2 f}$$

Using the stated human audible frequency levels, the corresponding wavelengths are $\lambda = [17m - 1.7\ m]$ at ambient conditions ($\rho_0 = 1.225\ kg/m^3$). This is equivalently a nondimensional viscous range $\mu^* = [10^{-11}, 10^{-3}]$. Hence, in the worst case, nondimensional viscosity is orders of magnitude smaller than convection, proving its inviscid behavior.

If both linear and inviscid conditions are applied to the Navier-Stokes governing equations, the linearized Euler equations and its variations are obtained. Those are by far the most commonly used governing equations in wave propagation simulations. Other alternatives are Euler equations or Linearized Navier-Stokes equations, which consider non-linearity and viscosity effects correspondingly.

In acoustics, another distinction is done between *tonal* and *broadband* noise. A sound is referred as "tonal" when a certain pitch can be assigned to it. This is the type of noise found in musical instruments. The classical reference for aerodynamic tonal noise is the wind blowing around a pole, such as ships shaft in a harbor. On rotating machinery tonal noise is also found when the blade is impinging on a fluid element with a periodic frequency, such as shed vortices,

or the interaction between the rotor wake and the stator. Broadband noise on the other side does not have a distinctive pitch and is composed of multiple frequencies. But it does have some defining characteristics such as "brightness". During Aircraft takeoff and landing strong broadband noise is emitted by engines propulsion and fluid/airframe interaction. For the last case, when the uncorrelated wing suction and pressure sides meet at the trailing edge, it generates a local strong non-stationary pressure spike [46, 62].

For most aerodynamically generated noise applications, noise sources can be explained by two phenomena [144]. The first is known as impulsive noise and results from the surface movement within a non-uniform flow. The fluid displaced by the immersed body generates a non-stationary aerodynamic load on the solid surface, which produces pressure fluctuations that are radiated as sound. This kind of noise has spatial and temporal resolution scales similar to the aerodynamic requirements. Therefore, it can be obtained "easily" from specifications for aerodynamic simulations. It is often the primary type of noise in rotating systems such as helicopter rotors, wind turbines, turbine engine fans, and ventilators. It is, in fact, this impulsive noise that gives the periodic tonal component to turbomachinery, with a frequency function of the rotating speed, and blade number. The second noise source mechanism is the result of turbulence, and therefore, arises in nearly every engineering application as a chaotic stream of eddies with a wide range of frequencies and velocities. Thus, a broadband type frequency spectrum is generated. As a matter of facts, acoustic radiation from turbulent energy occurs most efficiently in the vicinity of sharp edges (e.g., at the trailing edge of an aircraft wing), and therefore both types of noise sources tend to gather near solid surfaces and edges. Often, noise is referred as a broadband type sound with some narrow-band tonal components. In multiphysic problems additional noise sources might be found, probably being the combustion noise the most popular one. This is a complicated problem with stiff sources, caused by the result of chemical reactions and the corresponding sudden energy release.

According to theory, sound power emanating from turbulence will be proportional to the eighth power of flow velocity, and low Mach number flows will be extremely inefficient with orders of magnitude smaller than the turbulent structures ([81], p. 31). On the other side, generated waves are inversely proportional to the Mach number and have long wavelengths. For computational applications one might find wavelengths being too long for a specific computational domain, causing a scaling disparity problem. In fact, scaling disparity

are the main problems arising in CAA applications as reported by Tam [135].

1. **waves are compressible and unsteady in nature**. Acoustic timescales are very small compared to turbulence evolution in low Mach number problems and introduces a computational difficulty to capture both of them. If one would be interested only in the aerodynamics, it could solve the stationary problem, filtering acoustic waves out. However, to simulate the full problem with acoustic waves, unsteady (or frequency domain) simulations are required, where the aerodynamic evolution is constrained by the acoustic waves resolution. Developing numerical methods that successfully overcome this problem is a challenging task.

2. **Large Spectral Bandwidth**. When interest is in broadband noise, multiple frequencies must be computed. It is then necessary to use a mesh discretization fine enough to capture the highest frequency waves. At the same time, simulation time must be long enough such that the waves of smallest frequencies are captured. The combination of both requirements need from huge data storage resources. Alternatively, one might use frequency-based solvers. In that case, multiple frequency simulations need to be done.

3. **Length Scales**. Aeroacoustic problems are multiscale.

   A problem related to the *large spectral bandwidth* above, is when acoustic sources are gathered in shear layers and turbulent eddies, which are orders of magnitude smaller than the acoustic waves. The required mesh must be fine enough to resolve the source terms, resulting in timestep limitations.

   Another length scale disparity is the (pressure) wave amplitude to mean flow values. Recall, an acoustic wave at a maximum human audible pressure is of $200Pa$ (140 dB), whereas the atmospheric pressure is 10^5Pa. This is a ratio of 500.

   Finally, the propagation distance of an acoustic wave might be orders of magnitude bigger than the effective aerodynamic propagation. In combination with extremely fine grids for the aerodynamic region, very long simulations runtimes are needed for the acoustic waves to arrive the far-field.

4. **Radiation conditions**. Acoustic solutions are very sensitive to numerical noise introduced during simulation. Boundary conditions must avoid

noise accumulation by forcing outgoing waves not to reflect back, including acoustic, entropic or vorticity waves.

5. **Nonlinearity and Wave Steepening**. It has been demonstrated that most of the acoustic waves are weak enough and are governed by linear wave equations. Most of the numerical schemes make use of this simplification, although for stronger waves (taking 120 dB as a reference value) steepening might become important. In some cases even shock waves are formed. For example, in brash instruments [66].

6. **Wall Boundary Conditions**. Acoustic waves are very sensitive to wall boundary conditions. In general, accurate high-order conditions are needed to successfully capture noise. Especial care is required in curved domains, where problems can arise during runtime, and also for fitted grids construction.

It is around these numerical difficulties where most of the aeroacoustic research is carried out. In this thesis, the approach known as the hybrid methodology is followed. It works by splitting the problem into an aerodynamic and an acoustic part, which decouples involved scales and successfully solves some of the mentioned problems.

2.2 Governing equations

The governing equations for fluid dynamics, known as Navier-Stokes, are the set of *conservation laws* for mass, momentum, and total energy *conservative variables*. Conservation laws state how conservative variables in an isolated physical system do not change as the system evolves. These equations can be obtained by different approaches. A common procedure is computing the balance of the conserved variable over a finite control volume, relating transportation through the boundaries, chemical reactions, or external forces acting on the volume. Thereupon, they require the *continuum* principle, where variables are macroscopically defined in a continuous media.

Conservative variables are evaluated using directly measurable fluid *primitive variables* such as pressure, temperature, velocity and density. Navier-Stokes equations can be manipulated to be used either in primitive or conservative variables, if variables are smooth enough [104, 141]. In many cases, it boils down

to the experience and personal preference of the researcher. Nonetheless, primitive variables usually yield simpler equations and workflows with a vast number of applicable methods [125, 86]. Particularly for multiphysic problems such as combustion. Unfortunately, the use of governing equations in primitive variables (primitive equations) does not correctly represent conservation variables near discontinuities, or more precisely its Riemann invariants. For this reason, governing equations in primitive form might be favored for low Mach number problems and multiphysics, whereas conservative variables are best suited for high Mach number flows with possible shock formations. Nevertheless, nowadays techniques to deal with most situations using either conservative or primitive variables exist.

2.2.1 Compressible case

When fluid density is function of pressure, then it is governed by the compressible Navier-Stokes equations. Equations can be cast in different forms:

∗ **Conservative form**

$$\begin{aligned}
&\frac{\partial \rho}{\partial t} + \frac{\partial}{\partial x_j}(\rho u_j) = S_m, \\
&\frac{\partial \rho u_i}{\partial t} + \frac{\partial}{\partial x_j}\left(\rho u_j u_i + p\delta_{ij} - \tau_{ij}\right) = S_i, \quad i = 1, 2, 3 \\
&\frac{\partial \rho E}{\partial t} + \frac{\partial}{\partial x_j}\left(\rho H u_j - \tau_{ij} u_i + r_j\right) = S_e
\end{aligned} \tag{2.1}$$

where ρ, u_i, p, E and H are the density, velocity components, pressure, total energy, and total enthalpy respectively. j is the index for the dimension of the problem ($j = 3$ for three-dimensional problems). r_j represents the heat convection per unit mass. δ_{ij} stands for the Kronecker delta function. S_m, S_i and S_e are the mass, momentum and energy sources; they can also be seen as a mass injection, external body force, and heat addition respectively.

The most common fluid to be simulated is air, and it can be considered as a calorically perfect gas:

$$\begin{aligned}
p &= \rho R T = (\gamma - 1)\rho e \\
e &= c_v T
\end{aligned}$$

Where T is temperature, e is the internal energy, R is the "specific gas constant", E the total energy and H the total enthalpy. The "specific gas constant" R can be obtained from the specific heat at constant pressure c_p and constant volume c_v with the well-known formula $R = c_p - c_v$. At least for diatomic gases. Additionally the total energy E is related with internal energy e by:

$$\begin{aligned}\phi^2 &= \sum_{k=1}^{Dim} u_k \\ E &= e + \frac{\phi^2}{2} \\ H &= E + \frac{p}{\rho}\end{aligned}$$

A useful definition is the *speed of sound*, which for the isentropic case (valid if a disturbance is small enough) is,

$$c^2 = \left(\frac{\partial p}{\partial \rho}\right)_s = cst \tag{2.2}$$

which for a perfect gas relation ($p/\rho^\gamma = cst$),

$$c^2 = \gamma \frac{p}{\rho}$$

Heat conduction is assumed to follow Fourier's law:

$$r_j = -k \frac{\partial T}{\partial x_j}$$

Being k the heat conductivity coefficient.

Finally, for Newtonian fluids, the Stokes hypothesis can be used for the stress tensor:

$$\begin{aligned}\tau_{ij} &= \tau_{ji} = \mu \left(\frac{\partial u_i}{\partial x_j} + \frac{\partial u_j}{\partial x_i} - \frac{2}{3}\delta_{ij}\frac{\partial u_k}{\partial x_k}\right) \\ \frac{\partial \tau_{ij}}{\partial x_j} &= \mu \frac{\partial^2}{\partial x_j^2} u_i + \frac{1}{3}\mu \frac{\partial}{\partial x_i}\left(\frac{\partial u_j}{\partial x_j}\right).\end{aligned} \tag{2.3}$$

Rewriting equations in primitive form:

∗ **Primitive variables**

$$\begin{aligned}
&\frac{\partial \rho}{\partial t} + \frac{\partial}{\partial x_j}\left(\rho v_j\right) = S'_m \\
&\frac{\partial u_i}{\partial t} + u_j \frac{\partial u_i}{\partial x_j} + \frac{1}{\rho}\frac{\partial}{\partial x_j}\left(p\delta_{ij} - \tau_{ij}\right) = S'_i \qquad\qquad i = 1,2,3 \\
&\frac{\partial p}{\partial t} + u_j \frac{\partial p}{\partial x_j} + \gamma p \frac{\partial u_j}{\partial x_j} + (\gamma - 1)\left[\frac{\partial r_j}{\partial x_j} - \tau_{ij}\frac{\partial u_i}{\partial x_j}\right] = S'_e
\end{aligned} \tag{2.4}$$

Euler equations in vectorial form

Euler equations are a simplification of the Navier-Stokes equations for no heat conduction and no viscosity ($\tau_{ij} = r_j = 0$). With this simplification, vectorial notation is possible.

∗ **Conservative (vectorial) form**

$$\frac{\partial Q}{\partial t} + \frac{\partial F_j}{\partial x_j} = S \qquad\qquad j = 1, \ldots, Dim \tag{2.5}$$

$$Q = \begin{pmatrix} \rho \\ \rho u_i \\ \rho E \end{pmatrix} = \begin{pmatrix} q_0 \\ q_i \\ q_4 \end{pmatrix} \qquad F_j = \begin{pmatrix} q_j \\ \dfrac{q_i q_j}{q_0} + p\delta_{ij} \\ \dfrac{q_j}{q_0}(q_4 + p) \end{pmatrix} \qquad p = \frac{R}{c_v}\left(q_4 - \phi^2\right)$$

∗ **Primitive (vectorial) form**

$$\frac{\partial W}{\partial t} + \mathcal{A}_j \frac{\partial W}{\partial x_j} = S' \qquad\qquad j = 1, \ldots, Dim \tag{2.6}$$

$$W = \begin{pmatrix} \rho \\ u_i \\ p \end{pmatrix} \qquad \mathcal{A}_j = \begin{pmatrix} u_j & \rho\delta_{1j} & \rho\delta_{2j} & \rho\delta_{3j} & 0 \\ 0 & u_j & 0 & 0 & \delta_{1j}/\rho \\ 0 & 0 & u_j & 0 & \delta_{2j}/\rho \\ 0 & 0 & 0 & u_j & \delta_{3j}/\rho \\ 0 & \gamma p\delta_{1j} & \gamma p\delta_{2j} & \gamma p\delta_{3j} & u_j \end{pmatrix}$$

Conservative and primitive relation

The relation between the two forms is better observed in the quasilinear form. To get the conservative quasilinear form

$$\frac{\partial Q}{\partial t} + \mathscr{A}_j \frac{\partial Q}{\partial x_j} = 0 \tag{2.7}$$

we start by applying the chain rule to the flux derivative in (2.5), for a three-dimensional problem $u_j = \{u, v, w\}$.

$$\frac{\partial F_j}{\partial Q} = \mathscr{A}_j \frac{\partial Q}{\partial x_j}$$

$$\mathscr{A}_j = \begin{pmatrix} 0 & \delta_{1j} & \delta_{2j} & \delta_{3j} & 0 \\ a_1\phi^2/2\delta_{1j} - uu_j & u_j - a_2\delta_{1j}u & u\delta_{2j} - a_1\delta_{1j}v & u\delta_{3j} - a_1\delta_{1j}w & a_1\delta_{1j} \\ a_1\phi^2/2\delta_{2j} - vu_j & v\delta_{1j} - a_1\delta_{2j}u & u_j - a_2\delta_{2j}v & v\delta_{3j} - a_1\delta_{2j}w & a_1\delta_{2j} \\ a_1\phi^2\delta_{3j} - wu_j & w\delta_{1j} - a_1\delta_{3j}u & w\delta_{2j} - a_1\delta_{3j}v & u_j - a_2\delta_{3j}w & a_1\delta_{3j} \\ u_j(a_1\phi^2 - H) & a_1\delta_{1j} - a_1uu_j & a_1\delta_{2j} - a_1vu_j & a_1\delta_{3j} - a_1wu_j & \gamma u_j \end{pmatrix}$$

Being, $a_1 = (\gamma - 1)$ and $a_2 = (\gamma - 2)$.

Now, perform a change of variables with another chain rule,

$$\frac{\partial U}{\partial W}\frac{\partial W}{\partial t} + \mathscr{A}_j \frac{\partial U}{\partial W}\frac{\partial W}{\partial x_j} = 0.$$

Multiplying from the left by $\left(\frac{\partial U}{\partial W}\right)^{-1}$, the primitive form (2.6) is recovered by realizing,

$$\mathcal{A}_j = \left(\frac{\partial U}{\partial W}\right)^{-1} \mathscr{A}_j \frac{\partial U}{\partial W}$$

with

$$\frac{\partial U}{\partial W} = \begin{pmatrix} 1 & 0 & 0 & 0 & 0 \\ u_1 & \rho & 0 & 0 & 0 \\ u_2 & 0 & \rho & 0 & 0 \\ u_3 & 0 & 0 & \rho & 0 \\ \phi^2/2 & \rho u_1 & \rho u_2 & \rho u_3 & 1/a_1 \end{pmatrix}$$

$$\frac{\partial W}{\partial U} = \begin{pmatrix} 1 & 0 & 0 & 0 & 0 \\ -u_1/\rho & 1/\rho & 0 & 0 & 0 \\ -u_2/\rho & 0 & 1/\rho & 0 & 0 \\ -u_3/\rho & 0 & 0 & 1/\rho & 0 \\ a_1\phi^2/2 & -a_1u_1 & -a_1u_2 & a_1u_3 & a_1 \end{pmatrix}$$

In this thesis no source terms are considered.

$$S_m = S_i = S_e = S'_m = S'_i = S'_e = 0$$

Riemann invariants

A hyperbolic one-dimensional problem in the form of,

$$U_t + AU_x = 0,$$

being A a linear matrix of $n \times n$ size, can always be converted to an uncoupled diagonal form by using its left L and right R eigenvectors,

$$\begin{aligned} &LU_t + LARLU_x = 0 \\ &(LU)_t + LAR(LU)_x = 0 \\ &V_t + \Lambda V_x = 0 \end{aligned} \tag{2.8}$$

where Λ is the diagonal eigenvalues matrix. This is equivalent to a three plane-wave propagation system. V is also known as the *characteristic variables* or the *Riemann invariant*. Dependence between U and V variables can be found by the inverse of the identity $V = LU$,

$$U = RV$$

This solution means that any change in the solution U is composed off the sum of the characteristic variables, each of them proportional to the corresponding right eigenvector value. Unfortunately this analysis requires matrix A to be linear. If this is not the case, as for Euler and Navier-Stokes equations, only the linearized case can be proved.

$$L\partial U = \partial V$$

Solution for the primitive variables Euler equations is [104],

$$L\partial W = \partial W^c = \begin{pmatrix} \partial u - \frac{1}{\rho c}\partial p \\ \partial \rho - \frac{1}{c^2}\partial p \\ \partial u - \frac{1}{\rho c}\partial p \end{pmatrix} \quad \Lambda = \begin{pmatrix} u-c & 0 & 0 \\ 0 & u & 0 \\ 0 & 0 & u+c \end{pmatrix}$$

Where W^c denotes the characteristic variables of the primitive W system. The system for W^c becomes,

$$\begin{aligned} &\left(\frac{\partial u}{\partial t} - \frac{1}{\rho c}\frac{\partial p}{\partial t}\right) + (u-c)\left(\frac{\partial u}{\partial x} - \frac{1}{\rho c}\frac{\partial p}{\partial x}\right) = 0 \\ &\left(\frac{\partial \rho}{\partial t} - \frac{1}{c^2}\frac{\partial p}{\partial t}\right) + u\left(\frac{\partial \rho}{\partial x} - \frac{1}{c^2}\frac{\partial p}{\partial x}\right) = 0 \\ &\left(\frac{\partial u}{\partial t} + \frac{1}{\rho c}\frac{\partial p}{\partial t}\right) + (u+c)\left(\frac{\partial u}{\partial x} + \frac{1}{\rho c}\frac{\partial p}{\partial x}\right) = 0 \end{aligned} \tag{2.9}$$

Since from equation (2.2), the second variable is constant for an isentropic process, its evolution is related to entropy change. It is thus known as the *entropic wave*. The other two equations correspond to *acoustic waves* traveling at the speed of sound c. For an adiabatic isentropic flow, the characteristic variables can be analytically integrated,

$$\partial W^c = \begin{pmatrix} \partial u - \frac{1}{\rho c}\partial p \\ \partial \rho - \frac{1}{c^2}\partial p \\ \partial u - \frac{1}{\rho c}\partial p \end{pmatrix} = \begin{pmatrix} \partial\left(u - \frac{2}{\gamma-1}c\right) \\ \partial s \\ \partial\left(u + \frac{2}{\gamma-1}c\right) \end{pmatrix}$$

Nondimensional analysis

It is always a good practice to work with equations in nondimensionalization form. By this procedure, fluid variables are scaled to reference parameters, loosing their physical units. The main computational benefits are floating numbers rescaling, getting better round-off errors control; and on the mathematical side, negligible variables discrimination.

Consider the following reference parameters: $x_{ref}, u_{ref}, \rho_{ref}$, and c_{ref}. Then, variables are nondimensionalized by,

$$\begin{aligned} x^* &= \frac{x}{x_{ref}} & t^* &= t\frac{u_{ref}}{x_{ref}} & u^* &= \frac{u}{u_{ref}} \\ p^* &= \frac{p}{\rho_{ref}\ c_{ref}^2} & \rho^* &= \frac{\rho}{\rho_{ref}} & e^* &= \frac{e}{c_{ref}^2} \end{aligned} \tag{2.10}$$

Notice that two velocity reference values are being used u_{ref} and c_{ref}. The first is a suitable characteristic variable, such as far-field flow velocity. Whereas the second is the specific sound of speed. The use of two reference velocities is of interest for the low Mach number fluid analysis, as it will be shown next. Substituting all variables (2.10) in the primitive Navier-Stokes equations (2.4) and extracting μ from τ_{ij} as in equation (2.3) to form the Reynolds term, the following system of equations is obtained [106, 73] ('$*$' sign was dropped for convenience).

$$\begin{aligned} &\frac{\partial \rho}{\partial t} + \frac{\partial}{\partial x_j}\left(\rho v_j\right) = 0 \\ &\frac{\partial u_i}{\partial t} + u_j\frac{\partial u_i}{\partial x_j} + \frac{1}{\rho\, M^2}\frac{\partial}{\partial x_j}\left(p\delta_{ij}\right) = \frac{1}{\rho\, Re}\frac{\partial \tau_{ij}}{\partial x_j} \qquad i = 1,2,3 \\ &\frac{\partial p}{\partial t} + u_j\frac{\partial p}{\partial x_j} + \gamma p\frac{\partial u_j}{\partial x_j} = -\frac{\gamma - 1}{Pe}\frac{\partial q_j}{\partial x_j} + \frac{M^2\left(\gamma - 1\right)}{Re}\left(\frac{\partial \tau_{ij}u_i}{\partial x_j} - u_i\frac{\partial \tau_{ij}}{\partial x_j}\right) \end{aligned} \tag{2.11}$$

Where all variables are now nondimensional. Some well-known "nondimensional numbers" have been defined: Mach (M), Reynolds (Re), and Peclet (Pe).

$$M = \frac{u_{ref}}{c_{ref}} \qquad Re = \frac{u_{ref}\ x_{ref}\ \rho_{ref}}{\mu} \qquad Pe = \frac{x_{ref}u_{ref}}{q_{ref}}$$

The Mach number appears in the formulation in the form of $1/M^2$, introducing a singularity when Mach number tends to zero. Additionally, the nondimensional energy relationship becomes,

$$E = \rho e + \frac{M^2}{2}\rho u_k^2.$$

2.2.2 Incompressible case

Incompressibility condition is a simplification made when compressible Navier-Stokes equations are ill-conditioned. The most common case is for fluids with low-density variations with respect to pressure changes, such as liquids. But it

can also appear in other situations such as low Mach number flows, where the appearance of singularities was shown in the nondimensional analysis.

For the low Mach number case, the ill-conditioning stems from the speed difference between acoustic wave and aerodynamic modes propagation. Normalization of time with respect to the aerodynamic characteristic times, yield stiff pressure waves, which are no longer appropriately represented by time-derivatives. The incompressibility assumption solves all pressure fluctuations as instantaneously balanced in the domain, and thus no acoustic waves are simulated. A *low Mach number asymptotic* study will show that nondimensional equations (2.11) behave, in fact, as the incompressible equations [106, 73].

An excellent solution to compute acoustic waves in low Mach number applications is the usage of the hybrid formulation, where the aerodynamic part is solved first, and then the acoustic part. In other words, acoustic waves are removed from the compressible equations.

Performing a Mach number power expansion for system variables,

$$\begin{aligned}
\rho\,(x,t) &= \rho^{(0)} + M\ \rho^{(1)} + M^2\ \rho^{(2)} + \ldots + O(M^m) \\
u\,(x,t) &= u^{(0)} + M\ u^{(1)} + M^2\ u^{(2)} + \ldots + O(M^m) \\
p\,(x,t) &= p^{(0)} + M\ p^{(1)} + M^2\ p^{(2)} + \ldots + O(M^m)
\end{aligned}$$

Where each coefficient $\rho^{(i)}$, $u^{(i)}$, and $p^{(i)}$ on the series is function of space and time. Expanded variables are substituted into equations (2.11), and gathered by equal Mach powers. For continuity and energy equations $M^{(0)}$ are the smallest power terms. Whereas momentum equations include $M^{(-2)}$ and $M^{(-1)}$ terms, which are simplified to

$$\begin{aligned}
&\frac{\partial p^{(0)}}{\partial x_j}(x,t) = 0 \\
&\frac{\partial p^{(1)}}{\partial x_j}(x,t) = 0.
\end{aligned}$$

Therefore, $p^{(0)}$ and $p^{(1)}$ need to be spatially independent (but function of time).

$$\begin{aligned}
p^{(0)} &= p^{(0)}(x) \\
p^{(1)} &= p^{(1)}(x).
\end{aligned}$$

From the $M^{(0)}$ energy equation condition (2.11) we have

$$\frac{\partial p^{(0)}}{\partial t} + \gamma p^{(0)} \frac{\partial u_j^{(0)}}{\partial x_j} = -\frac{\gamma - 1}{Pe} \frac{\partial q_j^0}{\partial x_j}.$$

Which after integrating over the whole domain (Ω) and making use of the Gauss theorem (with $p^{(0)}$ being independent of space), we obtain

$$\frac{\partial p^{(0)}}{\partial t} \int_\Omega d\Omega + \gamma \; p^{(0)} \int_{\partial\Omega} u^{(0)} \cdot n \; d\Gamma = \frac{\gamma - 1}{Pe} \int_{\partial\Omega} q^{(0)} \cdot n \; d\Gamma. \tag{2.12}$$

Where n is the outward normal vector over the boundary ($\partial\Omega$). If we further assume no boundary compression,

$$\oint_{\partial\Omega} u^{(0)} \cdot n = 0 \, d\Gamma,$$

which is in fact a necessary condition when the fluid is not allowed to exit the domain (as is demonstrated in the next section), then (2.12) integral vanishes and $p^{(0)}$ is proven to be constant in time: $p^{(0)} = cst$.

Finally, gathering all zeroth order $M^{(0)}$ expansions we recover the incompressible Navier-Stokes equations with variable density,

$$\begin{aligned}
&\frac{\partial \rho^{(0)}}{\partial t} + u_j^{(0)} \frac{\partial \rho^{(0)}}{\partial x_j} = 0, \\
&\frac{\partial u^{(0)}}{\partial t} + u_j^{(0)} \frac{\partial u_i^{(0)}}{\partial x_j} + \frac{1}{\rho^{(0)}} \frac{\partial p^{(2)}}{\partial x_j} = \frac{1}{\rho^{(0)} Re} \frac{\partial \tau_{ij}^{(0)}}{\partial x_j}, \\
&\frac{\partial u_j^{(0)}}{\partial x_j} = 0.
\end{aligned} \tag{2.13}$$

For homogeneous initial density problems, equation (2.13) is trivially zero, and density is constant everywhere.

From this development it follows $p^{(2)}$ in the incompressible Navier-Stokes equations does not hold to the thermodynamic interpretation any longer; barely referred (in literature) as a Lagrangian multiplier which enforces divergence-free condition. A rigorous mathematical analysis for the asymptotic study can be found in [102, 88].

Considering the propagation medium as an isotropic Newtonian fluid in incompressible flow (with velocity divergence-free conditions), stress tensor in

equation (2.3) is simplified to [115],

$$\tau_{ij} = \mu \left(\frac{\partial u_i}{\partial x_j} + \frac{\partial u_j}{\partial x_i} \right).$$

Substitution in equations (2.13) and assuming initial homogeneous density conditions, the final system of equations is obtained (superscripts (0) and (2) are dropped for clarity).

$$\frac{\partial u_i}{\partial t} + u_j \frac{\partial u_i}{\partial x_j} + \frac{1}{\rho} \frac{\partial p}{\partial x_i} = \frac{1}{\rho\, Re} \frac{\partial^2 u_i}{\partial x_j^2} \tag{2.14}$$

$$\frac{\partial u_j}{\partial x_j} = 0 \tag{2.15}$$

These two equations represent the simplest general incompressible flow.

Initial velocity and normal to boundary velocity distributions are required for the well-posedness of the problem. Being the imposition of tangential velocity unnecessary, except for specific cases such as no-slip wall conditions. Under this conditions the problem is still well-posed, although the solution belongs to a higher regularity space ([118], p 4). On the other side, pressure should not be imposed within the domain nor on the boundary, since it can be computed (up to a constant) from the velocity distribution. Exceptions are the usage of certain boundary conditions such as moving walls. Imposed velocity boundary conditions are denoted with b,

$$b = u(t, x|_{\partial\Omega}).$$

A global incompressible condition on the boundary is obtained from the divergence theorem and equation (2.15),

$$\oint_{\partial\Omega} b_j \cdot n_j \, d\Gamma = 0. \tag{2.16}$$

Initial condition $u_j(0, x) = u_0(x)$ is given by

$$\frac{\partial u_0}{\partial x_j} = 0 \quad \text{in } \Omega.$$

From the combination of both equations we obtain a continuity condition

$$u_0(x|_{\partial\Omega}) \cdot n_j = b_j \cdot n_j \quad \text{in } \partial\Omega \tag{2.17}$$

Because of the velocity/pressure coupling, there is no available explicit equations for pressure, and the system is not easily solved. Fractional methods using the "pressure Poisson equation" are a popular way to uncouple both variables and reduce computational cost.

2.2.3 Pressure Poisson equation

The *pressure Poisson equation* (PPE) is introduced as a means to replace the incompressibility constrain (2.15), by obtaining an explicit equation for pressure. It is obtained applying the divergence operator to the momentum equation [151],

$$\frac{\partial^2 p}{\partial x_j} = \frac{\partial}{\partial x_j}\left(-\rho\,\frac{\partial u_j}{\partial t} - \rho\,u_i\frac{\partial u_j}{\partial x_i} + \frac{1}{Re}\frac{\partial^2 u_j}{\partial x_i^2}\right). \tag{2.18}$$

The use of the PPE is not entirely equivalent to the original system of incompressible equations (2.14 - 2.15). First of all, since higher derivatives are used, a more regular solution space (with higher smoothness) is required. Another challenging problem is setting new boundary conditions. Opposite to the original set of equations, this system needs from pressure boundary conditions. Gresho and Sani gave a good review on many of the alternatives proposed in literature, and studied which conditions are required such that the problem is well-posed [71]. Many of the methods are based on the idea that the PPE being an scalar equation, so the boundary condition should be. Therefore, the normal and the tangential scalar products on the (vectorial) governing equations are commonly used. Unfortunately, solutions are not unique since the use of one or the other results in different equations. Today, most of the authors use the normal scalar product,

$$\left.\frac{\partial p}{\partial n}\right|_{\partial\Omega} = \left(-\rho\,\frac{\partial u_j}{\partial t} - \rho\,u_i\frac{\partial u_j}{\partial x_i} + \frac{1}{Re}\frac{\partial^2 u_j}{\partial x_i^2}\right)\cdot n_j = \xi.$$

Although for smooth enough solutions both methods are correct [129, 71, 48].

Another condition is also required from equation (2.18). Rewriting it as,

$$\frac{\partial^2 p}{\partial x_j^2} = f \quad \text{in } \Omega$$

and using the Gauss theorem for p,

$$\int_\Omega \frac{\partial^2 p}{\partial x_j^2}\, d\Omega = \oint_{\partial\Omega} \frac{\partial p}{\partial x_j} \cdot n_j \, d\Gamma,$$

we get the solvability condition (p 225. [48]),

$$\int_\Omega f \; d\Omega = \oint_{\partial\Omega} \xi \; d\Gamma.$$

When the system is discretized, $Ax = \xi$, the solvability condition becomes $\xi^T l = 0$. Where l is the left eigenvector for matrix A. This is equivalent to the sum of ξ over all equations to be zero, and is a direct result of having a conservative divergence operator (p. 226 [48]).

In some cases, one of the following equations might also be required (p. 1116, 6 [71])

$$\begin{aligned} &\frac{\partial u_j}{\partial x_j}\bigg|_{\partial\Omega} = 0 \\ &\frac{\partial}{\partial x_i}\frac{\partial u_j}{\partial x_j} \cdot n_i \bigg|_{\partial\Omega} = 0. \end{aligned} \tag{2.19}$$

The first equation, known as the Kleiser condition, avoids harmonic solutions of the solenoidal condition (p. 150 [129], [118], [89]).

2.2.4 Turbulence

When considering best practice guidelines in CAA or CFD, turbulence resolution needs to be considered. In this section, we will provide a summary of common turbulence methods.

The best case scenario is a *direct numerical simulation* (DNS), where no modeling is introduced and all vortex scales and frequencies involved are resolved. Energy spectra for quantities of interest are monitored to judge fully resolved turbulence structures. In fully resolved problems high-frequency energy contents must tend to zero. Equivalently, two-point correlations in time and space should tend to zero. However, no real problem is solved by DNS due to the extreme computational cost. Computational cost reduction is achieved by modeling smallest flow structures of high-frequency content. This is achieved by averaging or filtering the governing equations, obtaining smoother solutions.

Large eddy simulation (LES) performs a spatial filtering on the "subgrid scale" structures, which are then modeled. This modeling introduces errors

that can strongly interact with the acoustic field and cause relevant errors in aeroacoustic applications [143]. In general, the spectral content of a solution should be kept fixed at the desired filter level [101]. To remove some filter errors statistical data processing and correlation can be employed. LES results are very accurate, but still expensive.

A less expensive simulation is obtained using the *Reynolds Averaged Navier-Stokes* equations (RANS). It is probably the most widely used turbulence modeling for aerodynamic applications due to its cheap computational cost, long-standing history, and thoroughly validated test cases. In this method, flow variables are split into a fluctuating and a mean part. The fluctuating part should contain frequencies orders of magnitude faster than the mean part. Applying appropriate "Ensemble" or "Favre" averaging, the so-called *Reynolds Stress* tensor is obtained, which requires further modeling to be fully determined. Usually transport equations for the turbulent mean kinetic energy and turbulent dissipation rates are constructed. This is known as the "turbulence closure problem". The mean part is usually assumed stationary, although it can also be unsteady if flow timescales are similar to the averaging timescales (see URANS below).

From RANS results fluctuating velocity components can be reconstructed, and therefore the noise caused by the unsteady field. This method is known as *Stochastic Noise Generation* (SNGR) or *Synthetic turbulence*, and is an active research field due to its interest in low-cost results [144]. Batten made this method popular in aeroacoustics by reconstructing coherent turbulent velocity fluctuations from a given dissipation rate and second-order moments [12].

For tonal noise problems, good results might be obtained using URANS simulations. Based on the RANS equations, it includes time dependency at a cost slightly higher than pure RANS simulations. Although it cannot accurately recover turbulence information, it captures the evolution of the biggest eddies in the flow. If those eddies are responsible for a periodic tonal sound, such as von Karman vortex shedding, the tonal noise might be successfully captured.

An increasingly popular strategy for turbulence resolution is the use of *hybrid approaches*. Here, different methods are blended on the domain, or a domain decomposition is applied. Hybrid RANS/LES techniques are probably the most common hybrid approach. For example, in surface interaction problems small turbulent structures are fully resolved near solid surfaces, whereas RANS modeling is used far from the surface. Hybrid methods are a growing research area, as an optimal solution for both RANS and LES. A significant challenge is the

information exchange between both regions. Since the RANS region only provides filtered mean quantities, the fluctuating data at the LES interface needs to be reconstructed. Typically synthetic turbulence reconstruction is performed, as Battens did in SNGR. Another popular hybrid method in CAA is the *Nonlinear Acoustic Solver* (NLAS). Not as popular as hybrid RANS/LES solver, it has the advantage of not having an interface between both filters. The method first requires a RANS computation of the full domain over which a perturbation simulation is performed.

2.2.5 Riemann problem

An initial value problem with two piecewise-continuous functions separated by a discontinuity is called a *Riemann problem*.

$$\frac{\partial u}{\partial t} + \frac{\partial f(u)}{\partial x} = 0, \tag{2.20}$$

$$u_0(x) = u(x,0) = \begin{cases} u^L \text{ if } x < 0 \\ u^R \text{ if } x > 0 \end{cases}$$

The solution to this problem is of great interest to understand governing equations behavior, and to construct suitable numerical methods.

When one talks about the Classical Riemann problem, it refers to the well-known Cauchy problem: piecewise-continuous functions with constant left and right states.

By understanding the behavior of the flux function $f(u)$, and the related *characteristic speed*, nonlinearity phenomena such as wave steepening can be studied. Assume a one-dimensional conservation equation in the form of (2.20). Using the chain rule, the quasilinear form is obtained,

$$\frac{\partial u}{\partial t} + \lambda(u)\frac{\partial u}{\partial x} = 0. \tag{2.21}$$

where

$$\lambda(u) = \frac{d}{du} f(u)$$

is the characteristic speed.

If one applies the same procedure to a system of hyperbolic equations, $\lambda(u)$ becomes the *Jacobian matrix* (not to be confused with the Jacobian determinant). This is equivalent to the Riemann invariant from section 2.8. Therefore,

solution is given by the *solution of characteristics*, which is the curve through which the total derivative of u is zero. Consider the characteristic curve $s(t)$ which satisfies,

$$\frac{ds}{dt} = \lambda(u), \qquad s_0 = s(0). \tag{2.22}$$

Then we compute the total derivative of u through the constructed characteristic line. Using the chain rule,

$$\frac{d}{dt}u\big(s(t),t\big) = \frac{\partial u}{\partial t} + \lambda(u)\frac{\partial u}{\partial s} = 0.$$

This equation satisfies the original PDE, and hence the total change of $u\big(s(t),t\big)$ must be zero. In other words, u is constant along the characteristic curve $s(t)$, and equal to the initial condition $u(s_0,0)$. Since u is constant along $\lambda(u)$, the characteristic curve is also a straight line in a $x-t$ representation. Equation (2.22) can be integrated to obtain

$$s(t) = s_0 + \lambda\big(u_0(s_0)\big)\,t.$$

Which can be converted to an implicit analytical solution,

$$u(s(t),t) = u_0\left(s - \lambda\big(u_0(s_0)\big)\,t\right) \tag{2.23}$$

$$= u_0\left(s - \lambda\big(u(s)\big)\,t\right). \tag{2.24}$$

The previous solution has the form of a linear advection equation, where initial data $u_0(x)$ is transported at a constant velocity $\lambda\big(u_0(s(t))\big)$. However, each characteristic line will have different velocity propagation, distorting the shape of the initial condition. This is the nonlinear effect.

Locations where two adjacent characteristic curves collide or diverge from each other will, develop *expansion* or *compression* regions. The first case leads to *shock waves*, and the later to *rarefraction waves*. In figure 2.2 both cases are represented. Its formation can be understood by the convexity property of the characteristic speed, $\lambda(u)$. Convexity means characteristic speed increases with an increasing u: $\lambda'(u) = f''(u) > 0$. If u^L is bigger than u^R, the characteristic curves will intersect each other at the shock location S, as can be seen in figure 2.2 (I). The opposite will occur if u^R is bigger than u^L, a region with no crossing characteristics is created, and an expansion area will happen as in figure 2.2 (II).

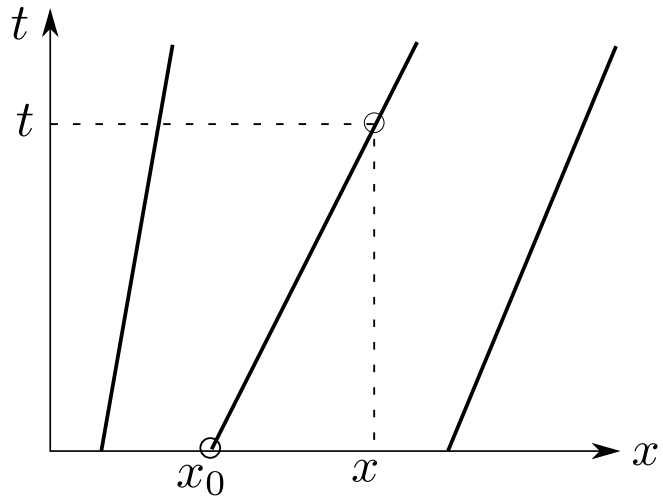

FIGURE 2.1: Characteristics based solution representation

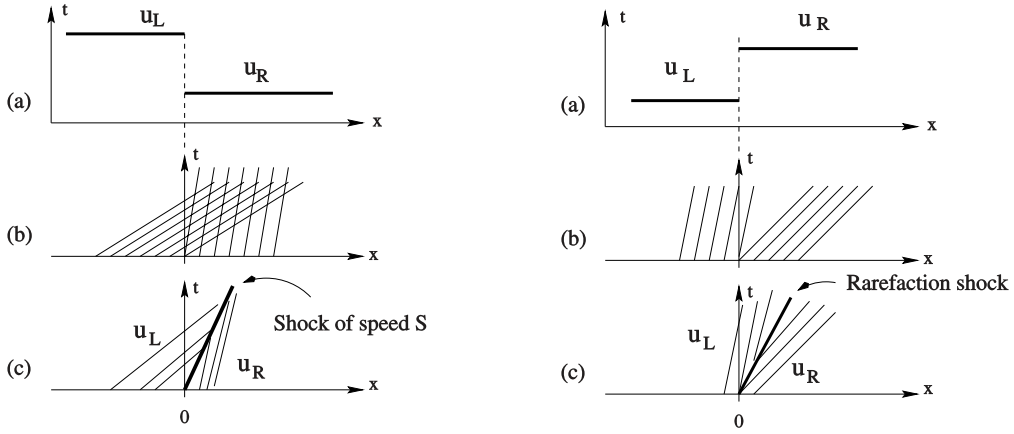

FIGURE 2.2: shock wave (I) and rarefraction shock (II) representations for Burgers' equation, from [141].

Equation (2.20) with a discontinuity is not well-posed, in terms of the classical differential-integral definitions. This framework should be cast in a more general weak formulation, or *distribution*. Selected notes on this topic will be introduced at the end of this section. However, an informal analysis of the classical problem will be done first. Take the integral of the balance law over a big enough domain (which includes the discontinuity), say $[x_L, x_R]$. Integrals

are then split around discontinuity $s(t)$,

$$f\big(u(x_L,t)\big) - f\big(u(x_R,t)\big) = \frac{d}{dt}\int_{x_L}^{s(t)} u(x,t)\,dx + \frac{d}{dt}\int_{s(t)}^{x_R} u(x,t)\,dx$$
$$f\big(u(x_L,t)\big) - f\big(u(x_R,t)\big) = [u(s_L,t) - u(s_R,t)]\,S + \int_{x_L}^{s(t)} u_t(x,t)\,dx + \int_{s(t)}^{x_R} u_t(x,t)\,dx.$$

Where S_L and S_R are the left and right limits of the discontinuity, function of time $S(t)$. Taking both x_L and x_R infinitely close to $s(t)$, both integrals vanish and the *Rankine-Hugoniot condition* is deduced.

$$\Delta f = S\Delta u. \tag{2.25}$$
$$\Delta f = f\big(u(x_R,t)\big) - f\big(u(x_L,t)\big)$$
$$\Delta u = u(x_R,t) - u(x_L,t).$$

It can be formally derived that a solution to the balance equation must satisfy the Rankine-Hugoniot condition. Unfortunately, multiple solutions can be obtained, from which only one can be the physically correct case. Extra solutions are called "spurious solutions". In order to obtain the correct result, additional conditions are required. In fluid dynamics this condition is the well-known *entropic condition*, which enforces systems to evolve such that entropy always increases. Different mathematical formulations can be constructed which satisfy the entropic condition, being the *Lax entropy condition* for shocks probably the simplest one: a shock can only be formed if the following condition is met.

$$f'\left(u^R\right) < S < f'\left(u^L\right).$$

The rarefraction shock in figure 2.2 (II) is therefore physically not correct: a continuous solution must be obtained.

A way to correctly construct the expansion zone is by using the Riemann invariants, since we know they hold constant along the characteristic lines. If u^R is bigger than u^L, there exists a unique solution to (2.20) given by [56],

$$u = \begin{cases} u^- & \frac{x}{t} < f'(u^-) \\ G & f'(u^-) < \frac{x}{t} < f'(u^+) \\ u^+ & \frac{x}{t} > f'(u^+) \end{cases}. \tag{2.26}$$

Where $G(x/t)$ is the auxiliary function,

$$G = G(x/t) = (f')^{-1}.$$

A discontinuity exists only at the origin for $t = 0$. For $t > 0$ no discontinuity (shock) is formed:

$$\begin{aligned} u_t + [f(u)]_x &= G'\left(-x/t^2\right) + f'(G)\, G_x \\ &= G'\left(-x/t^2\right) + f'\left((f')^{-1}\right)\, G'\left(1/t\right) \\ &= G'\left(-x/t^2\right) + G'(x/t^2) \\ &= 0. \end{aligned}$$

One of the properties of this solution is the self-similarity, where the solution follows a scaling rule in the form of x/t. This property is very useful since it allows obtaining a solution using the ratio between space and time.

The physically correct representation of the rarefraction zone is now depicted in figure 2.3

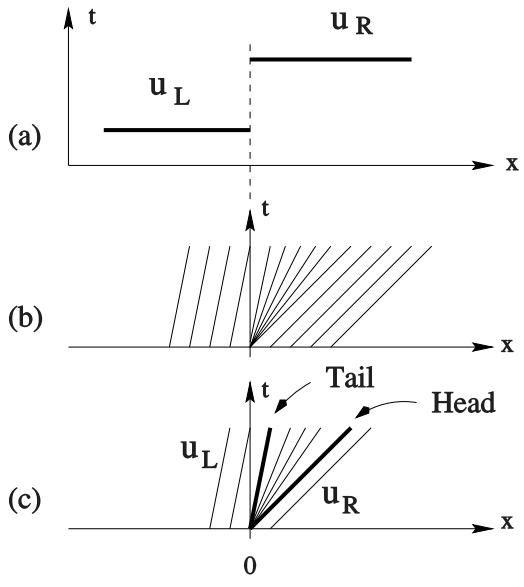

FIGURE 2.3: Entropic condition satisfying rarefraction wave [141].

A formal development to the previous results is obtained using the *weak formulation* approach. A function $u(x,t)$ is a weak solution of the conservation law (2.20) - note the conservation form - if for any sufficiently smooth with

compact support test function $\phi(x,t)$, it satisfies,

$$\int_0^\infty \int_{-\infty}^\infty u(x,t)\,\frac{\partial}{\partial t}\phi(x,t)\,dx\,dt + \int_0^\infty \int_{-\infty}^\infty f(x,t,u)\frac{\partial}{\partial x}\phi(x,t)\,dx\,dt = 0.$$

This definition will be the basis for many modern numerical methods. However, in practice, the integral is defined over a bounded space, in which case boundary terms are added to the previous equation, stemming from the integration by parts.

$$\int_0^\infty \int_a^b u(x,t)\,\frac{\partial}{\partial t}\phi(x,t)\,dx\,dt + \int_0^\infty \int_a^b f(x,t,u)\frac{\partial}{\partial x}\phi(x,t)\,dx\,dt - \\ - \int_0^\infty \Big[f(x,t,u)\phi(x,t)\Big]_a^b = 0. \tag{2.27}$$

Terms within square braces represent evaluation at boundary locations $x = a$ and $x = b$.

Inviscid Burgers' equation

Inviscid Burgers' equation is a convex equations which can be described by (2.20) and the specific characteristic speed

$$\lambda(u) = u$$
$$f(u) = \frac{1}{2}u^2$$

The shock discontinuity jump is obtained from the Rankine-Hugoniot relation,

$$S = \frac{1}{2}\left(u^L + u^R\right). \tag{2.28}$$

And the solution to the rarefraction wave is obtained from the Riemann invariant (2.26). Alternatively, since Burgers' equation is a simplification of the Navier-Stokes equation, one might consider solving the viscous version of the equation and approach the zero viscosity limit. In fact, equivalence between both methods has been proven.

$$u(x,t) = \lim_{\varepsilon \to 0} u_\varepsilon(x,t)$$

for

$$\frac{\partial u_\varepsilon}{\partial t} + u_\varepsilon \frac{\partial u_\varepsilon}{\partial x} = \varepsilon \frac{\partial^2 u_\varepsilon}{\partial x^2}.$$

Burgers solution for Classical Riemann problem is:

- if $u^L > u^R$

$$u(x,t) = \left\{ \begin{array}{ll} u^L & \text{if } x - St < 0 \\ u^R & \text{if } x - St > 0 \\ S = \frac{1}{2}(u^L + u^R) & \end{array} \right\} \tag{2.29}$$

- if $u^L < u^R$

$$u(x,t) = \left\{ \begin{array}{ll} u^L & \text{if } x/t < u^L \\ x/t & \text{if } u^L < x/t < u^R \\ u^R & \text{if } x/t > u^R \end{array} \right\} \tag{2.30}$$

Hyperbolic system of equations

In the case of a hyperbolic system of equations, a similar set of Rankine-Hugoniot relations are constructed. However, it is not possible to directly solve for S_i as was done for the scalar case.

By solving the Riemann invariants, $m - 1$ differential relations are constructed using the eigenvalues (λ_i) and eigenvectors ($K^{(i)}$) of the system of m equations [141].

$$\frac{dw_1}{k_i^{(i)}} = \frac{dw_2}{k_2^{(i)}} = \cdots = \frac{dw_m}{k_m^{(i)}}.$$

An appropriate solution to the Riemann problem has been an essential step in the comprehension of flow dynamics in supersonic conditions, where shock and rarefraction waves are formed. Solutions have been validated against experimental tests, such as the well-known “Shock tube” problems. In this tests a diaphragm which initially separates two states (u^L and u^R) is removed, and flow evolution is tracked.

Higher-order Riemann problem

Recall the Classical Riemann problem as the system with two piecewise constant states on both sides of a discontinuity. Equivalently, when the Riemann problem has piecewise linear values, it is known as the *Generalized Riemann Problem*. Whereas extension to fully nonlinear initial conditions is known as the *Derivative Riemann Problem* (*DRP*). Figure 2.4 illustrates the last two situations.

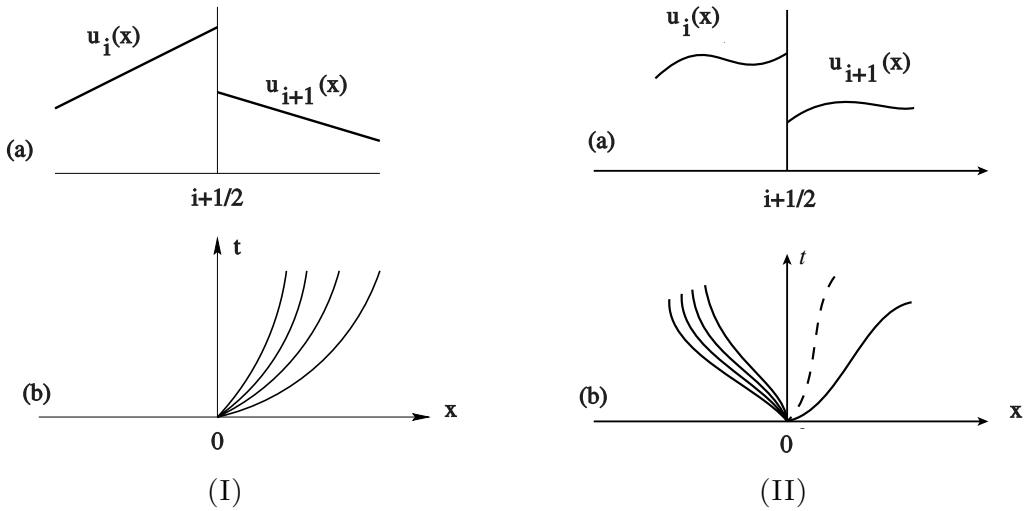

FIGURE 2.4: (I) Classical *GRP* problem (piecewise linear) and (II) *DRP* problem. Sources [25] and [141] with modifications.

The notation DRP_k is used to refer to the problem where space derivatives of order higher than k are zero. Hereafter, one can simply refer to the Classical Riemann problem as the DRP_0, since derivatives of order 1 are zero. Similarly, Generalized Riemann problems are represented by DRP_1.

In the previous section, analytical studies for DRP_0 were given, and explicit solutions for the Burgers' equation provided. Solutions to the Euler equations can also be found in literature [108]. And even solutions for Navier-Stokes equations [141]. But finding analytical solutions to DRP_1 problems is much more complicated. Finally, no relevant solution exists for higher-order problems (DRP_k). In fact, most of the finite volume schemes use solutions to the Classical Riemann problem. In this thesis, we will review the ADER family of numerical schemes, which are designed to numerically solve DRP_k problems.

2.3 Computational aeroacoustics

As introduced at the beginning of this chapter, many computational difficulties exist around acoustic simulations despite physics are well understood. Numerical techniques are found in two main CAA families: *Direct Noise Simulation* and *Hybrid Methods*.

Direct Noise Simulation (DNS) is the most straightforward since it directly simulates the flow using compressible governing equations, from which acoustic information is directly extracted. It requires no mathematical modeling for the acoustic part, but some turbulence or other physical properties may be modeled. DNS also stands for *Direct Numerical Simulation* in the CFD community. In that context turbulence is fully resolved, not modeled. In principle, common CFD methods could be applied for DNS. In practice, results obtained by traditional methods are very poor, since the stabilizing excess of numerical dissipation tends to smear off an already low energy content acoustic wave. Moreover, many numerical schemes are devoted to dump "spurious" acoustic waves. Hence, DNS methods use high-order schemes to capture the tiny acoustic waves, becoming extremely expensive simulations. Despite the huge cost, modest Reynolds number problems can be studied for sufficiently high Mach number flows, including the transonic regime. Higher Mach number is associated with bigger acoustic amplitudes and better conditioning number. DNS simulations can provide a validation benchmark and help understanding complex physics since no acoustic assumptions are done. This was the case of screech tones in a supersonic jet studied by Manning [103]. He found waves were emanating from the interaction between shear-layers and a jet-trapped wave-system. Other problems such as jet problems [64, 63], cavity flows [127] or vortex rings [121] have been computed using DNS.

For low Mach number problems DNS is not well suited due to the equation stiffness and small acoustic wave amplitudes. Hybrid methods are used instead, splitting aerodynamic and acoustic fields in two steps [42, 46]. In the first step, the aerodynamic field is obtained and injected into the acoustic simulation, which is solved in the second step. The splitting will cause flow-acoustic interactions to be lost, although some modifications can be done to partially recover them. For example, Lilley successfully modified Lighthill's equation to include jet convection effects [98]. On the other hand, the uncoupling allows using tailored solvers for each step. This way, little or no modifications are needed

for already existing aerodynamic codes, and specific high-order methods can be developed for the acoustic part. Nevertheless, high-order methods are also employed for the aerodynamic part, as noise creation and propagation is very sensitive to it. Additionally, different grids are used for each part. Acoustic grids do not include boundary layers because they are acoustically stable and do not emanate sound. They are also coarser than aerodynamic grids since wavelengths are typically larger than the turbulent structures.

Generally hybrid methods are the appropriate tool for industrial environments, where fast production cycles and low computational resources are simulation constraints. Particularly if they work under low Mach number conditions.

2.3.1 Hybrid methods

Hybrid methods are obtained from *flow decomposition* or *acoustic analogy* methods. Flow decomposition methods provide mathematical operations to extract the "disturbance" from the "mean" flow field. Different decompositions lead to different methods, such as the viscous/acoustic splitting, linearized Euler, and acoustic perturbation methods. Acoustic analogy, on the other side, rearranges the full Navier-Stokes equations to construct an inhomogeneous wave equation for pressure or density. The inhomogeneous part is moved to the right-hand side of the equation, and they are known as *acoustic sources*. Classically, this method requires all acoustic sources to be included in the *acoustic near-field* or *source region*, and the listener to be located in a quiescent *far-field*. These methods are often used in external aeroacoustic problems.

2.3.2 Acoustic analogy

Based on the rearrangement of the Navier-Stokes terms, the full physical meaning of the governing equations is kept in this analogy. As mentioned, wave propagation is represented by a wave operator, whereas all inhomogeneous "acoustic sources" on the right-hand side provide the noise creation mechanisms. Sound sources can be obtained by experimental testing, modeling, or by CFD simulations. In any case, an accurate representation of sound sources is critical for the analogy.

Lighthill came up with this methodology in 1952 [96]. His formulation was limited to unbounded domains, a difficulty that was solved in the following decades by authors such as Curle, or Ffowcs Williams and Hawkings [46].

Curle added immersed static walls to the flow field in the mid-fifties [43], a method that was further extended by Ffowcs Williams and Hawkings [148] by considering solid surfaces in motion. Up to these days, this is one of the most cited articles in CAA.

Lighthill's acoustic analogy

Starting from the conservative form of the compressible Navier-Stokes equations (2.1), take the time derivative of the continuity equation

$$\frac{\partial}{\partial x_i}\left(\frac{\partial \rho u_i}{\partial t}\right) = \frac{\partial^2 \rho}{\partial t^2}, \tag{2.31}$$

and the divergence of the momentum equation

$$\frac{\partial}{\partial x_i}\left(\frac{\partial \rho u_i}{\partial t}\right) = \frac{\partial^2}{\partial x_j\, \partial x_i}\left(\rho u_i u_j + p\delta_{ij} - \tau_{ij}\right). \tag{2.32}$$

For incompressible flows with homogeneous density initial conditions, divergences $\partial_{x_i} u_i$ and $\partial_{x_i} \rho u_i$ are zero. And from nondimensional analysis, they are expected to be small for low Mach number flows. Despite all, it turns out $\partial_{x_i}(\partial_t \rho u_i)$ cannot be neglected and that noise strongly depends on its measure. Lighthill proposed combining equations (2.31) and (2.32) to obtain,

$$\frac{\partial^2 \rho}{\partial t^2} - \frac{\partial^2 p}{\partial x_i^2} = \frac{\partial^2}{\partial x_i\, \partial x_j}\left(\rho v_i v_j - \tau_{ij}\right).$$

subtracting $c_\infty^2 \partial^2_{x_i^2} \rho$ from both sides we derive Lighthill's final form.

$$\frac{\partial^2 \rho}{\partial t^2} - c_\infty^2 \frac{\partial^2 \rho}{\partial x_i^2} = \frac{\partial^2 T_{ij}}{\partial x_i\, \partial x_j} \tag{2.33}$$

Where c_∞ is the speed of sound at listeners location (far-field). And T_{ij} is the second-order *Lighthill's stress tensor*

$$T_{ij} = \rho v_i v_j + \left(p - \rho c_\infty^2\right)\delta_{ij} - \tau_{ij}.$$

This tensor is composed of a nonlinear convective terms $\rho u_i u_j$ that reminds of the Reynolds stress tensor, a term that measures the deviation from the isotropic condition by means of equation (2.2), and the viscous effects which are generally negligible. Acoustic generation and phenomena such as refraction, diffraction,

and scattering are included in this tensor. It behaves as a quadrupole type source.

Lighthill provided the integral solution to his equation for an unbounded flow,

$$(\rho - \rho_\infty)(x,t) = \frac{1}{4\pi c_\infty^2} \frac{\partial^2}{\partial x_i \partial x_j} \int_\Omega T_{ij} \frac{1}{|x-y|} dy \tag{2.34}$$

In this equation, (x,t) represents the observer spatial and time coordinates. Whereas (y,τ) are the coordinates for sound emission. Both time variables are related by $\tau = t - |x-y|/c_\infty$, which is the time required for the wave to travel from y to x. τ is thus called the "retarded time".

When listeners position x is far enough, the solution in (2.34) can be simplified to,

$$(\rho - \rho_\infty)(\mathbf{x},t) = \frac{1}{4\pi c_\infty^2 x} \int_\Omega \frac{\partial^2 T_{ij}^{xx}(y,\tau)}{\partial \tau^2} dy. \tag{2.35}$$

In this case, T_{ij}^{xx} denotes the stress tensor in the direction given by the vector x to y.

When wall boundaries are present in the simulation, Lighthill's analogy cannot be used, and a more advanced acoustic analogy is required.

The most common choice is the Ffowcs Williams-Hawkings approach (FW-H) [107, 147, 23, 47], although other analogies exist in the literature. A detailed description of the formulation is given by [61, 67]. FW-H formulation has other additional benefits. First of all, only surface integrals are necessary. Additionally, the so-called permeable or open boundaries can be used, accounting for the exiting fluid structures noise contribution. Both conditions allow faster algorithms in smaller domains, yielding faster and cheaper computations.

Solutions to Lighthill's equation (2.33) and for FW-H can be constructed via Green's functions. Many aeroacoustic codes use this approach since it reduces computational time and numerical errors. For simple domains analytically solutions can be obtained. Unfortunately, for non-trivial domains, Green's function must be numerically obtained.

2.3.3 Flow decomposition methods

Flow decomposition methods consider sound as a *disturbance* around a *nominal* or *base* flow-field. Mathematically speaking, a perturbation (commonly

linearization) is performed. All decomposition formulations available in literature have a perturbed and a mean flow part. Typical methods are *nonlinear disturbance equations*, *acoustic/viscous splitting*, *linearized Euler equations* and *acoustic perturbation equations*. All these methods are based on a linearization of the base flow.

NLDE

Nonlinear disturbance equations (NLDE) are probably the most general linearization decomposition.

$$\begin{aligned}
\rho &= \overline{\rho} + \rho' \\
\rho u_i &= \overline{\rho u_i} + \rho' \overline{u}_i + \overline{\rho} u_i' \\
\rho E &= \overline{\rho E} + \rho' \overline{E} + \overline{\rho} E'
\end{aligned}$$

Overbar terms denote averaged quantities, and primed terms perturbations. After substitution in the Navier-Stokes equations (2.1), and assuming no heat convection ($r_j = 0$), the following system is obtained,

$$\frac{\partial Q'}{\partial t} + \frac{\partial F_j'}{\partial x_j} + \frac{\partial \tilde{F}_j'}{\partial x_j} = \overline{S}_j + S_j' - \frac{\partial \overline{Q}}{\partial t} - \frac{\partial \overline{F_j}}{\partial x_j} \tag{2.36}$$

$$Q' = \begin{cases} \rho' \\ \rho' \overline{u}_i + \overline{\rho} u_i' \\ \rho' \overline{E} + \overline{\rho} E' \end{cases}$$

$$F_j' = \begin{cases} \overline{\rho} u_i' + \rho' \overline{u}_i \\ \rho' \overline{u}_i \overline{u}_j + \overline{\rho}\, \overline{u}_i u_j' + \overline{\rho}\, \overline{u}_j u_i' + p' \delta_{ij} - \tau_{ij}' \\ u_i' (\overline{e} + \overline{p}) + \overline{u}_i (e' + p') - (u_k' \overline{\tau}_{ki}' + \overline{u}_k \tau_{ki}') \end{cases}$$

$$\tilde{F_j}' = \begin{cases} \rho' u_i' \\ \rho' u_i' \overline{u}_j + \overline{\rho} u_i' u_j' + \rho' u_i' u_j' \\ u_i' (e' + p') \end{cases}$$

$$\overline{F}_j' = \begin{cases} \overline{\rho}\, \overline{u}_i \\ \overline{\rho}\, \overline{u}^2 + \overline{p} - \overline{\tau}_{ji} \\ \overline{u}_i (\overline{p} + \overline{e}) - \overline{u}_k \overline{\tau}_{ki} \end{cases}$$

$$\overline{Q} = \begin{cases} \overline{\rho} \\ \overline{\rho u_i} \\ \overline{\rho E} \end{cases}$$

Primed flux F_j' is composed of linear perturbation terms, $\tilde{F_j}'$ contains non-linear terms while $\overline{F_j}$ represents averaged values. $\overline{Q}$ represent mean conservative variables and Q' the perturbation part. Source terms are treated accordingly. As a matter of facts, if time-averaging is applied to NLDE equations the Reynolds Averaged Navier-Stokes equations (RANS) are recovered.

The use of NLDE equations in aeroacoustics was first introduced by Morris [113]. He included a further variable decomposition to include subgrid scales in the form of a Smagorinsky LES model. His methodology consisted of an initial RANS simulation using $k - \epsilon$ turbulence modeling, from which mean flow quantities were extracted into a coarser acoustic mesh, better suited for DRP scheme wave propagation. Morris pointed out his methodology faced some difficulties to deal with high amplitude unsteady perturbations, in which case the method might fail. In a similar work by Batten [13], some acoustic intensities were predicted on several geometries using the *nonlinear acoustic solver* (NLAS). As for Morris, the first step consisted of a RANS simulation. However, in NLAS method the sub-grid scales are not solved as LES, but eddies are constructed through synthetic turbulence from available fine RANS statistical information. Reconstruction is done from well-known turbulence models itself, and values are introduced in the computation of the flux terms. Then acoustic source information is interpolated to the coarser acoustic grid, and acoustic field is solved. For both NLDE and NLAS solvers, explicit time stepping methods for the acoustic part are very popular. As opposite to the acoustic analogy, since the full Navier-Stokes is being solved, the interaction between acoustic and aerodynamic fields are included.

LEE

For very small perturbations, the use of linearization is enough to capture acoustic waves. For this case equation (2.36) is simplified by removing all non-linear terms.

Additionally, if averaged terms are assumed to satisfy the "averaged governing equations"

$$\frac{\partial \overline{Q}}{\partial t} + \frac{\partial \overline{F}_j}{\partial x_j} = \overline{S}_j \tag{2.37}$$

Then NLDE are simplified to the linearized Navier-Stokes equations.

$$\frac{\partial Q'}{\partial t} + \frac{\partial F'_j}{\partial x_j} = S'. \tag{2.38}$$

Recall,

$$Q' = \begin{cases} \rho' \\ \rho' \overline{u}_i + \overline{\rho} u'_i \\ \rho' \overline{E} + \overline{\rho} E' \end{cases}$$

$$F'_j = \begin{cases} \overline{\rho} u'_i + \rho' \overline{u}_i \\ \rho' \overline{u}_i \overline{u}_j + \overline{\rho}\, \overline{u}_i u'_j + \overline{\rho}\, \overline{u}_j u'_i + p' \delta_{ij} - \tau'_{ij} \\ u'_i \left(\overline{e} + \overline{p}\right) + \overline{u}_i \left(e' + p'\right) - \left(u'_k \overline{\tau}'_{ki} + \overline{u}_k \tau'_{ki}\right) \end{cases}$$

Condition (2.37) is particularly true if averaged terms are obtained from a steady RANS simulation.

Finally, linearized Euler equations are obtained if viscous term contributions are neglected, $\tau_{ij} = 0$.

The equivalent primitive variables system can be obtained with $W = (\rho, u_i, p)$ and assuming isentropic gas,

$$\frac{\partial W'}{\partial t} + \overline{\mathcal{A}}_j \frac{\partial W'}{\partial x_j} + \mathcal{A}'_j \frac{\partial \overline{W}}{\partial x_j} = \mathbb{S}'$$

$$\overline{\mathcal{A}}_j = \begin{pmatrix} \overline{u}_j & \delta_{1j}\overline{\rho} & \delta_{2j}\overline{\rho} & \delta_{3j}\overline{\rho} & 0 \\ 0 & \overline{u}_j & 0 & 0 & \frac{\delta_{1j}}{\overline{\rho}} \\ 0 & 0 & \overline{u}_j & 0 & \frac{\delta_{2j}}{\overline{\rho}} \\ 0 & 0 & 0 & \overline{u}_j & \frac{\delta_{3j}}{\overline{\rho}} \\ 0 & \gamma\delta_{1j}\overline{p} & \gamma\delta_{2j}\overline{p} & \gamma\delta_{1j}\overline{p} & \overline{u}_j \end{pmatrix}$$

$$\mathcal{A}'_j = \begin{pmatrix} u'_j & \delta_{1j}\rho' & \delta_{2j}\rho' & \delta_{3j}\rho' & 0 \\ 0 & u'_j & 0 & 0 & -\delta_{1j}\frac{\rho'}{\overline{\rho}^2} \\ 0 & 0 & u'_j & 0 & -\delta_{2j}\frac{\rho'}{\overline{\rho}^2} \\ 0 & 0 & 0 & u'_j & -\delta_{3j}\frac{\rho'}{\overline{\rho}^2} \\ 0 & \gamma\delta_{1j}p' & \gamma\delta_{2j}p' & \gamma\delta_{1j}p' & u'_j \end{pmatrix}.$$

As before, overbar denotes exclusive dependency to mean flow values, whereas a prime means evaluation using perturbed variables. Assuming small perturbations and smooth enough mean values, the product $\mathcal{A}'$ with the gradient of the mean flow are negligible, getting the approximated solution,

$$\frac{\partial W'}{\partial t} + \overline{\mathcal{A}}_j \frac{\partial W'}{\partial x_j} = \mathbb{S}' \tag{2.39}$$

Numerical instabilities

LEE equations can be solved using numerically cheap and efficient methods. Unfortunately, it is well-known that some instabilities might arise which cannot be dumped since no viscous or nonlinear mechanisms are contained in the LEE equations. Thus, instabilities tend to grow and cause the simulation to fail, or at least pollute acoustic results.

Instabilities can be studied from perturbation theory using the linearized Navier-Stokes equations, as with the Riemann invariants. For a one-dimensional problem three waves are emanated: *acoustic*, *entropic* and *vorticity* waves, also known as *modes* in the dedicated analysis by Chu [32]. An eigenvalue decomposition reveals acoustic waves propagate at the speed of sound, whereas vorticity and entropic waves are convected at the flow speed. It is the interaction between acoustic and vorticity modes what causes the first to grow unbounded during a simulation. More precisely, it is the gradient of the vorticity mean flow what causes the instability [18]. Consequently, instabilities are typically encountered in shear flows, where gradients are strong.

Significant research efforts were dedicated to understand and stabilize LEE simulations. Some authors included nonlinear terms to add damping mechanisms to the system [100]. However, this strategy increases the cost and complexity of the numerical method. A more popular approach is to reduce the convection operator by removing the mean flow gradient effects. Although this solution does, in fact, limit the vorticity mode amplification, it does not completely remove it, and instabilities still occur in strong shear-flows. Another type of stabilization for the LEE equations is by solving the frequency domain problem [5]. Nevertheless, note this method requires "direct solvers" since iteration methods still excite the vortical instability. Some formulations further stabilize the simulation by completely removing the vorticity mode from the solution, and filtering source terms to keep only acoustic mode exciting terms. *Acoustic perturbation equations* (APE) [57, 59] and *linearized perturbed compressible*

equations (LPCE) [132] are the most known methods. With this formulation the problem is transformed into a Poisson equation.

Acoustic sources

LEE formulation can be transformed into a wave type equation. Starting from the conservation form (2.38), subtract to time-derived continuity equation the divergence of the momentum equation,

$$\frac{\partial^2 \rho'}{\partial t^2} - \frac{\partial^2}{\partial x_i \partial x_j}\left(\widehat{(\rho u_i u_j)}' + p'\delta_{ij}\right) = \frac{\partial S'_m}{\partial t} - \frac{\partial S'_i}{\partial x_i}.$$
$$\widehat{(\rho u_i u_j)}' = \overline{\rho}\,\bar{u}_i\,u'_j + \bar{\rho}\,u'_i\,\overline{u}_j + \rho'\,\bar{u}_i\,\bar{u}_j$$

Then subtracting

$$c_\infty^2 \frac{\partial^2 \rho'}{\partial x_i \partial x_i}$$

from both sides, the wave equation for density is obtained,

$$\frac{\partial^2 \rho'}{\partial t^2} - c_\infty^2 \frac{\partial^2 \rho'}{\partial x_i \partial x_i} = \frac{\partial^2}{\partial x_i \partial x_j}\left(\widehat{(\rho u_i u_j)}' + (p' - c_\infty^2 \rho')\delta_{ij}\right) = \frac{\partial S'_m}{\partial t} - \frac{\partial S'_i}{\partial x_i}.$$

where c_∞ is the speed of sound at listener's location.

Obtained wave equation has a clear resemblance with Lighthill's equation (2.33), although in this development velocity momentum terms (gathered under a wide hat) are composed of linear perturbation products, whereas Lighthill's equation contains full nonlinear terms. In fact, conservation of meaningful physical properties during linearization is desired, including main flow features such as turbulence effects. This is not always satisfied since dropped perturbations might be necessary. In such case, those extra terms can be kept as source-terms. In a well-known case by Bailly [10], he decomposed linear perturbations into acoustic and turbulent contributions $Q' = Q'_{ac} + Q'_{tur}$, and then he included the turbulent-turbulent interactions rising in the NLDE process, S_i^+. Those terms are found to be very strong in shear-flow problems. Indeed, one can recover Lilley's wave equation adding this term, which is a very popular formulation in sheared flows, such as jet simulation.

$$S_i^+ = -u'_{tur_i}\frac{\partial u'_{tur_j}}{\partial x_i} + \overline{u}'_{tur_i}\frac{\partial u'_{tur_j}}{\partial x_i}.$$

Bailly was able to reconstruct the turbulent terms Q'_{tur} from RANS simulations, using synthetic turbulence techniques.

Finally, Billson [16] gathered in the source terms the full nonlinear Euler equations. He then proposed different simplifications for each appropriate type of flow condition.

Acoustic/viscous splitting

The Acoustic/viscous Splitting method was initiated by Hardin and Pope [76], with low Mach number applications in mind. Here sound radiation can be seen as an expansion around an (inviscid) incompressible flow. Therefore, the following flow decomposition is performed,

$$\begin{aligned} u_i &= U_i + u'_i \\ p &= P + p' \\ \rho &= \rho_0 + \rho_1 + \rho' \end{aligned} \tag{2.40}$$

where U_i, P and ρ_0 are respectively the incompressible velocity, pressure and density. u'_i, p' and ρ' are the acoustic perturbations. Whereas ρ_1 is the "incompressibility correction", which includes low Mach number compressibility effects, much bigger than the tiny acoustic waves. Although incompressible values are obtained from incompressible simulations, the decomposition is done for compressible flows, and hydrodynamic pressure corrections are computed assuming isentropic compression,

$$c^2\rho_1 = P - \lim_{T\to\infty} \frac{1}{T} \int_0^T P\, dt \tag{2.41}$$

Introducing system (2.40) into the compressible Navier-Stokes equations and subtracting the incompressible ones, the following first-order nonlinear-equations are yielded.

$$\begin{aligned} &\frac{\partial \rho'}{\partial t} + \frac{\partial f_i}{\partial x_i} = -\frac{\partial \rho_1}{\partial t} - U_i \frac{\partial \rho_1}{\partial x_i} \\ &\frac{\partial f_i}{\partial t} + \frac{\partial}{\partial x_j}\left[f_i\left(U_j + u'_j\right) + \left(\rho_0 + \rho_1\right) U_i u'_j + p'\delta_{ij}\right] = \\ &\qquad\qquad - \frac{\partial\left(\rho_1 U_i\right)}{\partial t} - U_j \frac{\partial\left(\rho_1 U_i\right)}{\partial x_j} \end{aligned} \tag{2.42}$$

where,

$$f_i = (\rho_0 + \rho_1)u_i' + \rho' \left(U_i + u_i'\right)$$

In summary, to compute an acoustic/viscous splitting the procedure requires first to obtain an incompressible simulation, on which the compressibility corrections are based. Finally, we obtain the acoustic field by solving the system (2.42) [58].

2.3.4 Extension to the far-field

Expensive numerical schemes and required grid refinement make the computation of sound sources very demanding for both direct and hybrid methods. Additionally, for direct methods, acoustic wave propagation might inadequately limit the overall simulation timestep, due to problems in scale differences as explained in the introduction and referenced by Tam [135].

In order to optimize costs, the use of *extension to far-field* methods can be employed [42]. The main idea is the limitation of expensive methods to reduced spatial subdomains (also known in this context as near-field), while extending the information to the rest of the domain (far-field) with lower cost algorithms. Two main techniques can be distinguished: extension of information into the whole far-field, or a point-wise calculation.

In the full far-field extension, cost reduction is achieved by using simpler governing equations and numerical schemes. For example, wave equation or LEE formulations. URANS methods are also possible for large eddies tracking. This was the case in the work by Quéméré and Sagaut [119, 144]. A common approach in the frequency domain is using Helmholtz equation in the far-field, which can be combined with a near-field time domain solution. With the new governing equations and conditions, timestep and grid spacing modifications should be studied. In which case, a correct near-field to far-field information transfer should be guaranteed through a domain "interface"; good interpolation methods are indispensable.

In the point-wise information extension, solutions are constructed by exploiting the analytical nature of the wave equation [42], in a principle similar to Lighthill's original work. Acoustic information in the far-field location is computed with Ffowcs Williams and Hawkings [149] or Kirchhoff equation [60], with

information from the near-field. Since no far-field grid is necessary, Boundary Element Method techniques are often used.

Finally, combinations of the previous ideas are possible. For example, LES simulation can be used in a near-field, whose modes can be propagated through a middle-field LEE extension, and acoustic data is then computed in the far-field using Kirchhoff equation.

2.4 Numerical methods

In literature, a plethora of numerical methods for fluid dynamics can be found, from which most popular schemes usually share good *high performance computing* (HPC) scaling properties, are robust to errors, and are simple to implement. Those qualities can be checked "a posteriori", but are vague enough to be impractical during new algorithm design. However, satisfying the following better-defined properties, the outcome usually leads into the same results.

- **Locality:** Keeping a small stencil, the number of cells involved in a computation is reduced and intercell communication is minimized. Accordingly, parallelization is improved by reducing the exchanged multiprocessor data.

- **Geometric flexibility:** The numerical method can run in unstructured complex geometries, and even in low "condition number" cells. By reducing mesh quality, the user meshing effort is simplified.

- **Adaptivity:** A method has adaptive properties when it modifies to some local needs. For example, if a solution develops a discontinuity, involved cells will adapt and employ limiters, stability preserving time-stepping, or apply cell subdivision. Adaptivity is a useful approach to optimize solvers cost to accuracy ratio.

- **Stability:** A method is stable when round-off errors are not amplified, and the solution stays the same under small initial conditions perturbations. The need for strong stability is especially beneficial for large industrial problems, where simulation breakdowns cause time and monetary losses. Furthermore, some time-constrained projects will trade-off accuracy for successfully obtaining a solution.

The finite volume method satisfies the previous conditions, and is, in fact, the most popular method for low-order aerodynamic simulations at an industrial level. Nevertheless, FV becomes less popular as a higher than second-order method, mainly because of its longer stencil use, loosing its locality, and hindering the geometric flexibility and parallelization.

For higher-order methods alternative schemes such as compact schemes, discontinuous Galerkin, flux reconstruction, or spectral techniques are more common; being discontinuous Galerkin (DG) one of the most popular. Most of these methods solve nonlinear systems of conservation laws employing solutions to the Riemann problem, being Godunov the pioneer who gave the first solution to a hyperbolic nonlinear system [68].

One of the most important characteristics of the first-order Godunov method is the preservation of *monotonicity*, a property essential to guarantee no artificial oscillations are formed around discontinuities. Godunov also demonstrated the following theorem: "a scheme that is linear and monotone, is at most first-order accurate". A theorem that is the founding pillar of higher-order schemes. First-order accuracy limitation is overcome by introducing constraints and nonlinearities into the interpolation, with the consequent monotonicity loss. Hence, other stability measures are employed, such as *Total Variation Diminishing* (TVD). TVD methods control the "variation" of reconstructed polynomial derivatives, such that the oscillations do never increase. Its theoretical background is only developed for one-dimensional homogeneous scalar equations, being second-order accurate at maximum when extended to multidimensional domains [24].

Many spatial reconstruction schemes are used in FV and FD methods. It is especially worth mentioning the ENO/WENO family, very popular today. ENO methods perform multiple reconstructions with different stencils, from which the smoothest one is taken as the final solution. ENO schemes are *Total Variation Bounded* (TVB), a stability condition weaker than the TVD property. WENO is a "weighted" combination of ENO polynomials.

Classically, temporal discretization is performed after spatial discretization. With Runge-Kutta (RK) being the most successful scheme for high-order time integration, benefiting from simple and convenient evaluations over several stages. However, it requires high storage values to save all intermediate stages, especially for methods of order higher than four, where the number of required coefficients grow exponentially. In order to reduce storage, "low-storage Runge-Kutta" schemes were designed. Another drawback of the RK method is the

lack of order adaptivity; one cannot easily change the order of integration for a unique cell without restarting the step.

At the beginning of this century, an alternative approach for high-order methods was developed by Toro: ADER family of methods [140]. Here, the Cauchy-Kowalewski procedure is used to solve higher-order Riemann problems, a procedure by which time derivatives are converted into spatial derivatives using the original PDE. ADER schemes belong to the multiderivative category, such as Taylor derivatives. Multiderivative methods are not popular strategies in the CFD community since they fast become overwhelming calculations for the multidimensional Navier-Stokes equation. However, as will be proven during this thesis, using Adomian method they are drastically simplified.

2.4.1 Finite volume

From the hyperbolic conservative PDE in equation (2.20), perform a spatial and temporal integration, and apply the Gauss divergence theorem to obtain,

$$\int_{i-1/2}^{i+1/2} u(x,t^{n+1})\,dx = \int_{i-1/2}^{i+1/2} u(x,t^{n})\,dx - \int_{t^n}^{t^{n+1}} f(x_{i-\frac{1}{2}},t)\,dt + \int_{t^n}^{t^{n+1}} f(x_{i+\frac{1}{2}},t)\,dt. \tag{2.43}$$

Given cell i in figure 2.5, define $\tilde{u}_i$ as the average of $u(x,t)$ over the entire cell,

$$\tilde{u}_i = \frac{1}{\Delta x}\int_{x_{i-\frac{1}{2}}}^{x_{i+\frac{1}{2}}} u(x,t)\,dx.$$

It can be proven $\tilde{u}_i$ is a second-order approximation to $u(x_i,t)$: $\tilde{u}_i = u(x_i,t) + \mathcal{O}(\Delta x^2)$. Therefore, it is often depicted in the center of the averaged cell. Injecting $\tilde{u}_i$ into equation (2.43), it simplifies to,

$$\tilde{u}_i^{n+1} = \tilde{u}_i^{n} + \frac{1}{\Delta x}\left(\tilde{f}_{i-\frac{1}{2}} - \tilde{f}_{i+\frac{1}{2}}\right) \tag{2.44}$$

with

$$\tilde{f}_{i+\frac{1}{2}} = \int_{t^n}^{t^{n+1}} f(u(x_{i+\frac{1}{2}},t))\,dt \qquad \tilde{f}_{i-\frac{1}{2}} = \int_{t^n}^{t^{n+1}} f(u(x_{i-\frac{1}{2}},t))\,dt$$

Since each $f_{i\pm1/1}$ is used in its corresponding left and right cells, the sum of all $\tilde{u}_i$ is conserved in time (except boundary conditions) from telescopic effects.

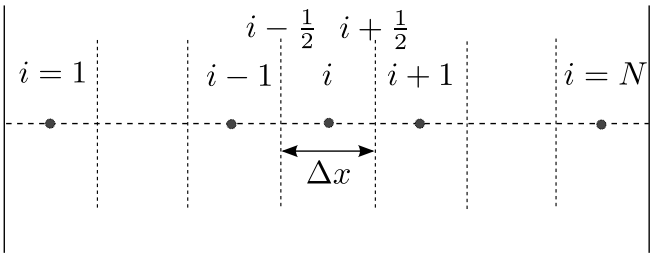

FIGURE 2.5: 1D mesh representation

This is a very desired property which keeps the system mass, momentum, and energy constant. The method is said to be *conservation preserving*.

The main problem in finite volume methods is the evaluation of the flux at the cell boundaries, $\tilde{f}_{i\pm\frac{1}{2}}$. Other properties as maximal relation preserving, or mentioned TVD methods, can also be achieved through appropriate flux manipulations. The same principle holds for multidimensional unstructured, although the flux evaluation becomes much more elaborated.

In the last decade, interest in higher-order methods has increased for high-accuracy demanding applications, since it is known to be more efficient than the use of finer grids and shorter timesteps with low-order schemes, for which the following difficulties arise. First of all, more FLOPS are needed to achieve the same accuracy levels. Data storage is also increased, especially if multiple timesteps are saved. Using explicit schemes might not be possible since strong mesh refinements will induce too severe timestep reductions. Hence, implicit schemes are forced even if explicit schemes are very well suited for high-accuracy needs. With the intense research in high-order methods, classical Riemann techniques have been extended in both space and time. Although (mixed) simultaneous space and time discretization can be done, more often the spatial discretization is applied first and temporal discretization to a set of ODEs later. In the following section the ADER type of time integration method is studied.

2.4.2 ADER solver

ODE integration can be divided into three classical categories. The multi-step family, where previously computed timesteps are used to construct higher-order results, such as the well-known Rosenbrock methods. Multistage schemes, based on a similar idea, compute intermediate stages within each timestep and constructs higher-order solutions using an appropriate weight combination of

the stages. In this group belongs the outstanding Runge-Kutta method. Finally, the Multiderivative schemes use higher-order derivatives, as in a Taylor expansion, to construct a higher-order extrapolation. In the PDE community, they are also known as Lax-Wendroff type, after Peter lax and Burton Wendroff, who first used a second-order time expansion. No big contributions in this family of methods were made until the last decade, probably due to the difficulty of expanding higher-order time derivatives for nonlinear PDEs, or even worse, for a system. This approach is neither well suited for eigendecomposition methods used in stabilization, such as in flux difference schemes [131]. Seal has recently proposed using a mixed multiderivative-multistage approach (potentially multiderivative Runge-Kutta methods) to build more efficient higher-order schemes [131], although he limits the numerical study to second-order multiderivative approximations. Therefore, no higher than second-order multiderivative methods have been successful.

Recently, Toro has introduced a new multiderivative approach known as ADER [110, 140]. As a multiderivative method, the solution is expanded in a series expansion. Take the following Taylor (Lax-Wendroff) expansion,

$$u(t) = u(0) + \sum_{k=1}^{K} \left[\frac{\partial^k}{\partial t^k} u(0) \right] \frac{t^k}{k!}. \tag{2.45}$$

Where each of the high-order time derivatives are obtained by the Cauchy-Kowalewski procedure.

Cauchy-Kowalewski procedure

Cauchy-Kowalewski is the procedure by which PDE time derivatives are expressed in terms of spatial derivatives. For example, consider the viscous Burgers' equation

$$\frac{\partial u}{\partial t} = u \frac{\partial u}{\partial x} + \frac{\partial^2 u}{\partial x^2}. \tag{2.46}$$

After computing time derivatives on both sides, the right-hand side time derivative is replaced with the original PDE, obtaining the second-order time-derivative,

$$\begin{aligned}\frac{\partial^2 u}{\partial t^2} &= \frac{\partial}{\partial t}\left(u\frac{\partial u}{\partial x}\right) + \frac{\partial}{\partial t}\frac{\partial^2 u}{\partial x^2} \\ &= \left(\frac{\partial u}{\partial x}\frac{\partial u}{\partial t} + \frac{\partial u}{\partial x}\frac{\partial^2 u}{\partial t\,\partial x}\right) + \frac{\partial^3 u}{\partial t\,\partial x^2} \\ &= u^2\frac{\partial^2 u}{\partial x^2} + u\frac{\partial u}{\partial x}\frac{\partial^2 u}{\partial x^2} + 2u\left(\left(\frac{\partial u}{\partial x}\right)^2 + \frac{\partial^3 u}{\partial x^3}\right) + \frac{\partial^4 u}{\partial x^4}.\end{aligned} \tag{2.47}$$

With the same procedure, third-order time-derivative is obtained,

$$\begin{aligned}\frac{\partial^3 u}{\partial t^3} = 18\left(\frac{\partial u}{\partial x}\right)^2\frac{\partial^2 u}{\partial x^2} + u^3\frac{\partial^3 u}{\partial x^3} + 16\frac{\partial^2}{\partial x^2}\frac{\partial^3 u}{\partial x^3} + 9\frac{\partial u}{\partial x}\frac{\partial^4 u}{\partial x^4} \\ + 3u^2\left(3\frac{\partial u}{\partial x}\frac{\partial^2 u}{\partial x^2} + \frac{\partial^4 u}{\partial x^4}\right) + 3u\left(2\left(\frac{\partial u}{\partial x}\right)^3\right. \\ \left. +4\left(\frac{\partial^2 u}{\partial x^2}\right)^2 + 6\frac{\partial u}{\partial x}\frac{\partial^3 u}{\partial x^3} + \frac{\partial^5 u}{\partial x^5}\right) + \frac{\partial^6 u}{\partial x^6}\end{aligned} \tag{2.48}$$

Cauchy-Kowalewski can be extended to any arbitrary order It is observed the third-order derivative is an already cumbersome expression, becoming intractable for higher-orders [150]. The expression gets more complicated for multi-spatial and multidimensional problems. Additionally, higher spatial-derivatives appear, requiring long stencils with appropriate interpolation functions and making the implementation more elaborated, especially in unstructured grids. This operation is well defined only for smooth initial conditions away from the interface.

Montecinos [112] performed some tests on several ADER schemes. In the following section two methods are explained: TT and HEOC methods [140, 142, 24, 112].

I. Toro and Titarev (TT)

Toro and Titarev used the series (2.45) to compute the evolution at the flux point $x_{i+1/2}$ [142].

$$u_{i+\frac{1}{2}}(t) = u_{i+\frac{1}{2}}(0) + \sum_{k=1}^{K}\left[\frac{\partial^k}{\partial t^k}u_{i+\frac{1}{2}}(0)\right]\frac{t^k}{k!}. \tag{2.49}$$

The leading term is obtained solving the associated Riemann problem (or a Godunov scheme type scheme), whereas for higher-order terms Cauchy-Kowalewski procedure is used to construct the time derivatives.

1. **$\mathbf{u_{i+\frac{1}{2}}}$ leading term**

   The authors used first-order Godunov method to compute the leading term $u_{i+\frac{1}{2}}$. Using, for example, the upwind method for the Burgers' equation (recall solution is given by (2.29) and (2.30)), solution is

   - if $u^L > u^R$

   $$u_{i+\frac{1}{2}}(t) = \left\{ \begin{array}{ll} u^L & \text{if } S > 0 \\ u^R & \text{if } S < 0 \\ S = \frac{1}{2}(u^R + u^L) & \end{array} \right\} \tag{2.50}$$

   - if $u^L < u^R$

   $$u_{i+\frac{1}{2}}(t) = \left\{ \begin{array}{ll} u^L & \text{if } u^L > 0 \\ 0 & \text{if } u^L < 0 < u^R \\ u^R & \text{if } u^R < 0 \end{array} \right\} \tag{2.51}$$

2. **High-order time derivatives**

   For higher-order terms, take the original PDE in quasi-linear form,

   $$\frac{\partial u}{\partial t} + \lambda(u)\frac{\partial u}{\partial x} = 0. \tag{2.21}$$

   and perform k number of space-derivatives. The solution can be rearranged as:

   $$\frac{\partial}{\partial t}\left(\frac{\partial^k u}{\partial x^k}\right) + \lambda(u)\frac{\partial}{\partial x}\left(\frac{\partial^k u}{\partial x^k}\right) = H(u)^k. \tag{2.52}$$

   Where $H(u)^k$ includes a number of spatial derivatives. In the case of the viscous Burgers' equation (2.46),

   $$\frac{\partial^2 u}{\partial t\,\partial x} = u\frac{\partial^2 u}{\partial x^2} + \frac{\partial^3 u}{\partial x^3} + \left(\frac{\partial u}{\partial x}\right)^2 \tag{2.53}$$

   $$= u\frac{\partial^2 u}{\partial x^2} + \frac{\partial^3 u}{\partial x^3} + H_1(u) \tag{2.54}$$

$$\frac{\partial^3 u}{\partial t\,\partial x^2} = u\frac{\partial^3 u}{\partial x^3} + \frac{\partial^4 u}{\partial x^4} + 3\frac{\partial u}{\partial x}\frac{\partial^2 u}{\partial x^2} \tag{2.55}$$

$$= u\frac{\partial^3 u}{\partial x^3} + \frac{\partial^4 u}{\partial x^4} + H_2(u) \tag{2.56}$$

With this procedure a set of non-conservative governing equations are obtained for the high-order space-derivatives. Each equation will have a characteristic speed function $\lambda(u)$, or a Jacobian matrix for a system of equations. It can be easily proved the characteristic speed, or Jacobian matrix, for the higher derivatives is the same as for the original PDE.

Toro and Titarev simplified equation (2.52) by neglecting $H(u)^k$ terms and linearizing $\lambda(u)$ around a solution point, obtaining a constant coefficient $\lambda^{(0)}_{LR} = \lambda(u_{i+\frac{1}{2}}(0))$. Consequently, the set of equations are transformed into classical linear homogeneous Riemann problems,

$$\frac{\partial}{\partial t}\left(\frac{\partial^k u(x,t)}{\partial x^k}\right) + A^{(0)}_{LR}\frac{\partial}{\partial x}\left(\frac{\partial^k u(x,t)}{\partial x^k}\right) = 0.$$

$$\frac{\partial^k u(x,0)}{\partial x^k} = \begin{cases} \dfrac{\partial^k u^L(x,0)}{\partial x^k} & \text{if } \; x < 0 \\ \dfrac{\partial^k u^R(x,0)}{\partial x^k} & \text{if } \; x > 0. \end{cases}$$

whose self-similar solution is given by the solution to the advection equations in (2.23),

$$\frac{\partial^k}{\partial x^k} u_{i+\frac{1}{2}}(t) = \begin{cases} \dfrac{\partial^k}{\partial x^k} u^L & \text{if } \; 0 < A^{(0)}_{LR} \\ \dfrac{\partial^k}{\partial x^k} u^R & \text{if } \; 0 > A^{(0)}_{LR} \end{cases} \tag{2.57}$$

From those spatial derivative evolution equations, high-order time derivatives are computed with the Cauchy-Kowalewski relation,

$$
\begin{cases}
\bullet & u_{i+\frac{1}{2}}(0) = \text{equation (2.50) and (2.51) evaluated at t=0} \\
\bullet & \dfrac{\partial}{\partial t} u_{i+\frac{1}{2}}(0) = u_{i+\frac{1}{2}}(0) \dfrac{\partial u_{i+\frac{1}{2}}(0)}{\partial x} + \dfrac{\partial^2 u_{i+\frac{1}{2}}(0)}{\partial x^2} \\
\bullet & \dfrac{\partial^2}{\partial^2 t} u_{i+\frac{1}{2}}(0) = u^2_{i+\frac{1}{2}}(0) \dfrac{\partial^2 u_{i+\frac{1}{2}}(0)}{\partial x^2} + u_{i+\frac{1}{2}}(0) \dfrac{\partial u_{i+\frac{1}{2}}(0)}{\partial x} \dfrac{\partial^2 u_{i+\frac{1}{2}}(0)}{\partial x^2} \\
& \qquad +2u_{i+\frac{1}{2}}(0) \left(\left(\dfrac{\partial u_{i+\frac{1}{2}}(0)}{\partial x} \right)^2 + \dfrac{\partial^3 u_{i+\frac{1}{2}}(0)}{\partial x^3} \right) + \dfrac{\partial^4 u_{i+\frac{1}{2}}(0)}{\partial x^4} \\
\bullet & \cdots
\end{cases}
\tag{2.58}
$$

3. **solution construction**

   In the last step, the flux term $\tilde{f}$ is constructed using the series terms (2.49) and evaluations (2.58),

$$
\tilde{u}_i^{n+1} = \tilde{u}_i^n + \frac{1}{\Delta x} \left(\tilde{f}_{i-\frac{1}{2}} - \tilde{f}_{i+\frac{1}{2}} \right) \tag{2.44}
$$

   with

$$
\begin{aligned}
\tilde{f}_{i+\frac{1}{2}} &= \int_{t^n}^{t^{n+1}} f\left(u(x_{i+\frac{1}{2}}, t) \right) dt \\
&\approx \int_{t^n}^{t^{n+1}} f\left(u_{i+\frac{1}{2}} + \frac{\partial u_{i+\frac{1}{2}}}{\partial t} t + \frac{\partial^2 u_{i+\frac{1}{2}}}{\partial t^2} t^2 + \cdots \right) dt \\
\tilde{f}_{i-\frac{1}{2}} &= \int_{t^n}^{t^{n+1}} f\left(u(x_{i-\frac{1}{2}}, t) \right) dt \\
&\approx \int_{t^n}^{t^{n+1}} f\left(u_{i-\frac{1}{2}} + \frac{\partial u_{i-\frac{1}{2}}}{\partial t} t + \frac{\partial^2 u_{i-\frac{1}{2}}}{\partial t^2} t^2 + \cdots \right) dt
\end{aligned}
$$

II. HEOC

We introduce here the second ADER scheme based on the work by Castro [24, 26], who reinterpreted the original scheme from Harten, Engquist, Osher and Chakravarthy [78] to include source terms and series expansions on both sides of the interface.

In this method, two Taylor expansions in time (2.45) are constructed: one for left and one for right sides of the interface,

$$u^L(\tau) = u^L(0) + \sum_{k=1}^{K} \left[\frac{\partial^k}{\partial t^k} u^L(0) \right] \frac{\tau^k}{k!} \tag{2.59}$$

$$u^R(\tau) = u^R(0) + \sum_{k=1}^{K} \left[\frac{\partial^k}{\partial t^k} u^R(0) \right] \frac{\tau^k}{k!}. \tag{2.60}$$

Hence, conceptually differs from the TT method, where a unique expansion was done with the solution to a DRP_k on the interface. Rather, the series expansion in this method is employed on the construction of multiple classical Riemann problems (DRP_0) at several time intervals τ_i. Then, the final solution is constructed using quadrature on the multiple Riemann problems,

$$\tilde{f}_{i\pm\frac{1}{2}} = \int_{t^n}^{t^{n+1}} f\left(u(x_{i\pm\frac{1}{2}}, t)\right) \, dt \approx \sum_{i}^{N} \omega_i \; f\left(u_{i\pm\frac{1}{2}}(\tau_i)\right). \tag{2.61}$$

1. **High-order time derivatives**

   To obtain the time derivatives, the Cauchy-Kowalewski procedure is computed with the left and right spatial interpolations. No Riemann problem is solved,

$$\begin{cases} \bullet \quad u^L(0) = u^L(0) \\ \bullet \quad \dfrac{\partial}{\partial t} u^L = u^L \dfrac{\partial u^L}{\partial x} + \dfrac{\partial^2 u^L}{\partial x^2} \\ \bullet \quad \dfrac{\partial^2}{\partial t^2} u^L = \left(u^L\right)^2 \dfrac{\partial^2 u^L}{\partial x^2} + u^L \dfrac{\partial u^L}{\partial x} \dfrac{\partial^2 u^L}{\partial x^2} \\ \qquad\qquad +2u^L \left(\left(\dfrac{\partial u^L}{\partial x} \right)^2 + \dfrac{\partial^3 u^L}{\partial x^3} \right) + \dfrac{\partial^4 u^L}{\partial x^4} \\ \bullet \quad \cdots \end{cases} \tag{2.62}$$

$$\begin{cases} \bullet & u^R(0) = u^R(0) \\ \bullet & \dfrac{\partial}{\partial t}u^R = u^R\dfrac{\partial u^R}{\partial x} + \dfrac{\partial^2 u^R}{\partial x^2} \\ \bullet & \dfrac{\partial^2}{\partial t^2}u^R = \left(u^R\right)^2\dfrac{\partial^2 u^R}{\partial x^2} + u^R\dfrac{\partial u^R}{\partial x}\dfrac{\partial^2 u^R}{\partial x^2} \\ & \qquad +2u^R\left(\left(\dfrac{\partial u^R}{\partial x}\right)^2 + \dfrac{\partial^3 u^R}{\partial x^3}\right) + \dfrac{\partial^4 u^R}{\partial x^4} \\ \bullet & \cdots \end{cases} \tag{2.63}$$

Twice as many spatial interpolations are needed in comparison to TT method. For this reason it is more appropriate for ENO and WENO type spatial interpolations, where multiple interpolations are performed anyway.

2. **Solving multiple classical Riemann problems**

Once Taylor series (2.59) and (2.60) are constructed on each side of the discontinuity, multiple Riemann problems are constructed for different time levels, τ_k. Note, given the Taylor coefficients, obtaining multiple intermediate timesteps is straight forward. For example, assuming $\tau_i = \frac{\Delta t}{2}$,

$$u^{L/R}\left(\frac{\Delta t}{2}\right) = u^{L/R} + \sum_{k=1}^{K}\left[\frac{\partial^k}{\partial t^k}u^{L/R}\right]\frac{t^k}{2^k k!}. \tag{2.64}$$

Then, self-similar solutions to the Riemann problems are obtained,

$$u_{i+\frac{1}{2}}(\tau_k) = RP\left(u^L(\tau_k), u^R(\tau_k)\right) \tag{2.65}$$

In figure 2.6 a representation of HEOC stages are given.

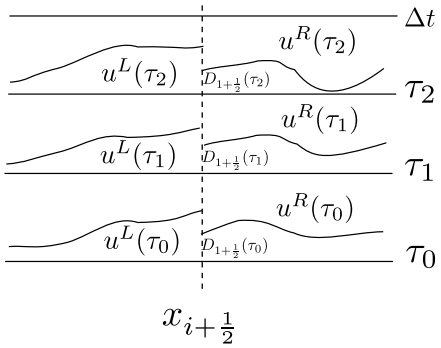

FIGURE 2.6: HEOC stages representation. $D_{i+\frac{1}{2}}$ represents a self-similar solution

3. **High-order numerical flux evaluation**

   From the previous intermediate Riemann solutions ($u_{i+\frac{1}{2}}(\tau_i)$), the high-order numerical flux is constructed using quadrature. Using finite volume nomenclature, the form (2.44) becomes,

$$\tilde{u}_i^{n+1} = \tilde{u}_i^n + \frac{1}{\Delta x}\left(\tilde{f}_{i-\frac{1}{2}} - \tilde{f}_{i+\frac{1}{2}}\right) \tag{2.44}$$

   with

$$\begin{aligned}\tilde{f}_{i+\frac{1}{2}} &= \int_{t^n}^{t^{n+1}} f\left(u(x_{i+\frac{1}{2}}, t)\right)\, dt \\ &\approx \sum_i^N \omega_i\, f\left(u_{i+\frac{1}{2}}(\tau_i)\right)\end{aligned}$$

$$\begin{aligned}\tilde{f}_{i-\frac{1}{2}} &= \int_{t^n}^{t^{n+1}} f\left(u(x_{i-\frac{1}{2}}, t)\right)\, dt \\ &\approx \sum_i^N \omega_i\, f\left(u_{i-\frac{1}{2}}(\tau_i)\right)\end{aligned}$$

   Where ω_i are the weights used for a particular numerical integration.

2.4.3 Discontinuous Galerkin

Research on numerical methods for wave propagation has made huge advances over the last decades. In 1985, the first finite difference method for the wave equation was constructed with second-order centered schemes both in space and time, providing proper stability and accuracy solutions. Unfortunately, that discretization makes the solution decay rapidly for very long waves, starting the race for higher-order methods [39]. After three decades, its study has not yet ended due to its huge applicability in problems solving. In fact, it is the base for any hyperbolic problem, which can be decomposed into a sum of propagating waves.

The biggest research effort has been devoted to the development of spatial higher-order methods, in view of high-order time schemes tending to be unstable. Only Dablain [44] successfully obtained a higher-order time discretization using a modified equation approach.

On top of this, finite difference methods are known to have difficulties adapting to complex geometries, hindering its use among researchers. A possible

solution is developing high-order finite volume or finite element type technologies, having each of these methods their own benefits and disadvantages. Finite volume method relies on reconstructing the flux values at cell interfaces by using neighboring data, whereas finite element method minimizes the error using test and trial functions with arbitrary polynomial orders. The main benefit of finite volume over finite element is the natural adaptation to discontinuities, its strong stability for hyperbolic problems, the simplicity of implementation, cell characteristic functions non-overlapping, and solver uncoupling at cell level in explicit schemes. Finite element on the other side is easier to extend for higher-order methods, especially in three-dimensional unstructured grids, and minimizes the L_2 error by solving a coupled system of overlapping trial and test functions.

Discontinuous Galerkin (DG) is a blending between both finite volume and finite element methods. As in the finite volume case, two adjacent cells are discontinuous and Riemann solvers are typically employed. At the same time, within each cell, trial functions are used to minimize L_2 error as in the finite element method. Discontinuous Galerkin has been for a long time a popular method for solving hyperbolic PDEs. In particular for wave propagation applications, were super-convergence results have been reported [83]. It has several useful mathematical properties studied in a series of papers by Cockburn [36, 38, 34, 37], including the possibility of using higher-order TVD Runge-Kutta time integration, and the use of limiters. DG methods are constructed using the weak formulation of a PDE. For conservative governing equations, a multidimensional variant of equation (2.27) is used.

One of the drawbacks of DG is the need of more unknowns compared to FE or FV methods, for the same grid and order. However, the overhead of the extra unknowns is balanced out by the bigger sparsity of the system compared to FE. The higher the order of the method, the smaller the overhead.

In this thesis, the DG method known as “quadrature-free” is employed for the primitive variables, W. Developed by Shu and Atkins [133] it is computationally cheaper than quadrature based schemes, at least for linear PDEs. The reader is referred to bibliography [133, 17] for an extended description. For the rest of this section, the tensorial notation will be used.

DG for Euler equations

When radiated acoustic waves are strong enough, nonlinear phenomena such as wave steepening and shock formation are observed. For example, in brash musical instruments, shock wave formation has been found at "fortissimo" levels [80]. Since shock formation cannot be captured by linear PDEs such as LEE, solving the full Euler equations is required. Typically, the conservative form of the equations is employed to appropriately capture the discontinuities propagation. However, since the work by Dal Maso et al. [45] (also known as DLM theory), advances in the non-conservative direction have been done. We highlight the work by Dumbser in mixed time-space discontinuous Galerkin and finite volume cases [53, 54, 52, 51], the applications by Rhebergen [124], and the work by Hulsen for smooth cases [85]. Finally, mention the limitations in the non-conservative formulation as shown by Abgrall [2], and its extension by Chalons [27].

Let $\mathcal{V}$ be the space of L^2 functions defined over the domain Ω. And $\mathcal{T}$ the equivalent for the time domain,

$$\mathcal{V} \equiv \{w \in L^2(\Omega)\} \tag{2.66}$$

$$\mathcal{T} \equiv \{\tau \in L^2(I_t)\}. \tag{2.67}$$

Then, solution W is required to belong to

$$W \in (\mathcal{V} \times \mathcal{T})$$

and satisfy the weak formulation (in DMS sense) constructed by multiplying the non-conservative governing equation (2.6) with a test function $\omega \in \mathcal{V}$ (Galerkin approximation), and integrating over the domain.

$$\int_\Omega \frac{\partial W}{\partial t}\omega \, d\Omega + \int_\Omega \mathcal{A}_j \frac{\partial W}{\partial x_j}\omega \, d\Omega = \int_\Omega S\omega \, d\Omega. \tag{2.68}$$

To numerically solve the previous equation, domain Ω is approximated by $\mathcal{N}_e$ non-overlapping elements,

$$\Omega = \sum_{i=1}^{\mathcal{N}_e} \Omega_i. \tag{2.69}$$

Additionally, variables defined on those elements are approximated with the set of polynomials $\mathcal{P}_p$. i.e. $\mathcal{V}$ is replaced by

$$\mathcal{V}^h \equiv \{b_k \in \mathcal{P}_p(\Omega_i) : i \leq \mathcal{N}_e\} \subset \mathcal{V}. \tag{2.70}$$

Hence, both test and trial functions are approximated,

$$\begin{cases} \mathrm{W}^h \in \left(\mathcal{V}^h \times \mathcal{T}\right) \\ \mathrm{W}^{h_j} = \begin{pmatrix} \sum_{k=1}^{\mathcal{N}} \alpha_{\rho\, k}(t) b_k(x,y) \\ \sum_{k=1}^{\mathcal{N}} \alpha_{u_1\, k}(t) b_k(x,y) \\ \sum_{k=1}^{\mathcal{N}} \alpha_{u_2\, k}(t) b_k(x,y) \\ \sum_{k=1}^{\mathcal{N}} \alpha_{p\, k}(t) b_k(x,y) \end{pmatrix} \\ \qquad = \begin{pmatrix} \alpha_{\rho\, 1}(t) + \alpha_{\rho\, 2}(t)x + \alpha_{\rho\, 3}(t)y + \alpha_{\rho\, 4}(t)x^2 + \cdots \\ \alpha_{u_1\, 1}(t) + \alpha_{u_1\, 2}(t)x + \alpha_{u_1\, 3}(t)y + \alpha_{u_1\, 4}(t)x^2 + \cdots \\ \alpha_{u_2\, 1}(t) + \alpha_{u_2\, 2}(t)x + \alpha_{u_2\, 3}(t)y + \alpha_{u_2\, 4}(t)x^2 + \cdots \\ \alpha_{p\, 1}(t) + \alpha_{p\, 2}(t)x + \alpha_{p\, 3}(t)y + \alpha_{p\, 4}(t)x^2 + \cdots \end{pmatrix} \end{cases} \tag{2.71}$$

and,

$$\begin{cases} \omega^h \in \mathcal{V}^h \\ \omega^h = \begin{pmatrix} \sum_{m=1}^{\mathcal{N}} b_m(x,y) \\ \sum_{m=1}^{\mathcal{N}} b_m(x,y) \\ \sum_{m=1}^{\mathcal{N}} b_m(x,y) \\ \sum_{m=1}^{\mathcal{N}} b_m(x,y) \end{pmatrix} \end{cases} \tag{2.72}$$

where $\alpha_{var\, k}$ are time dependent coefficients for variables in $var = \{\rho, u_1, u_2, p\}$.

The total number $\mathcal{N}$ of k and m terms in the expansion gives the desired order of the method, p. Both k and m values need to be the same for the system

to be determined. For a two-dimensional problem, their relation is,

$$\mathcal{N} = \frac{1}{2!}\prod_{k=1}^{2}(p+k)\,. \tag{2.73}$$

Substituting previous approximations into the weak equation (2.68), we get the discrete version. Assuming a smooth non-conservative solution, Hulsen formulation can be used [85], and a surface integral needs to be computed for $\mathbb{H}$,

$$\sum_{\Omega_i}\left\{\int_{\Omega_i}\frac{\partial W^h}{\partial t}\omega^h\,d\Omega + \int_{\Omega_i}\mathcal{A}_j\frac{\partial W^h}{\partial x_j}\omega^h\,d\Omega + \int_{\partial\Omega_i}\mathbb{H}\,\omega^h\,d\Gamma\right\} = \sum_{\Omega_i}\left\{\int_{\Omega_i}\mathbb{S}^h\omega^h\,d\Omega\right\}.$$

$$\mathbb{H}\left(W^{(i)}, W^{(l)}, n\right) = \int_{W^{(i)}}^{W^{(l)}}\mathcal{A}_j\,n_j\,dW$$

Where $W^{(i)}$ denotes the cell variables evaluated on the boundary, and $W^{(l)}$ the evaluation of the adjacent element on the same boundary. n is the outward pointing vector.

At this point h notation is dropped since provides no relevant information for the numerical scheme. Additionally, the system will only be studied for a single grid cell, and the linear summation operator is also dropped. Finally, no source terms are considered in this work, $\mathbb{S} = 0$. Simplifying the weak form of non-conservative variables to,

$$\int_{\Omega_i}\frac{\partial W}{\partial t}\omega\,d\Omega + \int_{\Omega_i}\mathcal{A}_j\frac{\partial W}{\partial x_j}\omega\,d\Omega + \int_{\partial\Omega_i}\mathbb{H}\,\omega\,d\Gamma = 0. \tag{2.74}$$

The reader is referred to the series of papers by Dumbser [52, 53, 54, 51] and Hulsen [85] to solve this system.

DG for LEE equations

When linearized Euler equations (2.39) are solved, recall matrix $\mathcal{A}_j$ is composed of the time-invariant mean values $\overline{\mathcal{A}}_j$, and therefore only needs to be (pre)computed once. As in this thesis, it can also be considered constant in space, in which case it becomes a scalar matrix and is pulled out from the integral.

After this procedure the weak formulation becomes conservative, and the boundary integral turns into the numerical flux for conservative equations (to be defined later) applying the divergence theorem, ($\mathbb{H} \rightarrow \mathcal{H}$).

$$\int_{\Omega_i} \frac{\partial W}{\partial t} \omega \, d\Omega + \overline{\mathcal{A}}_j \int_{\Omega_i} \frac{\partial \omega}{\partial x_j} W_j \, d\Omega + \int_{\partial\Omega_i} \mathcal{H}\, \omega \, d\Gamma = 0. \tag{2.75}$$

This gives an $\mathcal{N} \times \mathcal{N}$ system of equations for each variable var, per cell. The system is thus uniquely determined. In tensor notation,

$$M \frac{\partial \alpha_{var}}{\partial t} = F_{var} - H_{var} \tag{2.76}$$

where,

$$\begin{aligned}
&\alpha_{var\,k} = (\alpha_{var,1}, \alpha_{var,2}, \ldots, \alpha_{var,\mathcal{N}})^T \\
&b_m = (b_1, b_2, \cdots, b_{\mathcal{N}})^T \\
&M = \int_{\Omega} b_k \, b_m \, d\Omega \\
&F_{var} = \alpha_{var'\,k} \, \overline{\mathcal{A}}_{j\,var\,var'} \int_{\Omega_i} b_k \, \frac{\partial b_m}{\partial x_j} \, d\Omega \\
&H_{var} = \sum_{l \in I_j} \int_{\Gamma_{jl}} \mathcal{H}_{il} \, b_m \, d\Gamma
\end{aligned}$$

Since α_{var} is the only time-dependent variable, one can analytically precompute and store all integrals.

The Lax-Friedrichs numerical flux scheme is selected to solve the Riemann problem [126],

$$\mathcal{H}(W^{(i)}, W^{(l)}, n_l) = \frac{1}{2}\Big(f^n\left(W^{(i)}\right) + f^n\left(W^{(l)}\right)\Big) - \frac{1}{2}\alpha\Big(W^{(l)} - W^{(i)}\Big) \tag{2.77}$$

which for the linear equations involved it becomes,

$$\mathcal{H}_{il} = \frac{1}{2}\Big(\widehat{\mathcal{A}}^n\left(W^{(i)} + W^{(l)}\right)\Big) - \frac{1}{2}\alpha\Big(W^{(l)} - W^{(i)}\Big) \tag{2.78}$$

$$\widehat{\mathcal{A}}^n = \frac{\overline{\mathcal{A}_j}^{(l)} + \overline{\mathcal{A}_j}^{(i)}}{2} n_j \tag{2.79}$$

The scalar α needs to be larger than the largest $\widehat{\mathcal{A}}_j^n$ matrix eigenvalue. Recall $W^{(i)}$ denotes the cell variable evaluated into the boundary, while $W^{(l)}$ is the evaluation of the adjacent element into the same boundary. n is the outward

pointing vector. Then, H in equation (2.76) becomes,

$$\begin{aligned}\int_{\partial\Omega_{il}} \mathcal{H}_{il}\, b_m \; d\Gamma = \frac{1}{2}\left[\widehat{\mathcal{A}}^n + \alpha I\right]_{var\, var'} \alpha^{(i)}_{var'\, k} \int_{\partial\Omega_{il}} b_k^{(i)}\, b_m^{(i)} \; d\Gamma + \\ + \frac{1}{2}\left[\widehat{\mathcal{A}}^n - \alpha I\right]_{var\, var'} \alpha^{(l)}_{var'\, k} \int_{\partial\Omega_{il}} b_k^{(l)}\, b_m^{(i)} \; d\Gamma\end{aligned} \tag{2.80}$$

In order to simplify DG implementation, integrals are performed on a reference element and are then mapped into the real elements. We denote the mapping by $\mathcal{M}_i : \widehat{\Omega} \rightarrow \Omega_i$, and it is represented in figure 2.7. The reference element is an equilateral triangle, with unit side length.

Let $x_j = (x, y)$ denote the real element coordinates, and $\eta_l = (\eta, \xi)$ the reference element. A transformation matrix between both coordinates is given by,

$$\begin{pmatrix} x_j \\ y_j \end{pmatrix} = \begin{pmatrix} x_{0j} \\ y_{0j} \end{pmatrix} + |J| \begin{pmatrix} \eta \\ \xi \end{pmatrix} \tag{2.81}$$

Being $|J|$ the Jacobian,

$$|J| = \begin{vmatrix} \frac{\partial x}{\partial \eta} & \frac{\partial x}{\partial \xi} \\ \frac{\partial y}{\partial \eta} & \frac{\partial y}{\partial \xi} \end{vmatrix}. \tag{2.82}$$

Computing integrals in equation (2.76) with reference element coordinates,

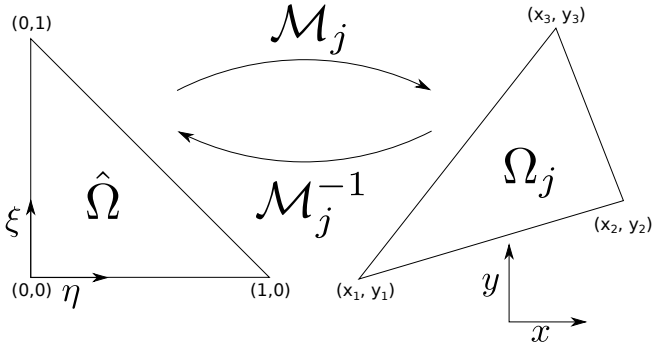

FIGURE 2.7: reference element mapping representation

- M term

$$\begin{aligned} M &= \int_{\Omega} b_k(x,y)\, b_m(x,y)\; d\Omega \\ &= |J| \int_{\widehat{\Omega}} b_k(\eta,\xi)\, b_m(\eta,\xi)\; d\widehat{\Omega} \\ &= |J|\, \widehat{M} \end{aligned}$$

- F term

$$\begin{aligned} F_{var} &= \alpha_{var'\,k}\; \overline{\mathcal{A}}_{j\,var\,var'} \int_{\Omega_i} b_k(x,y)\, \frac{\partial b_m(x,y)}{\partial x_j}\; d\,\Omega \\ &= \alpha_{var'\,k}\, \overline{\mathcal{A}}_{j\,var\,var'} \int_{\widehat{\Omega}_i} b_k(\eta,\xi) \left(\frac{\partial b_m(\eta,\xi)}{\partial \eta} \frac{\partial \eta}{\partial x_j} + \frac{\partial b_m(\eta,\xi)}{\partial \xi} \frac{\partial \xi}{\partial x_j} \right)\; d\,\widehat{\Omega} \end{aligned}$$

Since we are working with a linear mapping $\mathcal{M}_i$, all partial derivatives are constant (and available in the Jacobian), and are therefore pulled out from the integral

$$\begin{aligned} F_{var} &= \alpha_{var'\,k} \overline{\mathcal{A}}_{j\,var\,var'}\, |J|\, (J_{jl})^{-1} \int_{\widehat{\Omega}_i} b(\eta,\xi)_k \frac{\partial b(\eta,\xi)_m}{\partial \eta_l}\; d\,\widehat{\Omega} \\ &= |J|\, (J_{jl})^{-1}\, \widehat{F} \end{aligned}$$

- H term

$$\begin{aligned} H_{var} &= \sum_{l \in I_j} \int_{\partial\Omega_{il}} \mathcal{H}_{il}\, b_m\; d\Gamma \\ &= \frac{1}{2} \left[\widehat{\mathcal{A}}^n + \alpha I \right]_{var\; var'} \alpha^{(i)}_{var'\,k} \int_{\partial\Omega_{il}} b^{(i)}_k\, b^{(i)}_m\; d\Gamma + \\ &+ \frac{1}{2} \left[\widehat{\mathcal{A}}^n - \alpha I \right]_{var\; var'} \alpha^{(l)}_{var'\,k} \int_{\partial\Omega_{il}} b^{(l)}_k\, b^{(i)}_m\; d\Gamma \end{aligned} \tag{2.80}$$

When working with two-dimensional problems, surface integrals become line integrals. Using $s \in (0,1)$, we parametrize the integration path as $c(s) = \{x(s), y(s)\}$. Then, both integrals in H are obtained by restriction to the boundary, $\partial\Omega_{il}(x(s), y(s))$.

$$\begin{aligned} \int_{\partial\Omega_{il}} b^{(i)}_k(x,y)\, b^{(i)}(x,y)\, d\Gamma &= \int_{l_{jl}} b^{(i)}_k(s)\, b^{(i)}(s)\, |c(s)|\; ds \\ \int_{\partial\Omega_{il}} b^{(l)}_k(x,y)\, b^{(i)}(x,y)\, d\Gamma &= \int_{l_{jl}} b^{(l)}_k(s)\, b^{(i)}(s)\, |c(s)|\; ds \end{aligned}$$

where $|c(s)|$ is the boundary arclength,

$$|c(s)| = \sqrt{\left(\frac{\partial x}{\partial s}\right)^2 + \left(\frac{\partial y}{\partial s}\right)^2}. \tag{2.83}$$

It can also be computed in the reference element using the chain rule,

$$|\widehat{c}(s)| = \sqrt{\left(\frac{\partial x}{\partial u}\frac{\partial u}{\partial s} + \frac{\partial x}{\partial v}\frac{\partial v}{\partial t}\right)^2 + \left(\frac{\partial y}{\partial u}\frac{\partial u}{\partial s} + \frac{\partial y}{\partial v}\frac{\partial v}{\partial s}\right)^2}. \tag{2.84}$$

For a linear mapping, it is constant and it can be pulled out from the integral. In practice, H is computed using reference coordinates, but $|c(s)|$ is obtained from real coordinates.

2.4.4 Adomian algorithm

The power of Adomian method relies on decomposing nonlinear operators into a sum of *Adomian polynomials*, denoted by A_i. The unknown variable is then computed as the sum of a convergent infinite series. The original algorithm has been studied and modified by several authors [49], but we only consider the original algorithm reviewed by Adomian himself [3]. In the following, a short description is given. For more details, we refer to [50].

The first step consists in identifying the differential equations in the following form,

$$L(u) + R(u) + N(u) = 0$$

Where L and R are the linear parts of the differential operator, with L being easily invertible. N is the nonlinear part. In the context of this thesis, L is a time-derivative, and hence the inverse operator L^{-1} a time integral. Rewrite this equation by inverting the Linear operator L,

$$u = u(0) - L^{-1}R(u) - L^{-1}N(u) \tag{2.85}$$

Then, variables decomposition is applied as,

$$u = \sum_{n=0}^{\infty} u_n \qquad\qquad N(u) = \sum_{n=0}^{\infty} A_n(u) \tag{2.86}$$

where nonlinear operator $N(u)$ is decomposed into a series of Adomian polynomials A_n, evaluated by the explicit recurrence algorithm

$$A_n = \frac{1}{n!}\frac{d^n}{d\lambda^n}\left[N\left(\sum_{k=0}^{n}\lambda^k u_k\right)\right]_{\lambda=0}. \tag{2.87}$$

This particular Adomian decomposition yields a Taylor expansion: $u_n = \partial_t^n u(t)/n!$, and the final form of the solution is given,

$$\sum_{n=0}^{\infty} u_n = u_0 + L^{-1}R\left(\sum_{n=0}^{\infty} u_n\right) - L^{-1}\sum_{n=0}^{\infty} A_n \tag{2.88}$$

with

$$u_n = -L^{-1}R(u_{n-1}) - L^{-1}A_{n-1}. \tag{2.89}$$

When u is smooth, u_n terms are proof to converge [28] for big enough n.

Higher-dimensional Case

The multidimensional case is a direct extension to the one-dimensional problem [49]. Consider the following two-dimensional variables, u and v.

$$\begin{aligned} L_1(u) + R_1(u,v) + N_1(u,v) &= g \\ L_2(v) + R_2(u,v) + N_2(u,v) &= q. \end{aligned} \tag{2.90}$$

Decompose the variables in a series of sums,

$$u = \sum_{n=0}^{\infty} u_n \qquad\qquad v = \sum_{n=0}^{\infty} v_n$$

and build $N_1(u,v)$ and $N_2(u,v)$ operators with the corresponding Adomian polynomials $A_{(i),n}$,

$$N_1(u,v) = \sum_{n=0}^{\infty} A_{(1),n}(u,v) \quad N_2(u,v) = \sum_{n=0}^{\infty} A_{(2),n}(u,v)$$

$$A_{(1),n} = \frac{1}{n!}\frac{d^n}{d\lambda^n}\left[N_1\left(\sum_{k=0}^{n}\lambda^k u_k, \sum_{k=0}^{n}\lambda^k v_k\right)\right]_{\lambda=0} \tag{2.91}$$

$$A_{(2),n} = \frac{1}{n!}\frac{d^n}{d\lambda^n}\left[N_2\left(\sum_{k=0}^{n}\lambda^k u_k, \sum_{k=0}^{n}\lambda^k v_k\right)\right]_{\lambda=0}. \tag{2.92}$$

The solution for each u_i, v_i expansions is constructed with,

$$\sum_{n=0}^{\infty} u_n = u_0 + L_1^{-1} R_1 \left(\sum_{n=0}^{\infty} u_n, \sum_{n=0}^{\infty} v_n \right) - L_1^{-1} \sum_{n=0}^{\infty} A_{(1),n}$$
$$\sum_{n=0}^{\infty} v_n = v_0 + L_2^{-1} R_2 \left(\sum_{n=0}^{\infty} u_n, \sum_{n=0}^{\infty} v_n \right) - L_2^{-1} \sum_{n=0}^{\infty} A_{(2),n}$$

being

$$\begin{aligned} u_n &= -L_1^{-1} R_1(u_{n-1}, v_{n-1}) - L_1^{-1} A_{(1),n-1} \\ v_n &= -L_2^{-1} R_2(u_{n-1}, v_{n-1}) - L_2^{-1} A_{(2),n-1} \end{aligned} \tag{2.93}$$

Generalization to higher-dimensional spaces is straightforward, defining variables $\{u_1, u_2, \ldots, u_N\}$,

$$L_i(u_1, \ldots, u_N) + R_i(u_1, \ldots, u_N) + N_i(u_i, \ldots, u_N) = 0$$
$$u_i = \sum_{n=0}^{\infty} u_{i,n}$$
$$N_i\left(u_1, \ldots, u_N\right) = \sum_{n=0}^{\infty} A_{(i),n}\left(u_1, \ldots, u_N\right)$$
$$A_{(i),n} = \frac{1}{n!} \frac{d^n}{d\lambda^n} \left[N_i \left(\sum_{k=0}^{n} \lambda^k u_{1,k}, \ldots, \sum_{k=0}^{n} \lambda^k u_{N,k} \right) \right]$$

and solution for each $u_{i,n}$ is given by

$$u_{i,n} = -L_i^{-1} R_i\left(u_{1,n-1}, \ldots, u_{N,n-1}\right) - L_i^{-1} N_i\left(u_{1,n-1}, \ldots, u_{N,n-1}\right)$$

Chapter 3

Adomian Based Schemes (ABS)

3.1 ABS: derivation

We here derive a time integration method using the Adomian algorithm for the general case of Navier-Stokes equations.

To apply the Adomian decomposition technique described in section 2.4.4 to Navier-Stokes equations (2.4), we propose to set

$$L = \frac{\partial}{\partial t} \quad \text{and then} \quad L^{-1} = \int_0^t \tag{3.1}$$

Applying decomposition (2.86) to the primitive variables W in vector notation,

$$W = \sum_{k=0}^{\infty} W_k \tag{3.2}$$

The Adomian coefficients from (2.87) can be written as

$$A_n = \frac{1}{n!}\frac{\partial^n}{\partial \lambda^n}\left[\begin{array}{l}
\partial_x\left(\left(\sum_{k=0}^n \lambda^k \rho_k\right)\left(\sum_{k=0}^n \lambda^k u_k\right)\right) + \partial_y\left(\left(\sum_{k=0}^n \lambda^k \rho_k\right)\left(\sum_{k=0}^n \lambda^k v_k\right)\right) = 0 \\
\left(\sum_{k=0}^n \lambda^k u_k\right)\partial_x\left(\sum_{k=0}^n \lambda^k u_k\right) + \left(\sum_{k=0}^n \lambda^k v_k\right)\partial_y\left(\sum_{k=0}^n \lambda^k u_k\right) + \\
\qquad \left(\frac{1}{\sum_{k=0}^n \lambda^k \rho_k}\right)\partial_x\left(\sum_{k=0}^n \lambda^k p_k\right) - \mu\left(\partial_{x^2}\left(\sum_{k=0}^n \lambda^k u_k\right) + \partial_{y^2}\left(\sum_{k=0}^n \lambda^k u_k\right)\right) \\
\qquad\qquad - \frac{\mu}{3}\left(\partial_x\left(\partial_x\left(\sum_{k=0}^n \lambda^k u_k\right) + \partial_y\left(\sum_{k=0}^n \lambda^k v_k\right)\right)\right) = 0 \\
\left(\sum_{k=0}^n \lambda^k u_k\right)\partial_x\left(\sum_{k=0}^n \lambda^k v_k\right) + \left(\sum_{k=0}^n \lambda^k v_k\right)\partial_y\left(\sum_{k=0}^n \lambda^k v_k\right) + \\
\qquad \left(\frac{1}{\sum_{k=0}^n \lambda^k \rho_k}\right)\partial_y\left(\sum_{k=0}^n \lambda^k p_k\right) - \mu\left(\partial_{x^2}\left(\sum_{k=0}^n \lambda^k v_k\right) + \partial_{y^2}\left(\sum_{k=0}^n \lambda^k v_k\right)\right) \\
\qquad\qquad - \frac{\mu}{3}\left(\partial_y\left(\partial_x\left(\sum_{k=0}^n \lambda^k u_k\right) + \partial_y\left(\sum_{k=0}^n \lambda^k v_k\right)\right)\right) = 0 \\
\left(\sum_{k=0}^n \lambda^k u_k\right)\partial_x\left(\sum_{k=0}^n \lambda^k p_k\right) + \left(\sum_{k=0}^n \lambda^k v_k\right)\partial_y\left(\sum_{k=0}^n \lambda^k p_k\right) + \\
\qquad \gamma\left(\sum_{k=0}^n \lambda^k p_k\right)\left(\partial_x\left(\sum_{k=0}^n \lambda^k u_k\right) + \partial_y\left(\sum_{k=0}^n \lambda^k v_k\right)\right) \\
\qquad\qquad -(\gamma-1)\sum_{ij}\left(\left(\sum_{k=0}^n \lambda^k \tau_k\right)_{ij}\partial_{x_j}\left(\sum_{k=0}^n \lambda^k u_k\right)_i\right) = 0
\end{array}\right]_{\lambda=0} \tag{3.3}$$

Where Stokes' hypothesis (2.3) has been applied in the momentum stress tensor τ_{ij}. In the energy equation τ_{ij} is kept in tensorial notation. W_{n+1} terms are computed recursively by (2.93),

$$W_{n+1}(x,y,t) = \int_0^t A_n(x,y,t). \tag{3.4}$$

3.2 ABS: a recursive formula

Now let's develop the expression for vector $A_n = (A_{(\rho),n}, A_{(u),n}, A_{(v),n}, A_{(p),n})^t$, corresponding each component to an Adomian coefficient for each equation of the Navier-Stokes system. We will first derive the term A_n corresponding to the continuity equation. Then $A_{(u),n}, A_{(v),n}, A_{(p),n}$ will be obtained in a similar way.

From formula (3.3), $A_{(\rho),n}(x,y,t)$ is given by:

$$A_{(\rho),n} = \frac{1}{n!}\frac{\partial^n}{\partial\lambda^n}\left[\frac{\partial}{\partial x}\left((\sum_{k=0}^{n}\lambda^k\rho_k)(\sum_{k=0}^{n}\lambda^k u_k)\right) + \frac{\partial}{\partial y}\left((\sum_{k=0}^{n}\lambda^k\rho_k)(\sum_{k=0}^{n}\lambda^k v_k)\right)\right]_{\lambda=0}$$

Let's develop the first term in the summation. Start by exchanging the order of the derivative,

$$\frac{1}{n!}\frac{\partial^n}{\partial\lambda^n}\left[\frac{\partial}{\partial x}(\cdot)\right]_{\lambda=0} = \frac{1}{n!}\frac{\partial}{\partial x}\left[\frac{\partial^n}{\partial\lambda^n}(\cdot)\right]_{\lambda=0}.$$

Using the *Leibniz* formula we get

$$\frac{\partial^n}{\partial\lambda^n}\left((\sum_{k=0}^{n}\lambda^k\rho_k)(\sum_{k=0}^{n}\lambda^k u_k)\right) = \sum_{j=0}^{n}\binom{n}{j}\frac{\partial^{n-j}}{\partial\lambda^{n-j}}\left(\sum_{k=0}^{n}\lambda^k\rho_k\right)\frac{\partial^j}{\partial\lambda^j}\left(\sum_{k=0}^{n}\lambda^k u_k\right)$$

with

$$\begin{aligned}
&\frac{\partial^{n-j}}{\partial\lambda^{n-j}}\left(\sum_{k=0}^{n}\lambda^k\rho_k\right)\Big|_{\lambda=0} = (n-j)!\,\rho_{n-j} \qquad \binom{n}{j} = \frac{n!}{j!\;(n-j)!}\\
&\frac{\partial^{j}}{\partial\lambda^{j}}\left(\sum_{k=0}^{n}\lambda^k u_k\right)\Big|_{\lambda=0} = (j)!\,u_j
\end{aligned} \tag{3.5}$$

Then

$$\frac{1}{n!}\frac{\partial}{\partial x}\left[\frac{\partial^n}{\partial\lambda^n}\left((\sum_{k=0}^{n}\lambda^k\rho_k)(\sum_{k=0}^{n}\lambda^k u_k)\right)\right]_{\lambda=0} = \sum_{j=0}^{n}\frac{\partial}{\partial x}(\rho_{n-j}u_j) \tag{3.6}$$

Similarly, for the second summation term we have,

$$\frac{1}{n!}\frac{\partial}{\partial y}\left[\frac{\partial^n}{\partial\lambda^n}\left((\sum_{k=0}^{n}\lambda^k\rho_k)(\sum_{k=0}^{n}\lambda^k v_k)\right)\right]_{\lambda=0} = \sum_{j=0}^{n}\frac{\partial}{\partial y}(\rho_{n-j}v_j). \tag{3.7}$$

Substituting both equations (3.6 - 3.7) into $A_{(\rho),n}$ equation, we get the final formula

$$A_{(\rho),n} = \sum_{j=0}^{n}(\partial_x(\rho_{n-j}u_j) + \partial_y(\rho_{n-j}v_j)). \tag{3.8}$$

A similar formula for $A_{(p),n}$ is obtained. Even the stress tensor and velocity divergence yield the same form, since the stress tensor is composed of a summation of velocity (derivative) products, according to (2.3).

$$\sum_{ij}\left((\sum_{k=0}^{n}\lambda^k\tau_k)_{ij}\ \partial_{x_j}(\sum_{k=0}^{n}\lambda^k u_k)_i\right) = \sum_{k=0}^{n}\sum_{ij}\left((\tau_k)_{ij}\ \partial_{x_j}(u_{n-k})_i\right)$$

For $A_{(u),n}$ and $A_{(v),n}$, $\frac{1}{\sum_{k=0}^{n}\lambda^k\rho_k}$ is first developed in power series (note that λ can be considered close to zero since we are concerned by the limit)

$$\frac{1}{\sum_{k=0}^{n}\lambda^k\rho_k} = \sum_{k=0}^{\infty}\lambda^k\widehat{\rho}_k.$$

That is,

$$\begin{aligned}1 &= (\sum_{k=0}^{n}\lambda^k\rho_k)(\sum_{k=0}^{\infty}\lambda^k\widehat{\rho}_k)\\ &= \rho_0\widehat{\rho}_0 + \sum_{k=1}^{\infty}(\sum_{j=0}^{k}\rho_j\widehat{\rho}_{k-j})\lambda^k.\end{aligned}$$

Then we obtain the following recursive formula

$$\widehat{\rho}_0 = \frac{1}{\rho_0}$$
$$\widehat{\rho}_k = \frac{-1}{\rho_0} \sum_{j=1}^{k} \rho_j \widehat{\rho}_{k-j}, \qquad \text{for } k = 1, \ldots, \infty$$

Notice $\widehat{\rho}_k$ is an infinite sum regardless the maximum degree of $(\lambda^k \rho_k)$. However, the series will converge if $(\sum_{k=1}^{n} |\rho_k| < \rho_0)$. Nevertheless, as it will be proven, each term in $\widehat{\rho}_k$ will be multiplied by Δt^k, making the order of $\widehat{\rho}_k \sim \mathcal{O}\left(\Delta t^k\right)$, and accurate even for diverging $\widehat{\rho}$ as far as $t < 1$. We can consider using "mean squares" to approximate $\widehat{\rho}$ when the not satisfied by the algorithm above, although in this thesis is not further studied. Obviously $\widehat{\rho}$ will converge only if ρ converges. An important property is that modifying ρ_k term will only modify $\widehat{\rho}_{k'}$ terms, with $k' > k$. Finally, for the rest of this thesis, we consider $\widehat{\rho}_K$ a series with a number of expansions equal to ρ_K series.

We can now perform a change of variables in the system (3.3) by setting,

$$\left(\frac{1}{\sum_{k=0}^{n} \lambda^k \rho_k}\right) \partial_x \left(\sum_{k=0}^{n} \lambda^k p_k\right) = \left(\sum_{k=0}^{n} \lambda^k \widehat{\rho}_k\right) \partial_x \left(\sum_{k=0}^{n} \lambda^k p_k\right) \tag{3.9}$$
$$\left(\frac{1}{\sum_{k=0}^{n} \lambda^k \rho_k}\right) \partial_x \left(\sum_{k=0}^{n} \lambda^k p_k\right) = \left(\sum_{k=0}^{n} \lambda^k \widehat{\rho}_k\right) \partial_x \left(\sum_{k=0}^{n} \lambda^k p_k\right). \tag{3.10}$$

Then, the same deduction and simplification as for $A_{(\rho),n}$ is done. For the viscous terms the first term in the x-momentum equation is used as an example, assuming constant μ. After exchanging the second-order and λ derivatives, use identity (3.5). Here the procedure for the x-derivative,

$$\frac{\partial^n}{\partial \lambda^n} \left(\frac{\partial^2}{\partial x^2} (\sum_{k=0}^{n} \lambda^k u_k)\right)\Bigg|_{\lambda=0} = \frac{\partial^2}{\partial x^2} \left(\frac{\partial^n}{\partial \lambda^n} (\sum_{k=0}^{n} \lambda^k u_k)\right)\Bigg|_{\lambda=0} = \frac{\partial^2}{\partial x^2}\, n!\, u_n$$

Computing the same for all viscous derivatives in both momentum equations, we finally obtain the following formula for $A_n(x,y,t)$

$$A_n = \begin{cases} A_{(\rho),n} = \sum_{j=0}^{n}(\partial_x(\rho_{n-j}u_j) + \partial_y(\rho_{n-j}v_j)) \\ A_{(u),n} = \sum_{j=0}^{n}(u_{n-j}\partial_x u_j + v_{n-j}\partial_y u_j + \widehat{\rho}_{n-j}\partial_x p_j) \\ \qquad -\mu\left(\partial_{x^2}u_n + \partial_{y^2}u_n\right) - \frac{\mu}{3}\left(\partial_x\left(\partial_x u_n + \partial_y v_n\right)\right) \\ A_{(v),n} = \sum_{j=0}^{n}(u_{n-j}\partial_x v_j + v_{n-j}\partial_y v_j + \widehat{\rho}_{n-j}\partial_y p_j) \\ \qquad -\mu\left(\partial_{x^2}v_n + \partial_{y^2}v_n\right) - \frac{\mu}{3}\left(\partial_y\left(\partial_x u_n + \partial_y v_n\right)\right) \\ A_{(p),n} = \sum_{j=0}^{n}(u_{n-j}\partial_x p_j + v_{n-j}\partial_y p_j + \gamma p_j(\partial_x u_{n-j} + \partial_y v_{n-j})) \\ \qquad -(\gamma\text{-}1)\sum_{k=0}^{n}\sum_{ij}\left((\tau_k)_{ij}\ \partial_{x_j}(u_{n-k})_i\right) \end{cases} \tag{3.11}$$

3.3 ABS: exact time integration formula

Time integration (3.4) is not easy to compute with computer methods (except for symbolic software). Indeed, Adomian series coefficients are polynomials in time whose computed coefficients need to be stored. In the following, we will prove a Theorem that by simple multiplications of time t, it provides a systematic way to compute the integration.

***Theorem**: In formula (3.11), A_n can be expressed as*

$$A_n(x,y,t) = t^n\overline{A}_n(x,y) \tag{3.12}$$

Where $\overline{A}_n(x,y)$, is an expression depending only on spatial coordinates x and y.

Proof: We establish the proof by induction. We will do it only for the first momentum equation terms ($A_{(u),n}$), following the others a similar deduction.

Note that if equation (3.12) is fulfilled, a similar relation holds for field variables,

$$W_{n+1}(x,y,t) = -\int_0^t A_n(x,y,t)\,dt = -\frac{t^{n+1}}{(n+1)}\overline{A}_n(x,y) = -t^{n+1}\overline{W}_n(x,y).$$

Note also that in the recursive formula of $\widehat{\rho}_k$ the sum of the indexes is always equal to k, this implies $\widehat{\rho}_k$ will satisfy formula (3.12) as long as ρ_k satisfies it.

$$\widehat{\rho}_k(x,y,t) = t^k\widehat{\overline{\rho}}_k(x,y) \tag{3.13}$$

Now, to initialize the recursive proof, let's verify the relation for $A_{(u),0}$ and $A_{(v),1}$. From (3.11) We have

$$\begin{aligned} A_{(u),0}(x,y,t) &= u_0\partial_x u_0 + v_0\partial_x u_0 + \widehat{\rho}_0\partial_x p_0 - \mu\left(\partial_{x^2}u_0 + \partial_{y^2}u_0\right) \\ &\quad - \tfrac{\mu}{3}\left(\partial_x(\partial_x u_0 + \partial_y v_0)\right) \\ &= t^0\overline{A}_{(u),0}(x,y). \end{aligned}$$

Then a new state variable term is computed with (3.11),

$$W_1(x,y,t) = -\int_0^t A_0(x,y)\ dt = -t\,A_0(x,y). \tag{3.14}$$

And therefore a new Adomian polynomial,

$$\begin{aligned} A_{(u),1}(x,y,t) &= (u_1\partial_x u_0 + u_0\partial_x u_1 + v_1\partial_x u_0 + v_0\partial_x u_1 + \widehat{\rho}_1\partial_x p_0 + \widehat{\rho}_0\partial_x p_1) \\ &\quad -\mu(\partial_{x^2}u_1 + \partial_{y^2}u_1) - \tfrac{\mu}{3}(\partial_x(\partial_x u_1 + \partial_y v_1)). \end{aligned}$$

Recall from (3.13),

$$\widehat{\rho}_1 = t\,\widehat{\overline{\rho}}_1(x,y).$$

Substituting $\widehat{\rho}_1$ and W_1 into the expression of $A_{(u),1}$, it is easy to verify that $A_{(u),1}(x,y,t) = t\,\overline{A}_{(u),1}(x,y)$.

Now assume relation (3.12) is valid till index n and lets proof it for $n+1$. We proceed exactly as for A_1, since the relation is valid for order n we have

$$A_n(x,y,t) = t^n\overline{A}_n(x,y) \tag{3.15}$$

Then

$$W_{n+1}(x,y,t) = -\int_0^t A_n(x,y,t)\,dt = -\frac{t^{n+1}}{n+1}\overline{A}_n(x,y) = -t^{n+1}\overline{W}_n(x,y). \tag{3.16}$$

By substituting this expression in equation (3.11) we obtain for the first momentum $A_{(u),n+1}$.

$$\begin{aligned}
A_{(u),n+1} &= \sum_{j=0}^{n+1} (u_{n+1\text{-}j}\ \partial_x u_j + v_{n+1\text{-}j}\ \partial_y u_j + \widehat{\rho}_{n+1\text{-}j}\ \partial_x p_j) \\
&\qquad - \mu(\partial_{x^2} u_{n+1} + \partial_{y^2} u_{n+1}) - \tfrac{\mu}{3}(\partial_x(u_{n+1} + \partial_y v_{n+1})) \\
&= \sum_{j=0}^{n+1} \left[\left(t^{n+1\text{-}j}\overline{u}_{n+1\text{-}j}\right) \left(\partial_x t^j \overline{u}_j\right) + \left(t^{n+1\text{-}j}\overline{v}_{n+1\text{-}j}\right) \left(\partial_y t^j \overline{u}_j\right) + \left(t^{n+1\text{-}j}\widehat{\rho}_{n+1\text{-}j}\right) \left(\partial_x t^j \overline{p}_j\right) \right] \\
&\qquad - \mu(t^{n+1}\partial_{x^2}\overline{u}_{n+1} + t^{n+1}\partial_{y^2}\overline{u}_{n+1}) - \tfrac{\mu}{3}(\partial_x(t^{n+1}\partial_x\overline{u}_{n+1} + t^{n+1}\partial_y\overline{v}_{n+1})) \\
&= t^{n+1}\Big(\sum_{j=0}^{n+1} \left[\overline{u}_{n+1\text{-}j}\partial_x\overline{u}_{j\text{-}1} + \overline{v}_{n+1\text{-}j}\partial_y\overline{u}_j + \widehat{\rho}_{n+1\text{-}j}\partial_x\overline{p}_j \right] \\
&\qquad - \mu(\partial_{x^2}\overline{u}_{n+1} + \partial_{y^2}\overline{u}_{n+1}) - \tfrac{\mu}{3}(\partial_x(\partial_x\overline{u}_{n+1} + \partial_y\overline{v}_{n+1}))\Big)
\end{aligned}$$

Which is a monomial of degree $n+1$ in time, with an (overbar) coefficient depending only on x and y. Therefore $A_{(u),n+1}$ can be written as

$$A_{(u),n+1}(t,x,y) = t^{n+1}\overline{A}_{(u),n}(x,y) \tag{3.17}$$

Which completes the *proof.*

□

The ABS formula

Using equation (3.16) we can derive a formula for W_{n+1} that simplifies time integration,

$$W_{n+1}(x,y,t) = -\int_0^t A_n(t,x,y)\,dt = -\int_0^t t^n\overline{A}_n(x,y)\,dt \tag{3.18}$$

$$= -\frac{t^{n+1}}{n+1}\overline{A}_n(x,y) = -\frac{t}{n+1}\left[t^n\overline{A}_n(x,y)\right] \tag{3.19}$$

$$= -\frac{t}{n+1}A_n(t,x,y) \tag{3.20}$$

Substituting the expression of A_n we obtain

$$W_{n+1} = \begin{cases} \frac{-t}{n+1}\left[\sum_{j=0}^{n}\left(\partial_x(\rho_{n-j}u_j)+\partial_y(\rho_{n-j}v_j)\right)\right] \\ \frac{-t}{n+1}\left[\sum_{j=0}^{n}\left(u_{n-j}\partial_x u_j + v_{n-j}\partial_y u_j + \widehat{\rho}_{n-j}\partial_x p_j\right)\right. \\ \qquad \left. -\mu\left(\partial_{x^2}u_n+\partial_{y^2}u_n\right)-\frac{\mu}{3}\left(\partial_x(\partial_x u_n+\partial_y v_n)\right)\right] \\ \frac{-t}{n+1}\left[\sum_{j=0}^{n}\left(u_{n-j}\partial_x v_j + v_{n-j}\partial_y v_j + \widehat{\rho}_{n-j}\partial_y p_j\right)\right. \\ \qquad \left. -\mu\left(\partial_{x^2}v_n+\partial_{y^2}v_n\right)-\frac{\mu}{3}\left(\partial_y(\partial_x u_n+\partial_y v_n)\right)\right] \\ \frac{-t}{n+1}\left[\sum_{j=0}^{n}\left(u_{n-j}\partial_x p_j + v_{n-j}\partial_y p_j + \gamma(\partial_x u_{n-j}+\partial_y v_{n-j})p_j\right)\right. \\ \qquad \left. -(\gamma\text{-}1)\sum_{k=0}^{n}\sum_{ij}\left((\tau_k)_{ij}\partial_{x_j}\left(u_{n-k}\right)_i\right)\right] \end{cases} \tag{3.21}$$

As it can be seen, once $\{W_1,\ldots,W_n\}$ are calculated W_{n+1} is obtained without explicitly computing any integrals.

3.4 ABS-DG

Using Adomian, a recursive formulation only depending on initial conditions has been obtained, according to (3.18). Some literature can be found where Mathematica is used to directly obtain an analytical solution to a simple initial condition (see for example [50, 111]). Nevertheless, using symbolic software to obtain a real problem solution is, if possible, very expensive in terms of computational cost. Moreover, calculating the derivatives in a strong sense requires the initial condition to be smooth enough, which is not always the case.

We hereby propose considering space derivatives in the weak sense with numerical methods. Specifically, Shu's quadrature free discontinuous Galerkin (DG) is employed in this work [133], although any method can be used. We refer to the obtained (fully discretized) scheme *ABS-DG*.

3.4.1 Application to LEE

For the LEE case, and taking the two-dimensional form of equation (2.39), with $\overline{\mathcal{A}}_j = \{\mathcal{A}_0, \mathcal{B}_0\}$ and $x_j = \{x, y\}$, formula (3.21) is simplified in vector

notation to,

$$W_{n+1}(x,y,t) = \frac{-t}{n+1}\left[\mathcal{A}_0(x,y)\frac{\partial}{\partial x}W_n(x,y,t) + \mathcal{B}_0(x,y)\frac{\partial}{\partial y}W_n(x,y,t)\right]. \quad (3.22)$$

If we apply DG space discretization for each ABS series term, an equivalent formulation to (2.76) is obtained without time derivative. In tensor notation it writes,

$$M\,\alpha_{n\,;\,var} = \frac{-t}{n+1}\,(F_{var} - H_{var}) \quad (3.23)$$

$$W^N = \sum_{n=0}^{N} W_n = \sum_{n=0}^{N} \alpha_{n\,;\,var\,k}\,b_k \quad (3.24)$$

A semicolon is used in α to separate Adomian iteration number from tensor variables. W^N is the approximated solution, and N corresponds to the index for which $|W_N|$ is smaller than a given tolerance. A system (3.23) is constructed for each Adomian iteration n.

Order Zero The stability analysis of the formulation will depend on the whole Adomian terms summation, which is a power sum of multiple DG solutions. In order to have an insight into its properties, the zeroth order stability will be studied (equivalent to finite volume scheme). In such case, only $b_1 = 1$ exists, and its derivative becomes zero: the cell has a constant value.

Computing discontinuous Galerkin matrices for order zero, they reduce to a scalar value,

$$\begin{aligned} M &= |\Omega_i| \\ F_{var} &= 0 \\ H_{var} &= \sum_{l\in I_j}\int_{\partial\Omega_{il}} \mathcal{H}_{il}\,d\Gamma = \sum_{l\in I_j}\mathcal{H}_{il}\,|c(s)| \end{aligned}$$

with the Lax-Friedrichs numerical flux $\mathcal{H}_{il}$ being,

$$\begin{aligned} \mathcal{H}_{il} &= \frac{1}{2}\Big(\widehat{\mathcal{A}_0}^{\,n}\left(W_n^{(i)} + W_n^{(l)}\right) + \widehat{\mathcal{B}_0}^{\,n}\left(W_n^{(i)} + W_n^{(l)}\right)\Big) \\ &\quad - \frac{1}{2}\,\alpha\Big(\left(W_n^{(l)} - W_n^{(i)}\right)n_x + \left(W_n^{(l)} - W_n^{(i)}\right)n_y\Big). \end{aligned}$$

$$\widehat{\mathcal{A}}_0^n = \frac{\mathcal{A}_0^{(l)} + \mathcal{A}_0^{(i)}}{2}n_x \qquad \widehat{\mathcal{B}}_0^n = \frac{\mathcal{B}_0^{(l)} + \mathcal{B}_0^{(i)}}{2}n_y$$

Recall $|c(s)|$ is the arclength (or edge length) of the (constant) boundary integral, (2.83). $|\Omega_i|$ is the cell area. $W_n^{(i)}$ and $W_n^{(l)}$ are respectively the current cell and the neighboring cell boundary values for the Adomian iteration n.

From previous results, dividing equation (3.23) by scalar M we get the final algorithm,

$$(\text{ABS-DG})_0 \begin{cases} W_0^i = W(x, y, 0) \\ W_{n+1} = \dfrac{-t}{n+1} \dfrac{|c(s)|}{|\ \Omega_i\ |} \displaystyle\sum_{l \in I_j} \mathcal{H}_{il} \\ W^N = \displaystyle\sum_{n=0}^{N} W_n \end{cases} .$$

Being W_n constant in all the cell, its value can be represented by the value at the cell center with no loss of generality, and the formulation can be written with more traditional finite volume/difference notation, as used in the following section.

3.4.2 Stability analysis

We study stability for the one-dimensional linear wave propagation equation,

$$\frac{\partial u}{\partial t} + a \frac{\partial u}{\partial x} = 0, \tag{3.25}$$

using a zero order spatial ABS-DG formulation. For the rest of this section, the spatial discretization index i is written as a superindex, and Adomian iteration n as a subindex. This non-standard notation is intended to differentiate Adomian iterations from classical finite difference time levels, where n usually represents current time level and $n+1$ is the time level after a time increment. Adomian iteration terms (u_n) are given by the following discretization,

$$\begin{aligned} u_0^i &= u(x_i, 0) \\ u_{n+1}^i(t) &= \frac{-t}{n+1} \frac{1}{2\,h} \Big(a\big(u_n^{i+1} - u_n^{i-1}\big) - \alpha \left(u_n^{i+1} - 2u_n^i + u_n^{i-1}\right) \Big). \end{aligned} \tag{3.26}$$

Where the final solution is obtained by the sum of all the u_n contributions, namely; $u = \sum_n u_n$. In fact, round-off errors for each term (ε_n) are also governed by the same equation. After applying a Fourier decomposition for each error term, $\varepsilon_n^i(t) = \beta_n(t) e^{JK_n x_i}$, the error modes evolution is obtained,

$$\varepsilon_{n+1}^i = \frac{-t}{n+1} \frac{\beta_n}{2\,h} \Big(a\big(e_n^{i+1} - e_n^{i-1}\big) - \alpha \left(e_n^{i+1} - 2u_n^i + e_n^{i-1}\right) \Big). \tag{3.27}$$

From standard stability procedures, the solution is stable respect to round-off errors as long as their growth is kept bounded. *Von Neumann* stability approach is used for this study, with a growth rate amplification $G_n = \frac{e^i_{n+1}(t)}{e^i_n(t)}$. When equation (3.27) is plugged in, the following equation is obtained,

$$\begin{aligned} G_n &= \frac{-t}{n+1}\frac{1}{2\,h}\,\frac{1}{\beta_n e^{JK_n(x_i)}}\Big(a\Big(\beta_n e^{JK_n(x_i+h)} - \beta_n e^{JK_n(x_i-h)}\Big) \\ &\qquad - \alpha\Big(\beta_n e^{JK_n(x_i+h)} - 2\beta_n e^{JK_n(x_i)} + \beta_n e^{JK_n(x_i-h)}\Big)\Big) \\ &= \frac{-t}{n+1}\frac{1}{2\,h}\,\Big(a\Big(e^{JK_n(h)} - e^{JK_n(-h)}\Big) - \alpha\Big(e^{JK_n(h)} + e^{JK_n(-h)} - 2\Big)\Big). \end{aligned} \tag{3.28}$$

But with $\alpha = \frac{1}{2}\frac{h}{t}$,

$$G_n = \frac{-1}{2(n+1)}\,\Big(\frac{t}{h}a\left(e^{JK_n(h)} - e^{JK_n(-h)}\right) - \frac{1}{2}\left(e^{JK_n(h)} + e^{JK_n(-h)} - 2\right)\Big).$$

On the other hand we have

$$\begin{aligned} \left(e^{\frac{JK_n(h)}{2}} - e^{-\frac{JK_n(h)}{2}}\right)^2 &= -4\sin\left(\frac{JK_n(h)}{2}\right)^2 \\ &= e^{JK_n(h)} + e^{JK_n(-h)} - 2 \\ &= 2j\,\sin(JK_n(h)) - 2 \end{aligned}$$

By substitution in expression (3.28) for G_n, and setting $r = |\frac{at}{h}|$ and $\theta_n = K_n h$

$$\begin{aligned} G_n &= \frac{-1}{2(n+1)}\left(2rj\,\sin(\theta) + 2\,\sin\left(\frac{\theta}{2}\right)^2\right) \\ &= \frac{-1}{2(n+1)}\left(4rj\,\sin\left(\frac{\theta}{2}\right)\,\cos\left(\frac{\theta}{2}\right) + 2\,\sin\left(\frac{\theta}{2}\right)^2\right) \\ &\quad \frac{-2\,\sin\left(\frac{\theta}{2}\right)}{n+1}\left(rj\,\cos\left(\frac{\theta}{2}\right) + 0.5\,\sin\left(\frac{\theta}{2}\right)\right). \end{aligned}$$

Then

$$|G_n| = \frac{2\left|\sin\left(\frac{\theta}{2}\right)\right|}{n+1}\left(\sqrt{r^2\,\cos\left(\frac{\theta}{2}\right)^2 + 0.25\,\sin\left(\frac{\theta}{2}\right)^2}\right)$$

Now assume that $r^2 < \dfrac{(n+1)^2}{2}$ meaning that $|r| < \dfrac{n+1}{\sqrt{2}}$, we have

$$\begin{aligned} |G_n| &< 2\left|\sin\left(\frac{\theta}{2}\right)\right| \sqrt{0.5\,\cos\left(\frac{\theta}{2}\right)^2 + \frac{0.25}{(n+1)^2}\,\sin\left(\frac{\theta}{2}\right)^2} \\ &\leq 2\left|\sin\left(\frac{\theta}{2}\right)\right| \sqrt{0.5\,\cos\left(\frac{\theta}{2}\right)^2 + 0.25\,\sin\left(\frac{\theta}{2}\right)^2} \end{aligned}$$

In figure 3.1 the curve of $H\left(\overline{\theta}\right) = |\sin\left(\overline{\theta}\right)| \left(\sqrt{0.5\,\cos\left(\overline{\theta}\right)^2 + 0.25\,\sin\left(\overline{\theta}\right)}\right)$ as a function of $\overline{\theta}$ is depicted for $0 \leq \overline{\theta} \leq 2\pi$.

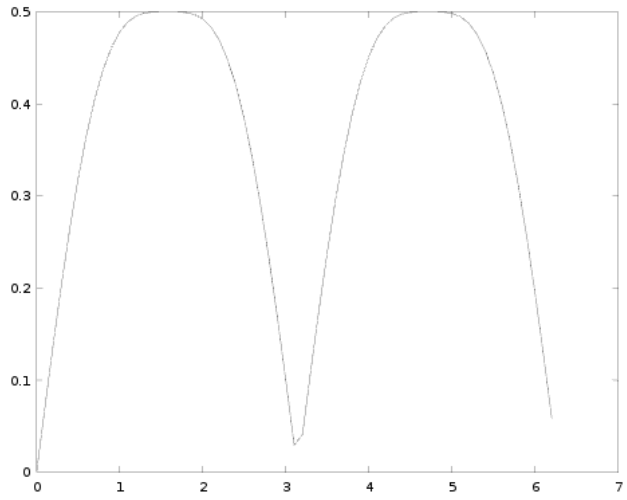

FIGURE 3.1: $H(\theta)$ function numerical evaluation

We deduce that

$$r = \left|\frac{at}{h}\right| < \frac{n+1}{\sqrt{2}} \quad \text{implies} \quad |G_n| < 1.$$

We conclude that a classical CFL condition is necessary to stabilize the first Adomian term (u_1) in the decomposition series (3.2). For the next terms, as n grows, the condition becomes less restrictive. Note that the first term requires $1/\sqrt{2}$ instead of the classical $1/2$ for finite volume with Lax-Friedrichs fluxes, which implies a slight improvement in stability.

3.4.3 Connection of ABS to RK

In this section we will establish a connection between the proposed ABS and the Runge-Kutta (RK) schemes for the linear case to solve the ODE

$$X' = f'(t, x)$$

the general form of RK scheme is given by

$$X_{n+1} = X_n + h \sum_{i=1}^{n} c_i k_i$$

where

$$\begin{aligned}
k_1 &= f(t_n, X_n) \\
k_2 &= f(t_n + \alpha_2 h, X_n + h\beta_{21} k_1(t_n, X_n)) \\
k_3 &= f(t_n + \alpha_3 h, X_n + h(\beta_{31} k_1(t_n, X_n)) + \beta_{32} k_2(t_n, X_n))) \\
&\vdots \\
k_m &= f(t_m + \alpha_m h, X_n + h(\sum_{j=1}^{m-1} \beta_{mj} k_j)
\end{aligned}$$

Setting $c_i = 1/i$ and $\alpha_j = 0$ for all $j = \{2, \ldots, m\}$ and $\beta_{kj} = 0$ for all $j = \{1, \ldots, m-1\}$ and $k = \{2, \ldots, m\}$ in the general Runge-Kutta formula we get the ABS scheme. Note that this is not true in the nonlinear case, it can be easily checked for the Burgers' equation for instance. The ABS for linear problems appears to be an efficient and a practical way of applying RK thanks to its recursive formula. Moreover, the order is dynamic and adaptive for each point of the domain at each timestep, function of the remainder of the Adomian series. Therefore, there is no need to fix the order as for the classical RK formulation in advance, and accuracy can be adjusted for an optimal cost.

3.5 Validation: propagating wave test case

To assess the performance of the proposed ABS-DG scheme, two test cases are used. First a wave propagation is considered, where the simulation is stopped before the wave reaches the boundary. Hence boundary effects are avoided. With this appropriate condition, grid convergence is studied, verifying that the expected spatial order for discontinuous Galerkin methods is achieved. In the second test, non-reflecting and wall boundary conditions are tested to verify aeroacoustic applications are properly solved.

3.5.1 Free-boundary conditions case

The test case consists of a Gaussian pulse centered at the origin, being propagated for three seconds. The simulation is stopped before the wave reaches domain boundary. Results are compared to second-order Runge-Kutta (RK-DG) simulations, and validated by comparison to the analytical solutions available from [136] (see $B1 - B11$ for details). Grid dimensions are 30×30 with a cell edge size of 0.19. Exact solution for pressure is,

$$p(x, y, t) = \frac{\varepsilon_1}{2\alpha_1} \int_0^\infty \left[e^{-\xi^2/4\alpha_1} cos(\xi t) J_0(\xi\eta)\xi \right] d\xi$$

Where $\eta = [(x - Mt)^2 + y^2]^{1/2}$ and J_0 is the zero order Bessel function. $\alpha_1 = 1/2 \ln(2b)$, b being the half-with of the Gaussian function. For the performed simulations we set $\alpha_1 = 1$ and $\varepsilon_1 = 10^{-5}$.

Timestep for reference method (RK-DG) is $\Delta t = 0.02$ (CFL $= 0.1$). This value is small enough to get high accuracy, required for aeroacoustic applications. For ABS-DG on the other side, a different strategy was adopted. From the fact that high-order methods are more efficient for high accuracy demands [92], a high CFL was selected and a small truncation error set to stop Adomian iterations ($|W_n| < 10^{-8}$). The algorithm is expected to use a high number of Adomian iterations, yielding a high-order result. Stable timesteps were found with values as high as $\Delta t = 0.5$ (CFL $= 2.5$). In summary, Adomian algorithm in equation (3.22) was computed with $t = 0.5$, and iterations stopped when $|W_n| < 10^{-8}$.

Next, obtained results are discussed regarding accuracy and cost-effectiveness. A grid convergence is also performed for ABS-DG, to ensure high-order convergence is obtained.

Accuracy assessment The relative L^2 error to the exact solution for both RK-DG and ABS-DG schemes are summarized in table 3.1 for different spatial orders. Results show that ABS-DG has smaller error values than RK-DG. For instance, error for the first spatial order ABS-DG is comparable to second-order RK-DG. This is probably explained by the high accuracy of ABS-DG in time, where the Adomian order is dynamically set to satisfy certain tolerance. Figure 3.2 shows some results for ABS-DG and RK-DG, compared to the exact Gaussian pulse propagation. We can see that ABS-DG fits better the exact solution.

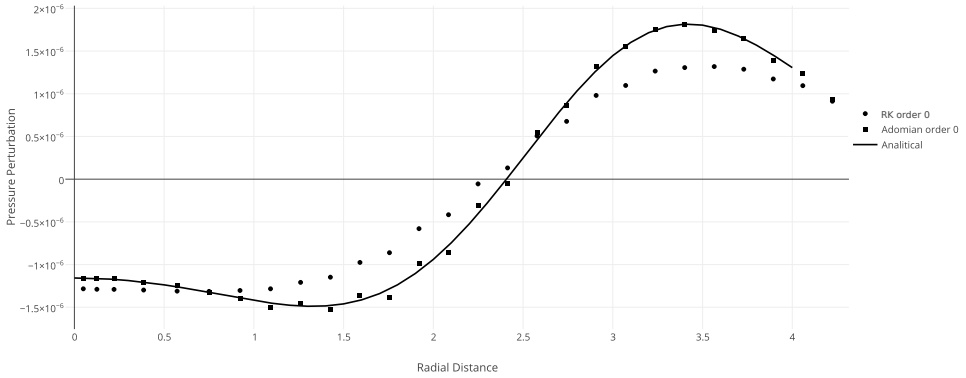

(I) Comparison of the first-order ABS-DG and RK-DG results to the exact solution

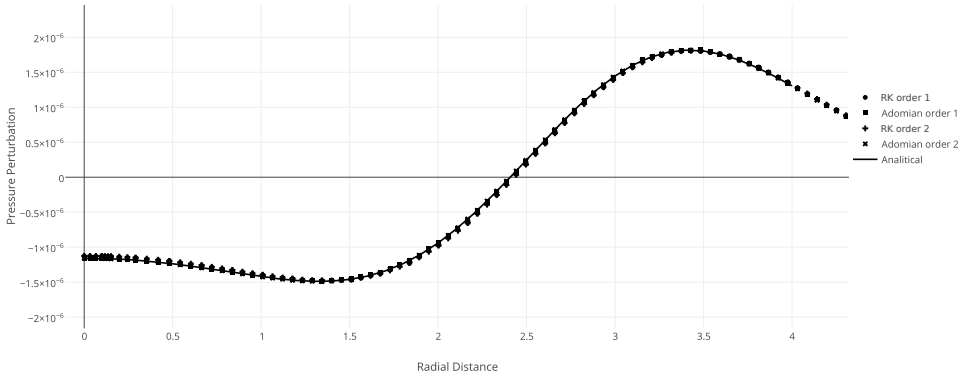

(II) Comparison of the second and third-order ABS-DG and RK-DG results to the exact solution

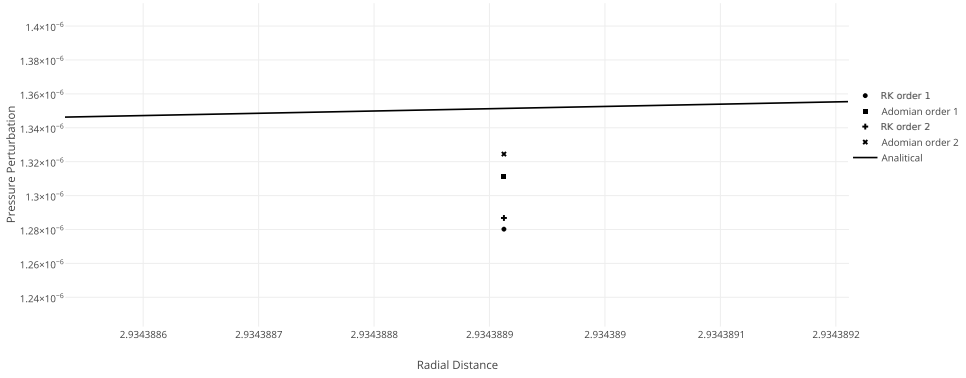

(III) Zoom on ABS-DG, RK-DG and exact solution

FIGURE 3.2: ABS-DG and RK-DG results comparison for 2D Gaussian propagation

TABLE 3.1: Relative L^2 error for DG vs ABS-DG

Order	RK-DG Method	ABS-DG Method
1	2.75E-001	6.28E-002
2	2.18E-002	2.45E-002
3	2.28E-003	1.26E-003

Cost-effectiveness assessment Evaluation of computational cost is done by comparing the number of computed stages for both RK-DG and ABS-DG, since they both have a similar cost per stage. In table 3.2 the values for three seconds of flow simulation are given. For ABS-DG, the worst case scenario is reported by showing the cell with the maximum number of stages; each cell has a different number of Adomian iterations from adaptivity. Results indicate that ABS-DG requires (at least) six times fewer evaluations for the first-order method, which in real time turns out to be a speedup of twenty. In the same way, the third-order case requires halve the evaluations at maximum. The total cost of ABS-DG is therefore smaller than RK-DG for the selected test case. This is mainly possible because of two reasons. First, the use of high CFL values implies that despite Adomian generally requires more stages per time iteration, a less restrictive CFL condition (CFL = 2.5) reduces the overall number of stages. Recall the total cost of the method is given by the product between the total number of timesteps with the number of stages per step. Second, the important adaptive property of the ABS-DG scheme allows each cell to compute only the required number of iterations to satisfy a tolerance threshold, and in this test many cells required only one Adomian term. Hence, big savings are obtained by avoiding irrelevant computations on the fly. This property has an important effect on the speedup and, as in any adaptive method, it is case dependent.

TABLE 3.2: Number of RK-DG, and ABS-DG stage-iterations for 3 seconds simulation. For ABS-DG, the maximum number of iterations over all cells are reported.

Order	RK-DG	ABS-DG (max over all cells)
1	300	50
2	300	90
3	300	170

Grid convergence To study ABS-DG grid convergence, four different meshes with different "edge sizes" are generated in SALOME, a tool for mesh generation used on the current work [15]. Simulations are stopped after two seconds flow simulation, and the relative (to the exact) error is computed. Table 3.3 shows the errors for different h sizes, and in figure 3.3 their logarithmic curves are plotted. For clarity, each curve is separately shown in figure 3.4. In dash line the theoretical order of convergence is plotted. The solid line represents the numerical solution. These results demonstrate that we get the right convergence values.

TABLE 3.3: Relative error magnitude for several Adomian orders at different Mesh sizes

Order	$h = 1.4$	$h = 0.7$	$h = 0.5$	$h = 0.26$
1	5.49E-001	2.80E-001	1.87E-001	8.36E-002
2	2.49E-001	7.69E-002	4.08E-002	1.10E-002
3	7.79E-002	8.36E-003	3.66E-003	3.49E-004

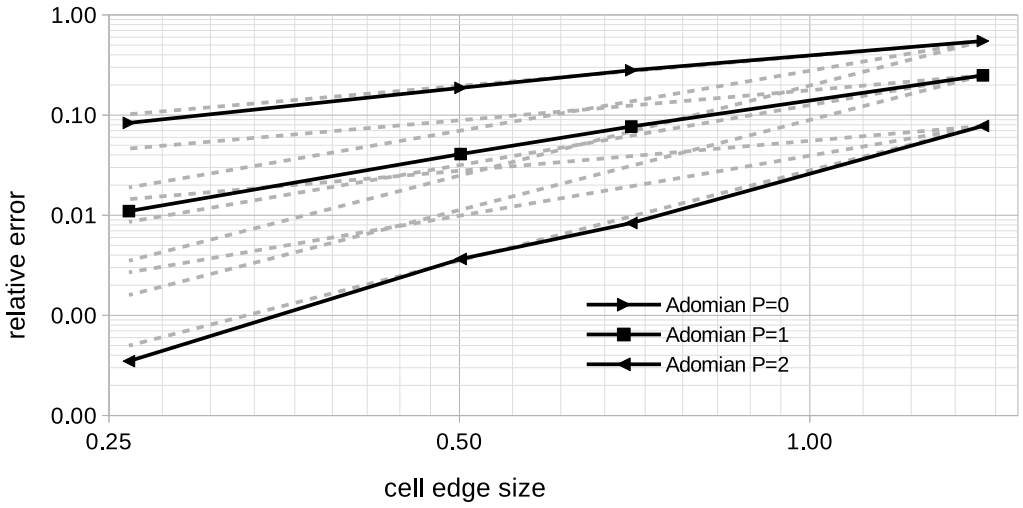

FIGURE 3.3: Discontinuous Galerkin grid convergence study for Gaussian propagation

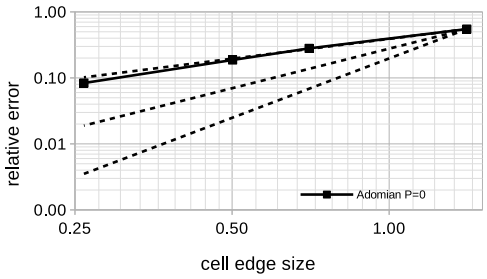

(I) Grid convergence order 0

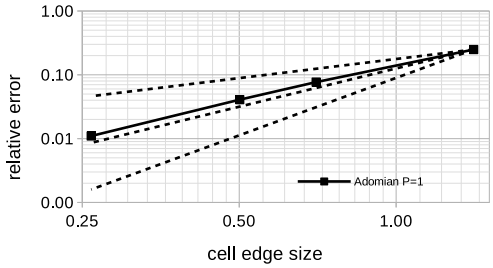

(II) Grid convergence order 1

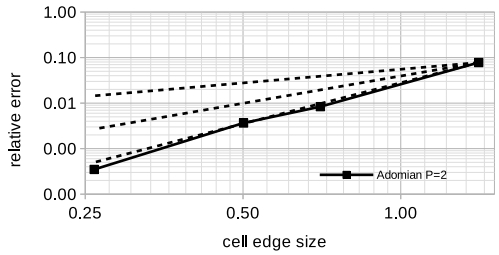

(III) Grid convergence order 2

FIGURE 3.4: Individual orders representation of discontinuous Galerkin grid convergence results

3.5.2 Tests with boundary conditions

The objective of this test is to show how to appropriately impose boundary conditions to the ABS-DG method. Two relevant in aeroacoustic boundary conditions are considered: slip wall and non-reflective conditions. To make the solution fulfill the imposed boundary conditions, we force each of the ABS-DG series terms to satisfy them. The slip wall BC are implemented in a weak sense by nullifying the normal to the boundary component of the momentum flux. Non-reflective BC is achieved according to the standard procedure based on the characteristics for boundary conditions. To estimate the accuracy of the ABS-DG and since an exact solution is not available, a 5^{th} order RK-DG simulation is run on a fine grid (mesh size of 0.1) and its solution is considered as the reference. The ABS-DG test is run on a mesh with 0.19 edge size. Simulations are run till 6 seconds flow time. Table 3.4 shows the relative (to reference DG solution) error for different ABS-DG orders. Very good agreement is found with errors comparable to those obtained in the case of boundary-free tests. Figures 3.5 and 3.6 show the solutions obtained by the reference, and 1st, 2nd, and 3rd order (in space) ABS-DG schemes. These tests demonstrate that imposing the boundary conditions on each term of the series for the ABS-DG scheme is an appropriate approach.

TABLE 3.4: ABS-DG results compared to reference DG solution (relative error)

Order	Wall condition	Non-reflective condition
1	9.39E-002	9.97E-002
2	3.78E-002	2.27E-002
3	3.50E-003	1.22E-003

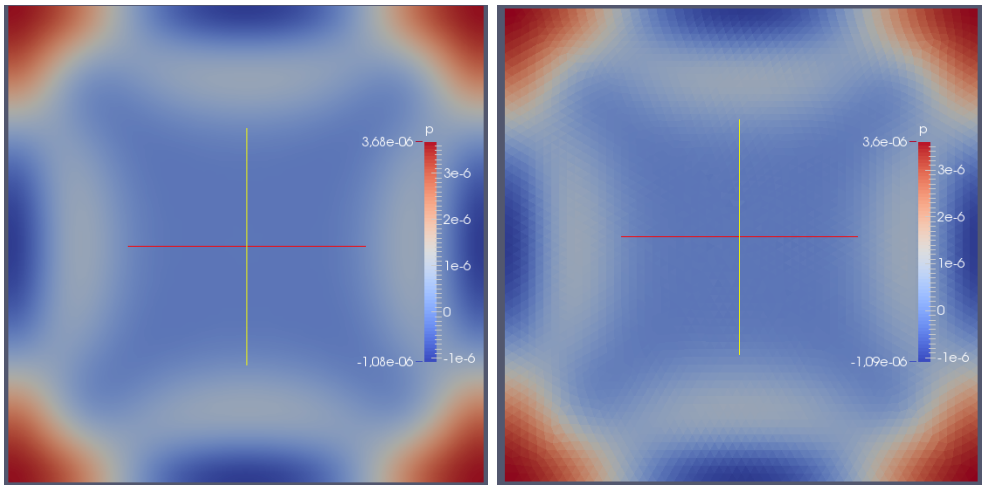

(I) Reference solution (II) P0 Adomian solution

(III) P1 Adomian solution (IV) P2 Adomian solution

FIGURE 3.5: RK-DG Reference and ABS-DG solutions after 6 seconds, for wall boundary conditions

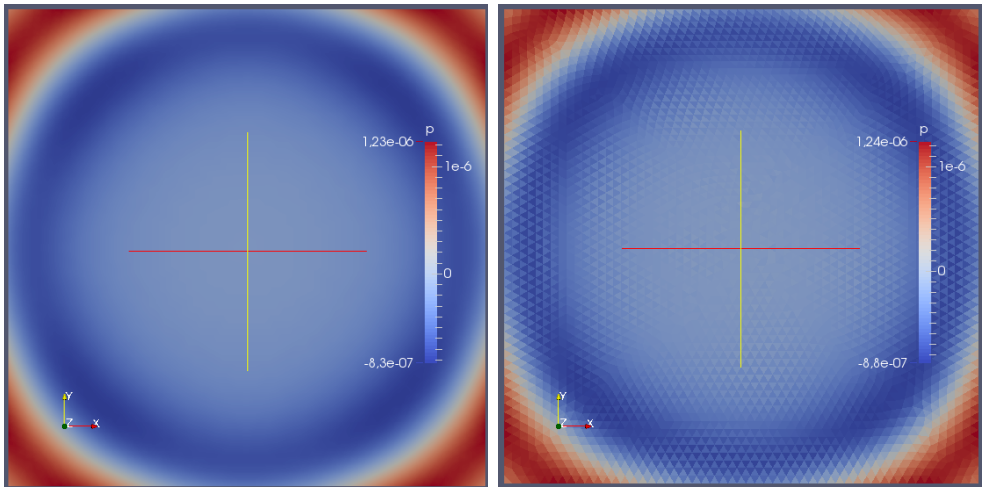

(I) Reference solution (II) P0 Adomian solution

(III) P1 Adomian solution (IV) P2 Adomian solution

FIGURE 3.6: RK-DG Reference and ABS-DG solutions after 6 seconds, for non-reflective boundary conditions

Chapter 4

ABS for Low Mach Number Flows

Although every fluid is physically compressible, the use of compressible governing equations becomes singular and numerically stiff in cases such as liquids or low Mach number flows. The stiffness increases the computational cost and hinders the accuracy and convergence of numerical methods. As studied in chapter 2, the source of the singularity is the eigenvalues difference between acoustic and entropic or vorticity waves. It is generally accepted that for aerodynamic simulations of gases under 0.1 Mach number the incompressible Navier-Stokes equations are better suited. For such cases, acoustic results can be obtained by post-processing aerodynamics results using hybrid CAA methods.

The computation of sound sources in the first hybrid method step is the most computationally demanding task for high Reynolds broadband noise problems [42]. In this chapter, the ABS method developed in chapter 3 is proposed to alleviate the computational cost of such aerodynamic simulations.

4.1 Incompressible Navier-Stokes simulation

There are several ways to solve incompressible Navier-Stokes momentum equations. However, a straightforward solution of equations leads to pressure and velocity coupling, resulting in extremely expensive solvers. Therefore, methods that uncouple pressure and velocity have been largely debated in the literature, still being an active area of research in engineering and mathematical analysis. Among the most popular methods, we fined the use of pressure Poisson equation (PPE) introduced in section 2.2.2. The proposed formulation

allows obtaining an explicit expression for pressure which enforces divergence-free conditions. Unfortunately, this might not be enough to uncouple velocity and pressure when naive methods are used.

Consider the incompressible Navier-Stokes equations (2.13) with constant density $\rho = 1$. Then discretize momentum equations with b Dirichlet boundary conditions on $\partial\Omega$:

$$\frac{u^{n+1} - u^n}{\Delta t} + \frac{\partial p^{n+1}}{\partial x_j} = \frac{1}{Re}\frac{\partial^2 u_i^{n+1}}{\partial x_j^2} - u_j^n \frac{\partial u_i^n}{\partial x_j} \tag{4.1}$$

$$u\,|_{\partial\Omega} = b \tag{4.2}$$

Take divergence and rearrange to obtain the following PPE,

$$\frac{\partial}{\partial x_i}\left(\frac{u_i^{n+1}}{\Delta t} - \frac{1}{Re}\frac{\partial^2 u_i^{n+1}}{\partial^2 x_j}\right) + \frac{\partial^2 p^{n+1}}{\partial^2 x_j} = \frac{\partial}{\partial x_i}\left(\frac{u_i^n}{\Delta t} - u_j^n \frac{\partial u_i^n}{\partial x_j}\right) \tag{4.3}$$

This new equation (altogether with $\int b \cdot n \; d\Gamma = 0$ condition) enforces incompressibility. Gathering all equations,

$$\frac{u^{n+1} - u^n}{\Delta t} + \frac{\partial p^{n+1}}{\partial x_j} = \frac{1}{Re}\frac{\partial^2 u_i^{n+1}}{\partial x_j^2} - u_j^n \frac{\partial u_i^n}{\partial x_j} \tag{4.4}$$

$$\frac{\partial^2 p^{n+1}}{\partial^2 x_j} = \frac{\partial}{\partial x_i}\left(\frac{u_i^n}{\Delta t} - u_j^n \frac{\partial u_i^n}{\partial x_j}\right) \tag{4.5}$$

$$u^{n+1}\big|_{\partial\Omega} = b \tag{4.6}$$

$$\left.\frac{\partial u_i^{n+1}}{\partial x_i}\right|_{\partial\Omega} = 0 \tag{4.7}$$

Since two boundary conditions are set for velocity and none for pressure, it is not possible to uncouple equations, and they need to be solved simultaneously.

Historically Chorin [31, 30] and Temam [137, 138] introduced what today are known as *Projection Methods*, which can be seen as a category of *Fractional-Step Methods*. In the rest of this chapter, we will use the second terminology, to avoid any confusion with the projection operator $\mathcal{P}$. Before Chorin's contribution, pressure and velocity coupling was successfully split by Harlow and Welch in Los Alamos with a method known as the MAC scheme. Today, this method is considered as a fractional-step case, although this was first unnoticed. Fractional-step methods are probably the most popular for unsteady incompressible simulations since they effectively reduce the cost of the simulation. Diverse formulations can be found in [118, 146, 72].

In the following section, the general description of the fractional-step solver is given, in particular for applications with MAC type grid.

4.2 Standard fractional-step method

This methods are based on the projection operator $\mathcal{P}$, by which a vector field U is made solenoidal U^d. The projection operation is denoted as,

$$U^d = \mathcal{P}(U) \tag{4.8}$$

The mathematical ground is based on the *Hodge decomposition.*

Theorem 1. ***Hodge decomposition:*** *Any vector field U in Ω admits a unique orthogonal decomposition*

$$U = U^d + \frac{\partial \phi}{\partial x_j} \tag{4.9}$$

where U^d is a solenoidal field (zero divergence) with zero normal component on the boundary Γ. And $\partial_{x_j}\phi$ is an irrotational (curl-free) field.

Taking the divergence of the Hodge-decomposition the solenoidal part is vanished,

$$\frac{\partial U_j}{\partial x_j} = \frac{\partial^2 \phi}{\partial x_j^2} \tag{4.10}$$

From where ϕ variable is computed. Hence, solving for U^d, the exact continuous projection operator is found to be (for constant unit density),

$$\mathcal{P}(U) = \left[\delta_{ij} - \frac{\partial}{\partial x_i} \left(\frac{\partial^2}{\partial x_j^2} \right)^{-1} \frac{\partial}{\partial x_j} \right] U. \tag{4.11}$$

This projection operator is stable with $\| \mathcal{P}(U) \|_2 \leq \|U\|_2$. Projections satisfy the idempotent property $\mathcal{P}^2 = \mathcal{P}$ [122]. That is,

$$\mathcal{P}(\mathcal{P}(U)) = \mathcal{P}(U). \tag{4.12}$$

This property is useful since it implies once the velocity field is projected into the solenoidal space, further projections have no effect.

A fractional-step method consists of two steps

- *Prediction step*, an evolved velocity field is guessed:
  $U^n \to U^*$.
- *Correction step*, the new state is projected into the divergence-free field
  $U^* \to \mathcal{P}(U^*) = U^{n+1}$.

In bibliography it is sometimes referred as a prediction-correction method.

Multiple fractional-step schemes for the incompressible Navier-Stokes have been developed during the past decades [72]. Among them, the *pressure-correction* methods, including "incremental-pressure schemes". They are particularly useful when pressure needs to be accurately computed, being the most popular category in the fractional-step family. Explicit pressure terms (if any) can be used in the velocity prediction step, while in the correction the pressure is updated using a pressure-update equation. Another class is the *velocity-correction* schemes, which follows the same idea as the pressure-correction schemes, but switches the role of velocity and pressure in the algorithm. Meaning viscous terms can be potentially ignored in the prediction (or included in explicit schemes), and then velocity field is corrected. Finally, we have the *Consistent-splitting* methods, which by taking the L^2-inner product of the momentum equation with $\partial_{x_i} q$ and using $(\partial_t u_i, \partial_{x_i} q) = -(\partial_{x_i} u_i, q) = 0$, a weak formulation equation is obtained,

$$\int_\Omega \frac{\partial p}{\partial x_i}\frac{\partial q}{\partial x_i}\, d\Omega = \int_\Omega \left(f + \frac{1}{Re}\frac{\partial^2 u_i}{\partial x_j^2} \right) \frac{\partial q}{\partial x_j}\, d\Omega. \tag{4.13}$$

Another concern is whether fully explicit, implicit [72] or semi-implicit [48] schemes should be used. The choice will yield different stability and accuracy properties. A recent formulation considers using the intermediate velocity u^* in the nonlinear advection term. Furthermore, three type of semi-implicit methods can be obtained: skew-symmetric, divergence form and rotational form. The three methods are stable whether one uses u^* or u^n [72].

The main drawback of fractional-step methods is the difficulty to obtain higher pressure convergence orders. It is even not clear if higher than two orders can be obtained. Additionally, one needs to compute expensive Poisson type problems to enforce incompressibility, the bottleneck of the whole process. Despite all, it is still one of the best approaches available for unsteady incompressible flow simulation.

As introduced in section 2.2.2, a compatibility conditions must be satisfied for the incompressible equations. Recall, equations (2.16, 2.17), and optionally (2.19):

- Continuity between initial and boundary conditions

$$u_j|_\Gamma \cdot n_j = b_j \cdot n_j \quad \text{in } \partial\Omega \tag{2.17}$$

- zero net flux through boundary

$$\oint_{\partial\Omega} b \cdot n \; d\Gamma = 0 \tag{2.16}$$

- divergence-free boundary condition

$$\frac{\partial}{\partial x_i}\frac{\partial u_j}{\partial x_j} \cdot n_i \Big|_{\partial\Omega} = 0. \tag{2.19}$$

We now describe the explicit pressure-projection family of methods.

4.2.1 Fully explicit fractional-step

The fractional-step method can be applied before or after discretization. In this thesis the fractional-step is performed first, obtaining split governing equations, and then time and space discretizations are computed.

Lets start rearranging (density simplified) Navier-Stokes momentum equation (2.14) into the following form,

$$\frac{\partial u_i}{\partial t} + \frac{\partial(\widehat{p} + \varphi)}{\partial x_j} = \frac{1}{Re}\frac{\partial^2 u_i}{\partial x_j^2} - u_j\frac{\partial u_i}{\partial x_j}. \tag{4.14}$$

Notice pressure is substituted by $p = \widehat{p} + \varphi$. For a fully explicit fractional-step method, we can summarize the algorithm as follows,

- **STEP 1:** Initial data for velocity (u) and pseudo-pressure ($\widehat{p}$) are provided at time n. Density (ρ) is also needed for inhomogeneous problems.
- **STEP 2:** velocity data might be modified such that divergence-free values are obtained at cell face edges. MAC grid schemes automatically satisfy this condition if appropriately discretized.

- **STEP 3:** Solve for intermediate velocity u^*

$$\frac{\partial u_i^*}{\partial t} = \frac{1}{Re}\frac{\partial^2 u_i^n}{\partial x_j^2} - \frac{\partial \widehat{p}^n}{\partial x_j} - u_j^n \frac{\partial u_i^n}{\partial x_j} \tag{4.15}$$

- **STEP 4:** if needed, density ρ and other scalar values can be advanced in time.

- **STEP 5:** Compute the correction term using the PPE,

$$\frac{\partial^2 \varphi^{n+1}}{\partial x_j^2} = \frac{1}{\Delta t}\frac{\partial u_j^*}{\partial x_j} \tag{4.16}$$

- **STEP 6:** Update velocity estimation u_i^* to get a solenoidal solution u^{n+1}.

$$u_i^{n+1} = u_i^* - \Delta t \frac{\partial \varphi^{n+1}}{\partial x_j} \tag{4.17}$$

- **STEP 7:** Update pseudo-pressure. For a fully explicit STEP 3,

$$\widehat{p}^{n+1} = \widehat{p} + \varphi \tag{4.18}$$

- **STEP 8:** Start next time iteration

Chorin's projection method is used in order to obtain the pressure Poisson equation in STEP 5. Chorin realized that the incompressible equation could be seen as a Hodge decomposition in the form of equation (4.9), where temporal evolution u_t is the solenoidal part and pressure gradient the irrotational field,

$$U_i^d = \frac{\partial u_i}{\partial t} \tag{4.19}$$

$$U_i = \frac{\partial u_i^*}{\partial t} = \frac{1}{Re}\frac{\partial^2 u_i}{\partial x_j^2} + \frac{\partial \widehat{p}}{\partial x_j} - u_j \frac{\partial u_i}{\partial x_j} \tag{4.20}$$

$$\frac{\partial \phi}{\partial x_j} = \frac{\partial \varphi}{\partial x_j} \tag{4.21}$$

The Poisson equation is constructed from equation (4.10) and the previous relations. Taking a first-order in time discretization for u_t^*, and assuming u^n is divergence-free from the last iteration,

$$\frac{\partial}{\partial x_j}\left(\frac{u_j^* - u_j^n}{\Delta t}\right) = \frac{\partial^2 \varphi}{\partial x_j^2} \tag{4.22}$$

simplifies to equation (4.16).

Solving the Poisson equation for pseudo-pressure is usually the bottleneck of the fractional-step method. It is an elliptic type equation which needs to be solved simultaneously in all the domain. Many techniques have been developed to increase accuracy and reduce computational cost for the Poisson equation. Indeed, practice has shown the solution is very sensitive to the solver employed and to boundary conditions. In this thesis, our interest is the solution of the advection-diffusion equation (prediction step), and therefore a basic Gauss-Seidel method is used for the Poisson.

To achieve a correct updating formula in STEP 7, replace equations (4.19 - 4.21) into equation (4.15) (STEP 3), and subtract the original equation (4.14) to obtain equation (4.21). Making the approximation $\widehat{p} = p^n$, equation (4.18) is obtained. $\widehat{p}$ is also called pseudo-pressure, and φ pressure-correction term for obvious reasons. If instead we take $\widehat{p} = 0$ (as in Kim and Moin method), then $\varphi = p^{n+1}$. For the first case, the following relationship can be proven [87, 70],

$$p = \widehat{p} + \mathcal{O}\left(\frac{k}{Re}\right). \tag{4.23}$$

Pressure update formula is easy to obtain when fully explicit methods are used. However, it is not the case for implicit or semi-implicit methods.

4.2.2 MAC scheme

The use of traditional collocated grids in finite volume, where both velocity and pressure values are stored at the same spatial coordinate, is known to be a source of instability for the incompressible Navier-Stokes equations. It is a consequence of the pressure and velocity data uncoupling during discretization, creating effectively four independent grids that do not interact with each other. It is particularly notorious the instability leading to the checkerboard problem. One of the most effective strategies to overcome this difficulty was already introduced by Harlow and Welch [77], with what is known as the MAC grid in finite differences schemes. Here, pressure values are stored at cell centers, whereas velocity values are located at cell faces. Alternatively, a staggered grid can be used where pressure is typically stored at cell centers and velocity at cell nodes. Both MAC and staggered grids produce a pressure and velocity coupling, yielding a stable numerical scheme; especially with the first method. Additionally, MAC scheme is conservative, and no creation or destruction of

variables happen. A sketch for all three grid types are shown in figure 4.1, and a more detailed MAC representation for finite volume in figure 4.2. Three overlapping local cells are appreciated in the MAC grid, where each of them has been constructed around the corresponding variable being solved. Unfortunately, implementation of MAC type schemes for non-Cartesian or unstructured meshes is somewhat complicated. And in the Cartesian case, data reconstruction is the price to pay for the staggering. Especially velocity data for Godunov-type methods. Despite all, it is known to give accurate results. In fact, it has extensively been used for DNS simulations with turbulent and/or multiphase applications [90, 94].

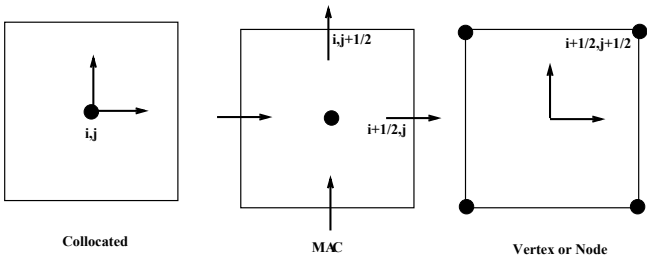

FIGURE 4.1: Collocated, MAC-staggered and standard-staggered mesh discretizations. Taken from [48]

In its origins, the classical MAC scheme was proposed by Harlow and Welch as a fully explicit finite-difference scheme for multiphase applications. Nevertheless, nowadays is considered as a fundamental fractional-step method. We now proceed to give a more detailed review of a general MAC type scheme, by analyzing the STEPs for the general fractional-step method above. The original MAC scheme is given in [77].

The formulation of boundary conditions is not included in the STEPs, and its discussion is given in a separated subsection.

NOTE: For an accurate description of the MAC scheme, Cartesian coordinates tuple (i, j) will be used. And tensor notation will be avoided for clarity. u will denote the x component of velocity and v the y component.

- **STEP 3:** we first compute the intermediate velocity u^* and v^* using equation (4.15), with no pressure term, $\widehat{p} = 0$. Note, velocity is no longer centered around (i, j) coordinates, and local cells are constructed around

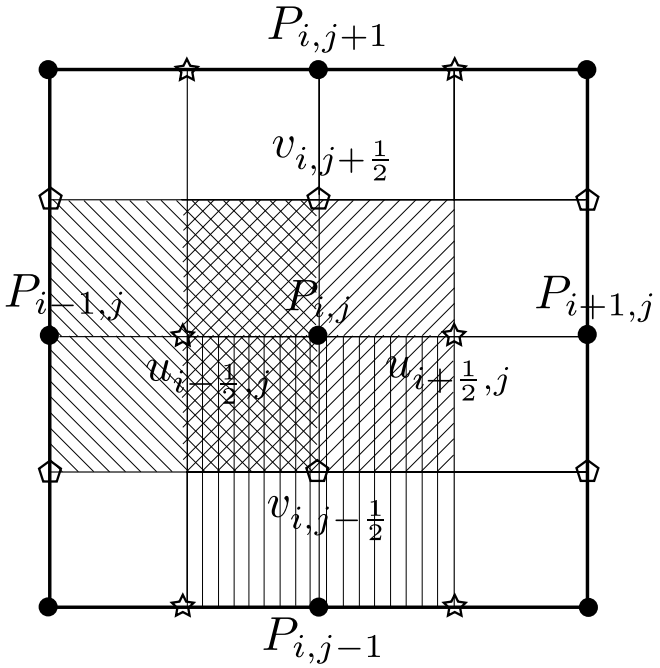

FIGURE 4.2: Detailed MAC scheme grid layout. Each momentum and the pressure variable is stored at a different staggered location: "\" bars for u variable momentum equation, "/" for v variable and "|" for Pressure variable. Black points denote pressure locations, stars u velocity variables locations and pentagons v velocity locations

velocity variables.

$$u^*_{i+\frac{1}{2},j} = u^n_{i+\frac{1}{2},j} - \Delta t \left(\tilde{u}\frac{\partial \tilde{u}}{\partial x} + \tilde{v}\frac{\partial \tilde{u}}{\partial y} \right) + \frac{\Delta t}{Re}\left(\frac{v_{i+\frac{3}{2},j} - 2v_{i+\frac{1}{2},j} + u_{i-\frac{1}{2},j}}{\Delta x^2} + \frac{u_{i+\frac{1}{2},j+1} - 2u_{i+\frac{1}{2},j} + u_{i+\frac{1}{2},j-1}}{\Delta y^2} \right) \tag{4.24}$$

$$v^*_{i,j+\frac{1}{2}} = v^n_{i,j+\frac{1}{2}} - \Delta t \left(\tilde{u}\frac{\partial \tilde{u}}{\partial x} + \tilde{v}\frac{\partial \tilde{u}}{\partial y} \right) + \frac{\Delta t}{Re}\left(\frac{v_{i+1,j+\frac{1}{2}} - 2v_{i,j+\frac{1}{2}} + v_{i,j-\frac{1}{2}}}{\Delta x^2} + \frac{v_{i,j+\frac{3}{2}} - 2v_{i,j+\frac{1}{2}} + u_{i,j-\frac{1}{2}}}{\Delta y^2} \right). \tag{4.25}$$

Convective terms are obtained from an appropriate Godunov type upwinding.

- **STEP 5:** Pressure is again obtained from a PPE involving the velocity divergence. However, calculations are now done in the MAC grid, and

discretization for velocity divergence is given by,

$$\frac{\partial u^*_{i,j}}{\partial x} + \frac{\partial v^*_{i,j}}{\partial y} = \frac{u^*_{i+1/2,j} - u^*_{i-1/2,j}}{\Delta x} + \frac{v^*_{i,j+1/2} - v^*_{i,j-1/2}}{\Delta y}. \tag{4.26}$$

Equivalently, pressure is computed by,

$$\frac{p_{i+1,j} - 2p_{i,j} + p_{i-1}}{\Delta x^2} + \frac{p_{i,j+1} - 2p_{i,j} + p_{i,j-1}}{\Delta y^2} = \frac{1}{\Delta t}\left(\frac{\partial u^*_{i,j}}{\partial x} + \frac{\partial v^*_{i,j}}{\partial y}\right) \tag{4.27}$$

- **STEP 6:** Finally, predicted velocity is corrected using centered finite differences,

$$u^{n+1}_{i+1/2,j} = u^*_{i+1/2,j} - \Delta t \frac{p_{i+1,j} - p_{i,j}}{\Delta x} \tag{4.28}$$

$$v^{n+1}_{i+1/2,j} = v^*_{i,j+1/2} - \Delta t \frac{p_{i,j+1} - p_{i,j}}{\Delta y} \tag{4.29}$$

If the gradient of a scalar stored at u-variable location is needed, it can be obtained by,

$$G_{i+1/2,j} = \begin{pmatrix} \dfrac{\phi_{i+1,j} - \phi_{i,j}}{\Delta x} \\ \\ \left[\dfrac{\phi_{i,j+1} - \phi_{i,j}}{4\Delta y} + \dfrac{\phi_{i,j} - \phi_{i,j-1}}{4\Delta y}\right. \\ \left.\dfrac{\phi_{i+1,j+1} - \phi_{i+1,j}}{4\Delta y} + \dfrac{\phi_{i+1,j} - \phi_{i+1,j-1}}{4\Delta y}+\right] \end{pmatrix}. \tag{4.30}$$

For v-variable,

$$G_{i,j+1/2} = \begin{pmatrix} \left[\dfrac{\phi_{i+1,j} - \phi_{i,j}}{4\Delta y} + \dfrac{\phi_{i,j} - \phi_{i-1,j}}{4\Delta y}\right. \\ \left.\dfrac{\phi_{i+1,j+1} - \phi_{i,j+1}}{4\Delta y} + \dfrac{\phi_{i,j+1} - \phi_{i-1,j+1}}{4\Delta y}+\right] \\ \\ \dfrac{\phi_{i,j+1} - \phi_{i,j}}{\Delta x} \end{pmatrix}. \tag{4.31}$$

The scheme only requires a five-point stencil to compute the Laplacian and the gradient of a two-dimensional flow, strongly simplifying the algebra involved and increasing the efficiency of linear solvers.

Nowadays, when a method refers to a MAC scheme, it usually means a staggered grid is used together with a Poisson type solution for pressure. And

it doesn't necessarily satisfy the original multiphase scheme. In this thesis, we build a new solver for the incompressible Navier-Stokes equations based on a MAC grid type.

Boundary conditions

Despite its essential impact on the overall performance of the method, description of boundary conditions has been avoided because of its complexity and huge research background. Nevertheless, in this section some considerations are pointed out.

Without considering any specific boundary condition, it was mentioned in section 2.2.2 Dirichlet conditions for velocity are the appropriate way to set the problem. Recall that pressure is implicitly computed from the PDE system. Then a PPE was deduced to obtain an explicit equation for pressure, and additional Neumann pressure boundary conditions were included.

With the fractional-step method however, new nonphysical variables appear: $u^*, \widehat{p}$ and φ. It should be then considered if boundary values are required for them, and if so, what are their appropriate values.

$\widehat{p}$ is a function involving previous timestep pressure values and does not require any boundary condition for STEPs 3 and 7. Velocity u^* does require boundary conditions, but its correct definition depends on the approximation of other terms in the equation: if second-order methods are used for advection, diffusion and $\widehat{p}$, then $u^* = u^{n+1} + \mathcal{O}(\Delta t^2)$ (p. 103 [75], [14]). In this case boundary condition can be approximated as,

$$u^*|_{\partial\Omega} = u^{n+1}\big|_{\partial\Omega}\,. \tag{4.32}$$

Kim and Moin [87] also obtained an overall second-order method, but they used $\widehat{p} = 0$. This is possible with the appropriate selection of boundary conditions (p. 105 [75])

$$Eu_j^* \cdot n_j\big|_{\partial\Omega} = 0 \tag{4.33}$$

$$u_j^* \cdot \tau_j\big|_{\partial\Omega} = \left(u_j^{n+1} + \frac{\partial\varphi}{\partial x_j}\right) \cdot \tau_j\Bigg|_{\partial\Omega}\,. \tag{4.34}$$

Where E represents an extrapolation from the domain interior.

Alternatively, for $\widehat{p} = 0$, a first-order scheme is also built by selecting more simple boundary conditions (which will in fact get second-order accuracy for

certain cases)

$$u_j^* \cdot n_j\big|_{\partial\Omega} = u_j^{n+1} \cdot n_j\big|_{\partial\Omega} \tag{4.35}$$

$$u_j^* \cdot \tau_j\big|_{\partial\Omega} = \left(u_j^{n+1} + \frac{\partial\tilde{\varphi}^{n+1}}{\partial x_j}\right) \cdot \tau_j\Big|_{\partial\Omega} \tag{4.36}$$

Here $\frac{\partial\tilde{\varphi}^{n+1}}{\partial x_j}$ needs to be approximated. The following first-order method seems to work.

$$\frac{\partial\tilde{\varphi}^{n+1}}{\partial x_j} = \frac{\partial\varphi^n}{\partial x_j} \tag{4.37}$$

Independently from STEP 3, boundary conditions for φ are required at elliptic Poisson equation in STEP 5. This boundary condition is obtained from the compatibility condition imposed through equation (4.17) in the fractional-step method. Taking its normal derivative on the boundary,

$$\left(\Delta t \frac{\partial\varphi^{n+1}}{\partial x_j}\right) \cdot n_j\Big|_{\partial\Omega} = \left(u_j^* - u_j^{n+1}\right) \cdot n_j\big|_{\partial\Omega}\,. \tag{4.38}$$

Which from approximation in (4.32), it simplifies to

$$\left(\frac{\partial\varphi^{n+1}}{\partial x_j}\right) \cdot n_j\Big| \approx 0. \tag{4.39}$$

For the second-order Kim and Moin method, equations (4.33 - 4.34) are complemented with

$$\left(\frac{\partial\varphi^{n+1}}{\partial x_j}\right) \cdot n_j\Big|_{\partial\Omega} = \left(u_j^* - u_j^{n+1}\right) \cdot n_j\big|_{\partial\Omega}\,. \tag{4.40}$$

Whereas for the first-order case, equations (4.35 - 4.36) need the homogeneous boundary condition for the Poisson equation,

$$\left(\frac{\partial\varphi^{n+1}}{\partial x_j}\right) \cdot n_j\Big|_{\partial\Omega} = 0. \tag{4.41}$$

In this thesis, the MAC discretization is used as described in the previous section, with $\widehat{p} = 0$. Since no extrapolation for the gradient of u^* is implemented (to satisfy equation (4.33)) boundary conditions are expected to resemble first-order Kim and Moin equations (4.35 - 4.36) and (4.41). Which for nonslip wall

boundary conditions ($u_i^{n+1} = 0$) simplifies to

$$u_j^* \cdot n_j \Big| = 0 \tag{4.42}$$

$$u_j^* \cdot \tau_j \Big| = \left(\frac{\partial \varphi}{\partial x_j}\right) \cdot \tau_j \Big|_{\partial\Omega} \tag{4.43}$$

$$\left(\frac{\partial \varphi^{n+1}}{\partial x_j}\right) \cdot n_j \Big|_{\partial\Omega} = 0 \tag{4.41}$$

Studies for high-enough (but not too high) Reynolds values reveal that a good approximation for wall pressure is obtained setting the normal derivative to zero (p. 1119 (9) [71]).

$$u_j(t) \cdot n_j = 0 \tag{4.44}$$

$$u_j(t) \cdot \tau_j = 0 \tag{4.45}$$

$$\left(\frac{\partial p}{\partial x_j}\right)_i \cdot n_i = 0. \tag{4.46}$$

It resembles a second-order boundary condition for variables u^* and φ, except in the tangential direction.

Additionally, when a first-order explicit scheme is used to discretize pressure with Neumann type boundary conditions, no Gaussian points are required outside the domain ($u|_{\partial\Omega}$ Gaussian points). This is in fact representative of the real continuous situation, where no extra pressure boundary conditions were required for the PPE. In the discrete case, this is possible from the cancellation between the Poisson equation and the imposed Neumann boundary conditions (p. 160 [117]). Lets demonstrate it by assuming a vertical boundary is located at $i - \frac{1}{2}$ in figure 4.2. That means point $P_{i,j}$ belongs inside the domain, whereas $P_{i-1,j}$ is an external Gauss point. Take the pressure discretization at (i, j) given by STEP 5 in the MAC section. Merging both equations (4.26) and (4.27) it can be written in the following form.

$$\begin{aligned} &\frac{1}{\Delta x}\left(\frac{p_{i+1,j}^{n+1} - p_{i,j}^{n+1}}{\Delta x} - \frac{p_{i,j}^{n+1} - p_{i-1,j}^{n+1}}{\Delta x}\right) \\ &\qquad + \frac{1}{\Delta y}\left(\frac{p_{1,j+1}^{n+1} - p_{1,j}^{n+1}}{\Delta y} - \frac{p_{1,j}^{n+1} - p_{1,j-1}^{n+1}}{\Delta y}\right) \\ &\qquad\qquad = \frac{1}{\Delta t}\left(\frac{u_{i+1/2,j}^* - u_{i-1/2,j}^*}{\Delta x} + \frac{v_{1,j+1/2}^* - v_{1,j-1/2}^*}{\Delta y}\right). \end{aligned} \tag{4.47}$$

Additionally, discretization of boundary condition in the general form (4.38) is given by

$$\frac{1}{\Delta x}\left(p_{i+1,j}^{n+1}-p_{i,j}^{n+1}\right)=-\frac{1}{\Delta t}\left(u_{i-1/2,j}^{n+1}\right). \tag{4.48}$$

Which by direct substitution into (4.47), boundary term $u^*_{i-1/2,j}$ is canceled. Thus, the solution is independent respect to the boundary value $u^*|_{\partial\Omega}$, and no Gaussian point for pressure is required. A side effect is that no control over the tangential direction of the boundary is possible, and therefore equation (4.43).

An important phenomena of incompressible projection is the growth of an artificial numerical boundary layer from pressure not fully satisfying forced boundary conditions, triggered by the operator splitting. This layer is found from the beginning of the simulation since pressure propagates infinitely fast. Consequently, it is very hard to obtain higher than second-order convergences for pressure since it pollutes all the domain [72].

Some alternative pressure boundary condition approaches have been developed. For example, a rotational formulation was proposed by [139] where the rotational formulation is used. It is a consistent and improved normal boundary condition, although it still contains tangential direction errors [72, 21]. Overall, significant research efforts have been made in the scientific community to obtain appropriate boundary conditions.

4.2.3 Convergence and stability

Accuracy and stability for incompressible Navier-Stokes method depend on multiple factors involving space and time derivatives. For example, combining equations (4.24) in STEP 3 and (4.28) in STEP 6, a first-order in time method is reconstructed for u-variable.

$$\begin{aligned}\frac{u_{i+1/2,j}^{n+1}-u_{i+1/2,j}^{n}}{\Delta t}=&-\left(\tilde{u}^n\frac{\partial\tilde{u}^n}{\partial x}+\tilde{v}^n\frac{\partial\tilde{u}^n}{\partial y}\right)-\frac{p_{i+1,j}-p_{i,j}}{\Delta x}\\&+\frac{1}{Re}\left(\frac{u_{i+\frac{3}{2},j}^{n}+u_{i+\frac{1}{2},j}^{n}+u_{i-\frac{1}{2},j}^{n}}{\Delta x^2}+\frac{v_{i+\frac{1}{2},j+1}^{n}+u_{i+\frac{1}{2},j}^{n}+u_{i+\frac{1}{2},j-1}^{n}}{\Delta y^2}\right)=0\end{aligned} \tag{4.49}$$

The stability of the projection scheme is the stability of the associated equation (4.49) (p. 162 [117]). Although not considered in the steps above, implicit methods can also be used. Implicit methods are more stable, whereas explicit methods are easier to be implemented and require less computational memory.

A combination of both can be found in many semi-implicit methods, where convection terms are solved explicitly while keeping viscous terms implicit. A stability and accuracy study for semi-explicit Navier-Stokes equations can be found in [87]. Stability range is strongly Reynolds value dependent. For low Reynolds number values, viscous terms play the predominant stability role, while for the higher Reynolds numbers it is the convective term.

In the fractional-step method, accuracy is not only function of the discretization schemes selected, a second-order barrier appears from the induced numerical boundary layer. Consequently using higher-order numerical schemes doesn't follow up as one would expect. Reduction of timestep size is nevertheless an effective way to increase accuracy. Explicit methods are thus preferred for accurate simulation since they are cheaper per timestep iteration compared to implicit methods. Unfortunately, for high Reynolds values, extremely thin grid cells are required to capture the tiny boundary layers. The effect of timestep size in turbulent applications has been extensively analyzed [29, 65]. One should make a careful assessment in order to appropriately select implicit or explicit time discretization.

4.3 New formulation of the fractional-step methods using ABS approach

In the previous section it was shown how fractional-step method splits time advancement into two steps. In the first step the intermediate velocity estimation is performed, whereas in the second step the elliptic nature of the problem is solved. In this section a new formulation of the fractional-step method is proposed. This is achieved by modifying the scheme using ABS method developed in chapter 3 to solve the advection-diffusion equation,

$$\begin{aligned}\frac{\partial u^*}{\partial t} &= -\frac{\partial (uu)^n}{\partial x} - \frac{\partial (vu)^n}{\partial y} + \frac{1}{Re}\left(\frac{\partial^2 u^n}{\partial x^2} + \frac{\partial^2 u^n}{\partial y^2}\right) \\ \frac{\partial v^*}{\partial t} &= -\frac{\partial (uv)^n}{\partial x} - \frac{\partial (vv)^n}{\partial y} + \frac{1}{Re}\left(\frac{\partial^2 v^n}{\partial x^2} + \frac{\partial^2 v^n}{\partial y^2}\right).\end{aligned} \tag{4.50}$$

This equation appears in the STEP 3 of the fractional-step method described. Bear in mind, that since a first-order projection method is used, the final convergence order will be formally first-order in time regardless of the velocity scheme.

Highlight again that the motivation of this modification is not to increase the order, but to improve accuracy, speedup and, stability of the scheme.

Since expected results are first-order in time, first-order boundary approximations are used. When solving advection-diffusion equations in a MAC grid with first-order approximations in space and time, equations (4.24-4.25) are recovered. Therefore, Dirichlet boundary conditions are used,

$$u^* \mid_{\partial\Omega} = b_1 \tag{4.51}$$

$$v^* \mid_{\partial\Omega} = b_2 \quad . \tag{4.52}$$

The ABS scheme developed in section 3.1 for the Navier-Stokes equations was ($\mu = Re^{-1}$)

$$W_{n+1} = \begin{cases} \frac{-t}{n+1}\left[\sum_{j=0}^{n}\left(\partial_x(\rho_{n-j}u_j) + \partial_y(\rho_{n-j}v_j)\right)\right] \\ \frac{-t}{n+1}\left[\sum_{j=0}^{n}\left(u_{n-j}\partial_x u_j + v_{n-j}\partial_y u_j + \widehat{\rho}_{n-j}\partial_x p_j\right) - Re^{-1}\left(\partial_{x^2}u_{k-1} + \partial_{y^2}u_{k-1}\right)\right] \\ \frac{-t}{n+1}\left[\sum_{j=0}^{n}\left(u_{n-j}\partial_x v_j + v_{n-j}\partial_y v_j + \widehat{\rho}_{n-j}\partial_y p_j\right) - Re^{-1}\left(\partial_{x^2}v_{k-1} + \partial_{y^2}v_{k-1}\right)\right] \\ \frac{-t}{n+1}\left[\sum_{j=0}^{n}\left(u_{n-j}\partial_x p_j + v_{n-j}\partial_y p_j + \gamma(\partial_x u_{n-j} + \partial_y v_{n-j})p_j\right)\right]. \end{cases} \tag{3.21}$$

which for constant homogeneous density and no pressure influence, $p = 0$ and $\rho = 1$, they reduce to the advection-diffusion equations (or viscous Burgers' equations).

Spatial discretization (ABS-FV)

The ABS scheme for viscous Burgers' equations (3.21) is discretized in space using finite volume technique on a MAC grid. As in chapter 3, we refer to the obtained method by ABS-FV.

To obtain the maximum computational cost speedup, the use of high-order interpolation and flux estimation is only done for the first Adomian stage, whereas simple yet accurate centered schemes are used for the subsequent stages. Obtained results show that this strategy still improves accuracy while maintaining a low computational cost of the method. In the following, some details about the discretization are provided, and Taylor-Green vortex and vortex shedding test cases are performed to demonstrate the efficiency of the proposed ABS-fractional-step method.

For 0^{th} order Adomian iteration reconstruction is done using upwinded parabolic interpolation from Colella [41, 40, 109, 128]. Which is third-order accurate (in one dimension), or fourth-order if cells are equally spaced. For the MAC grid a simplification was done for the velocity terms,

$$\text{in the x-momentum equation:} \quad v_{i-\frac{1}{2},j+\frac{1}{2}} = \frac{v_{i,j+\frac{1}{2}} + v_{i,j+\frac{1}{2}}}{2}$$
$$\text{in the y-momentum equation:} \quad u_{i+1,j-\frac{1}{2}} = \frac{u_{i+\frac{1}{2},j} + u_{i-\frac{1}{2},j-1}}{2}$$

The flux was computed with the Lax-Friedrich scheme (2.78).

For higher-order Adomian iterations all interpolations are reduced to simple central second-order methods, and fluxes are computed by algebraic averaging.

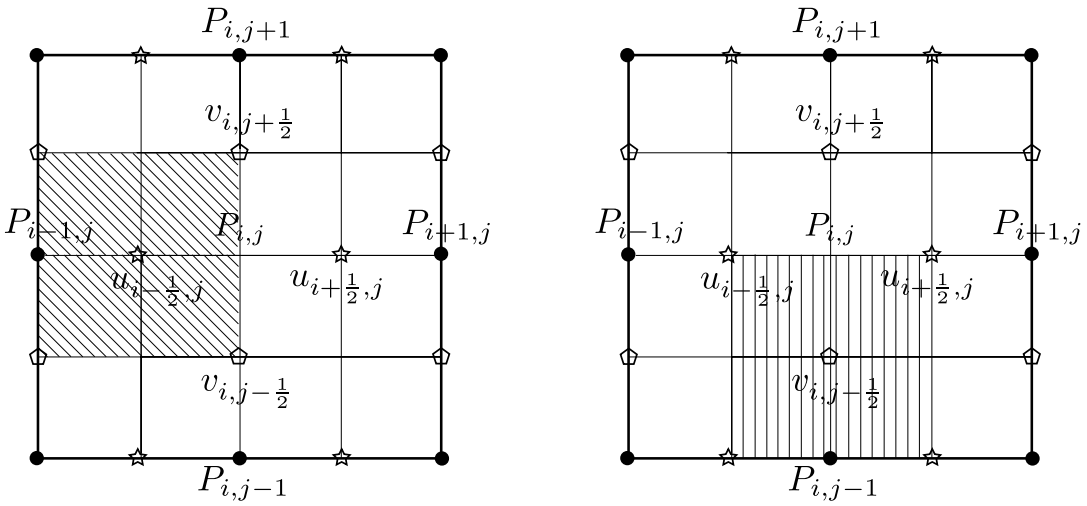

(I) x-momentum (II) y-momentum

FIGURE 4.3: MAC type grid, local cell discretization

Boundary conditions

In this section, we will review boundary conditions implemented for ABS-FV. For the pressure Poisson equation, a standard Helmholtz decomposition is used: null normal pressure and velocity derivatives. Further description is given by Weinan [146], but no further details are given here since is not the objective of this thesis.

- Inlet boundary conditions: Constant in time (per time iteration) Dirichlet boundary condition (u_D, v_D) are assumed. The value is matched by the

zeroth Adomian expansion for every inlet boundary node $\mathbf{x}_i$.

$$u_0(\mathbf{x}_i) = u_D \quad ; \quad v_0(\mathbf{x}_i) = v_D$$
$$u_j(\mathbf{x}_i) = 0 \quad ; \quad v_j(\mathbf{x}_i) = 0 \quad ; \quad \forall j \geq 1$$

- Outlet boundary conditions: Continuative outlet boundary conditions are given by

$$\frac{\partial u}{\partial \mathbf{n}} = 0 \qquad \frac{\partial v}{\partial \mathbf{n}} = 0$$

This is achieved by introducing ghost points, $\mathbf{x}_G$, in the outlet boundary $\mathbf{x}_o$. Ghost points are also implemented for pressure solution. Extrapolation of first-order is done.

$$u_j(\mathbf{x}_G) = u_j(\mathbf{x}_o) \quad ; \quad v_j(\mathbf{x}_G) = v_j(\mathbf{x}_o) \quad ; \quad \forall \quad j \geq 0$$

- Nonslip wall boundary condition: Nonslip boundary conditions are strongly imposed at wall boundaries, $\mathbf{x}_w$. Velocity and normal to boundary pressure derivative are zero. Ghost points, $\mathbf{x}_G$ for pressure are used

$$u_j(\mathbf{x}_G) = 0 \quad ; \quad v_j(\mathbf{x}_G) = 0 \quad ; \quad \forall j \geq 1$$
$$p(\mathbf{x}_w) = p(\mathbf{x}_o)$$

- Slip wall boundary conditions: Slip boundary conditions imply no flow normal to the wall. Implementation is done removing the normal to the wall velocity and pressure derivatives. Again ghost points, $\mathbf{x}_G$ are used.

4.4 Validation

4.4.1 Taylor-Green vortex test case

In order to study the accuracy of the modified fractional-step with ABS-FV, simulations are compared to an exact solution of the incompressible NS equations for the Taylor-Green vortex test case. The exact solution in time is

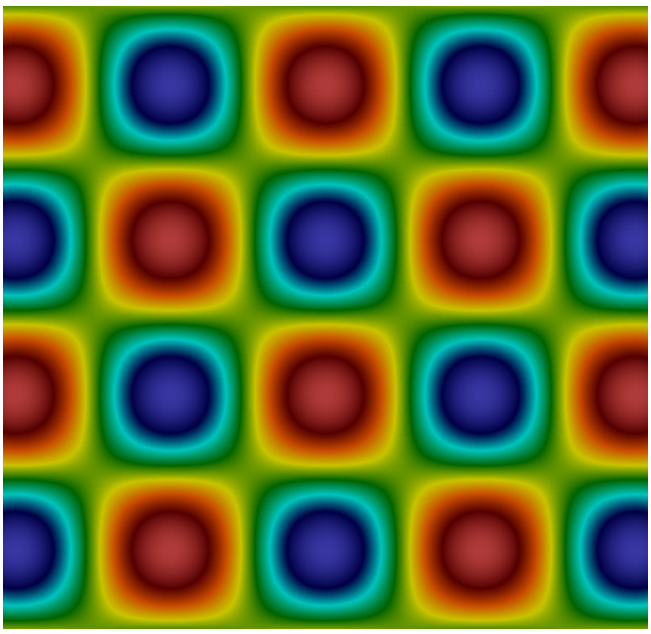

FIGURE 4.4: Taylor-Green test case x-component velocity field representation

given by,

$$u = -\cos(kx)\ \sin(ky)\ e^{-2k^2t/Re} \tag{4.53}$$

$$v = \sin(kx)\ \cos(ky)\ e^{-2k^2t/Re} \tag{4.54}$$

$$p = -\frac{1}{4}\left[\cos(2kx) + \cos(2ky)\right]\ e^{-4k^2t/Re} \tag{4.55}$$

In figure 4.4 the solution pattern is given. This pattern is constant, although its amplitude evolves depending on the fluid viscosity and time.

In this test case, ABS-FV has been tested for $Re = 2000$ and $k = 20$, in a periodic 1×1 square. Three different mesh sizes with two CFL conditions have been tested. In table 4.1, relative errors are reported for both first-order forward Euler method (FE) and ABS-FV simulations after 10 iterations.

ABS-FV simulations required from four to six Adomian iterations to converge within all the domain. Nevertheless, the predominant error in the finest grid is not of temporal source since no difference is found between FE and Adomian results. These errors might come from space discretization, or the projection step for example. The second option would mean ABS-FV can, in fact, approximate better the intermediate velocity u^*, but the error improvement is meaningless in fine grid projection simulations. Similar results are found for the medium mesh with smallest timesteps: both Adomian and FE based schemes produce the same errors. Indeed, the error size is linearly proportional to the

TABLE 4.1: Taylor-Green test case relative error for FE and ABS-FV after 10 iterations.

ABS-FV Relative Error ($\times 10^{-3}$)			
	N=100	N=200	N=400
CFL 0.25	2.5	1.2	0.35
CFL 0.5	4.8	1.8	0.70
FE Relative Error ($\times 10^{-3}$)			
	N=100	N=200	N=400
CFL 0.25	3.1	1.3	0.34
CFL 0.5	6.2	2.4	0.70

timestep size, which is explained by the first-order condition in fractional-step methods.

However, for the coarsest mesh (but also the case with CFL = 0.5 in the average mesh), Adomian scheme yields better results than FE although being in the same order of magnitude. It is expected the error produced during the intermediate velocity computation influenced the projection error.

Further analysis is required to fully understand this test case error results. Nevertheless, an overall positive result is obtained from the ABS-FV method, improving the error produced by forward Euler alternative.

4.4.2 Vortex shedding test case

In order to test the ABS-FV projection in a real test case, a two-dimensional square-cylinder vortex shedding example was selected. This test case has been extensively used to validate turbulence models. It presents multiple complex flow behaviors such as vortices and wall detachment. However, since accuracy has been tested in the previous section (and no exact solution exists for this problem), here focus is set on the computational cost and performance of the algorithm. Therefore, no boundary layer, turbulence or boundary conditions studies are included. Nevertheless, ABS-FV simulations are again run and compared to forward Euler time discretization for the Reynolds values $Re = \{500, 2000, 5000\}$.

The test case is set as follows: a cylinder is located in a domain of 1 m height, and 3 m length. Cylinder sides are 0.1 m length, and its center is located at 1 m distance from the inlet. A structured uniform mesh is used with equidistant cell edges of 7 mm length. Inflow is forced with *inlet boundary conditions* with a velocity and pressure values 1.0. Exit on the right boundary is a *outlet boundary* condition. Cylinder walls are set to *nonslip walls*, whereas

top and bottom domain walls are *slip* walls. The mathematical definition of this boundary conditions can be found in section 4.3.

In table 4.2 computational costs are reported. Solutions were obtained after simulating one second flow evolution from an already evolved common result. Adomian speedup ratios are given compared to FE case, and maximum stable CFL for the FE scheme are also reported for which results have been taken. ABS-FV was always computed with a constant (and stable) CFL = 0.5.

An average speedup of two was obtained, but bigger speedups are obtained with increasing Reynolds values. Two main reasons are found. First, gradients in high Reynolds values are better defined, such that large Adomian expansions are only needed in few cells. Second, a substantial decrease in the stable CFL value of FE involves more timesteps, and hence more computational effort. In fact, for high enough Reynolds values it is well-known centered FE scheme is unstable, whereas Adomian (and high-order RK schemes) are linearly stable [22]. Stability for ABS-FV is achieved by increasing the number of Adomian iterations.

Figure 4.5 shows an example for $Re = 2000$ after 0.2 seconds simulation. In (I) the horizontal velocity is displayed, and (II) shows the number of Adomian expansion terms required to achieve convergence using ABS-FV. As mentioned, most of the Adomian expansions are located at steep gradients, next to wall boundaries and vortices.

A maximum number of 10 expansions were needed at the cylinder corners to achieve the desired accuracy. This order would be impossible by standard Taylor series expansions, and one would need to decrease the overall timestep value.

On top of that, more robust simulations are obtained with Adomian. As previously shown, and practice confirms, using Adomian yields big stability ranges, which increase by adding further iterations. Hence, when a theoretically stable timestep becomes unstable, adding extra Adomian terms can stabilize the solution at a small cost. In other words, timestep size can be pushed to optimize computational cost with smaller safety margins, while for non-adaptive methods a rule of thumb is using smaller than theoretically stable timestep size.

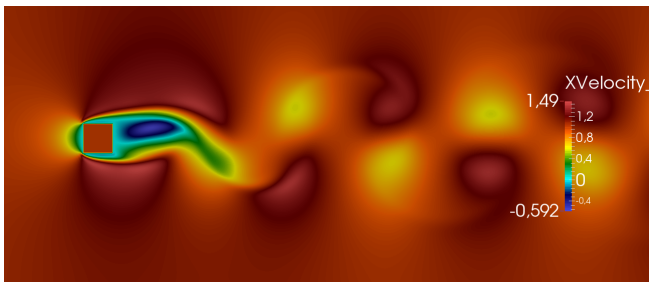

(I) x component of the velocity field

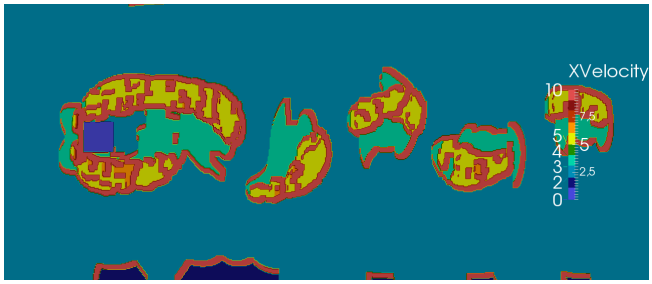

(II) number of Adomian expansions to get converged solution

FIGURE 4.5: Square cylinder vortex shedding after 5000 iterations using ABS-FV and a tolerance of 10^{-2}

Re	$ABS-FV$ Speedup	FE CFL_{max}
500	1.4	0.5
2000	2.1	0.2
5000	3.2	0.1

TABLE 4.2: ABS-FV vs FE speedup values.

4.5 Modified ADER-HEOC

ADER has been introduced in chapter (2.4.2) as a modern high-order alternative to the standard finite volume method. The described HEOC algorithm performs a time series expansion, which based on Cauchy-Kowalewski procedure, it reduces to spatial derivatives. When solved with finite volume discretizations long stencils are expected for high-order derivatives.

Since an Adomian expansion represents an alternative Taylor series expression, it can be used to construct a new type of ADER scheme, known as ABS-ADER. More precisely, a modified HEOC scheme is constructed.

This successful approach gives a simpler and compact (short stencil) ADER scheme. For clarity, spatial coordinate subindex (e.g., u_{i+1}) are replaced with Adomian indexes.

The steps for the modified HEOC ABS-ADER scheme are given next.

1. **Time series expansions**: For convenience, the algorithm is subdivided in two substeps.

   (a) *Adomian terms computation*: First, the Adomian expansions are computed,

   $$u^L = \sum_k^\infty u_k^L \qquad\qquad u^R = \sum_k^\infty u_k^R \tag{4.56}$$

   In contrast to the original method in equations (2.59) and (2.60), they represent Adomian and not Taylor expansions, with the ABS algorithm given by equation (3.21) for $\rho = 1$ and $p = 0$. For example, take the second x-momentum Adomian stage,

   $$u_2 = u_0 \frac{\partial u_1}{\partial x} + u_1 \frac{\partial u_0}{\partial x} + \frac{\partial^2 u_1}{\partial x^2}.$$

   When left and right approximations are done, two options can be considered. Individually computing each term, for example

   $$u_2^{L/R} = u_0^{L/R} \frac{\partial u_1^{L/R}}{\partial x} + u_1^{L/R} \frac{\partial u_0^{L/R}}{\partial x} + \frac{\partial^2 u_1^{L/R}}{\partial x^2},$$

   which resembles the original approach of HEOC method (equations (2.62) and (2.63)). Or reconstructing left and right sides after the Adomian algorithm is applied. Hence, only one interpolation per Adomian step is required.

   $$u_2^{L/R} = \left(u_0 \frac{\partial u_1}{\partial x} + u_1 \frac{\partial u_0}{\partial x} + \frac{\partial^2 u_1}{\partial x^2} \right)^{L/R} \tag{4.57}$$

   In this thesis, the second option is adopted.

   Remark: To solve this substep, exactly the same number of operations as ABS-FV in section 4.3 are needed. Therefore, the modified HEOC ABS-ADER is understood as an ABS-FV extension.

   Although the referenced ABS-FV was developed for a MAC grid type, it can be easily adapted to collocated grids, particularly for 1-D problems.

   (b) *Left and right interpolations*: After Adomian terms are computed, u_i^L and u_i^R terms in equation (4.57) are reconstructed. In this particular

example, linear and parabolic reconstructions are used. Limiters such as minmod or Van Leer can be added.

2. **Solving multiple classical Riemann problems:**

   Following the original method, multiple classical Riemann problems are constructed for specific time values (τ_i) using obtained series expansions.

   Then, each Riemann problem is solved using an appropriate method.

3. **High-order numerical flux evaluation:**

   As in the original method, numerical quadrature is employed to interpolate a high-order numerical flux. In this thesis, a third-order Runge-Kutta scheme is used.

Experience has shown that using a strongly stable Riemann solver in the first step with purely centered schemes in higher Adomian terms give stable solutions.

4.5.1 Validation: one-dimensional Gaussian

In order to compare the performance of different numerical methods, advection and Burgers' equations have been solved using finite volume with three different time schemes: standard RK (RK-FV), Adomian (ABS-FV) and the Modified HEOC scheme (ABS-ADER). Accuracy is studied for all cases, and some considerations on dispersion and dissipation.

In this test case an amplitude one Gaussian pulse is advected over a unit length periodic mesh. The mesh is composed of 50 elements, and the timestep corresponding to CFL = 1.0 is set.

$$u(t=0) = exp\left[-100\,(x-0.5)^2\right] \tag{4.58}$$

We recall centered schemes are unstable when combined with low-order time interpolation schemes, but linearly stable for smooth solutions and high-order time integration methods such as RK4. The following conditions were satisfied in the setup:

- Second and fourth-order centered schemes are used for flux reconstruction.
- In ABS-FV and RK-FV methods four steps/stages are used, yielding in both cases fourth-order time integration schemes.

- For the ABS-ADER, the solution from ABS-FV is taken for the first substep in section 4.5, and the spatial reconstruction for the second substep is done with the same order as used in ABS-FV step (such that ABS-FV and ABS-ADER match in order).

  For example, if the following orders are used in the ABS-FV formulation: [4, 4, 2, 2], the same orders are used in the reconstruction process of modified HEOC.

- Numerical flux is computed with Lax-Friedrichs scheme, and fourth-order Simpson's rule is used for high-order integration in step (3),

$$\tilde{f}_{i+\frac{1}{2}} = \sum_{i}^{N} \frac{1}{8}\left(f\left(u_{i+\frac{1}{2}}(0)\right) + 3f\left(u_{i+\frac{1}{2}}\left(\frac{2}{3}\Delta t\right)\right) + 3f\left(u_{i+\frac{1}{2}}\left(\frac{1}{3}\Delta t\right)\right) + f\left(u_{i+\frac{1}{2}}\left(\Delta t\right)\right)\right)$$

Advection equation

The advection equation is a linear PDE used in acoustic wave propagation. It advects initial condition without shape modification. In figures 4.6 the final solution is represented for the employed solvers. In table 4.3 the L_2 errors are reported.

Despite the fact that ADER method has worse L_2 error compared to both RK and Adomian methods, figures show good wave amplitude preservation. Error is introduced by oscillations and wiggles which pollute the solution. As expected, the bigger the interpolation orders, the lower the L_2 error.

Comparing Adomian and RK, equivalent accuracy results are obtained at fully second or fourth-order simulations. However, when stage orders are mixed, for example orders [4, 4, 2, 2], Adomian algorithm have better results. In fact, small differences exist between orders [4, 4, 2, 2] and [4, 4, 4, 4] for the Adomian case.

Although not formally studied, this behavior can be explained by the weight each Adomian stage has in the final Taylor expansions. Because Runge-Kutta method uses weighted sums to construct the solution, each term in the Taylor series will be a combination of respective weights. Therefore, a combination of second and fourth-order methods will give a combination of second and fourth-order terms. Whereas in Adomian and Taylor (multiderivative) methods, terms are computed in order, and lower terms do not depend on the higher ones.

Hence, each term order can be arbitrarily selected in a monotonically decreasing condition. As a particular multiderivative type, Adomian does indeed have this behavior, where higher-order terms are conditioned by lower-order's accuracy.

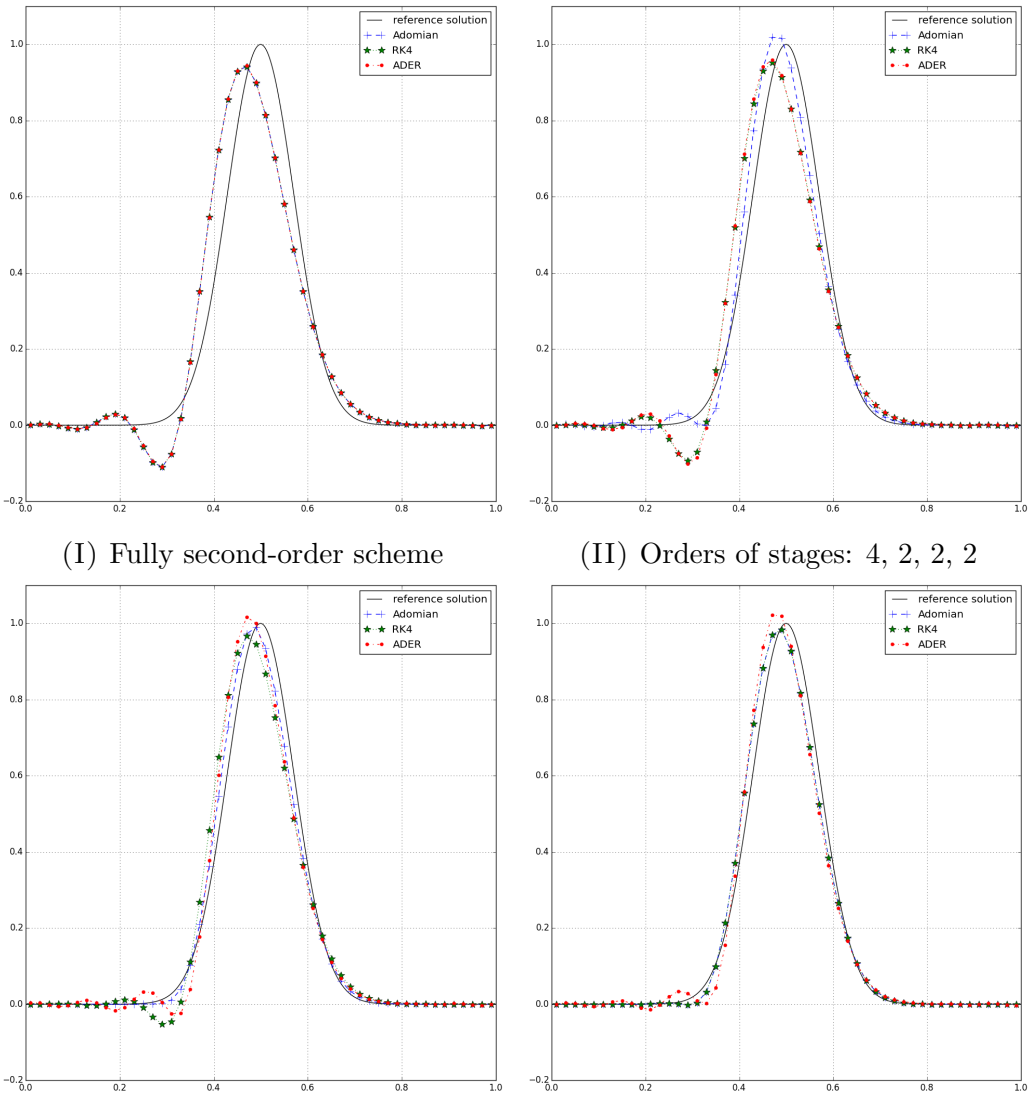

(I) Fully second-order scheme

(II) Orders of stages: 4, 2, 2, 2

(III) Order of stages: 4, 4, 2, 2

(IV) Fully fourth-order scheme

FIGURE 4.6: Adomian (ABS-FV), ADER (ABS-ADER), and RK (RK-FV) results after a periodic advection cycle.

TABLE 4.3: Advection test case error summary

Reconstruction scheme order	RK-FV	ABS-FV	ABS-ADER
2, 2, 2, 2	0.46	0.46	0.49
4, 2, 2, 2	0.39	0.14	0.49
4, 4, 2, 2	0.25	0.08	0.34
4, 4, 4, 4	0.092	0.092	0.144

Burgers' equation

As known, solving Burgers' equation is more complicated than the advection equation due to nonlinearity. In this test, the three methods are compared to a Gaussian shape propagation, both when solution is smooth and after shock formation.

smooth solution

Solutions are compared after four time iterations at CFL = 1.0, with a combination of second and fourth-order centered schemes. A representative figure 4.7, and a detailed errors table 4.4 are reported.

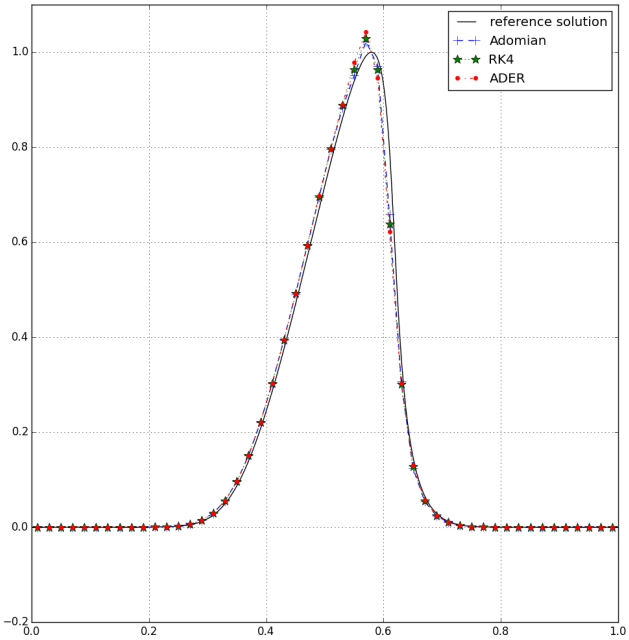

FIGURE 4.7: Adomian (ABS-FV), ADER (ABS-ADER), and RK (RK-FV) smooth results for Burgers' equations after four time iterations

TABLE 4.4: Smooth Burgers test case error summary

Reconstruction scheme order	RK-FV	ABS-FV	ABS-ADER
2, 2, 2, 2	0.056	0.055	0.058
4, 2, 2, 2	0.053	0.044	0.056
4, 4, 2, 2	0.047	0.038	0.052
4, 4, 4, 4	0.038	0.037	0.044

Similar to the advection case, modified HEOC scheme shows comparable or worse results compared to both Adomian and RK schemes. Also, comparison of

RK and Adomian case reveals the same accuracy for fully second or fourth-order solutions. However, far better results are obtained for the Adomian case when mixed order stages are considered. The same reasoning as in the advection case is expected.

shocked solution

Solution is taken after 20 iterations with CFL = 1.0. At this point, a shock is formed, and centered schemes are unstable. Hence slope limiters and upwinding are introduced.

For ABS-FV and ABS-RK an upwinded parabolic reconstruction is used. For ABS-ADER fully second-order ABS-FV is used in the first substep [2, 2, 2, 2], and the conditions used in ABS-FV and ABS-RK are applied in the second substep (upwinding and limiters included). Parabolic reconstruction with limiters can be found in [109].

In figure 4.8 can be seen both ABS-ADER and ABS-RK schemes are stable, whereas ABS-FV is unstable despite upwinding and limiters. Indeed, limiters and upwinding methods were developed for first-order time discretizations, and its extension to higher-order methods is elaborated (see strong stability preserving methods (SSP)). Further study should be done to stabilize Adomian expansions. In the summary, a possible Adomian and HEOC combination is proposed to overcome this difficulty.

Summary

When solving smooth problems, ABS-FV and RK-FV methods are faster and more accurate than ABS-ADER. However, for shocked problems ABS-FV is unstable, and ABS-ADER needs to be used. We propose exploiting the substepping of the modified HEOC scheme, by using the following combination (although it was not tested in this thesis):

1. Apply full ABS-FV algorithm in all computational domain
2. Compute slope limiters
3. For cells with active limiters, further compute the second substep of the ABS-ADER scheme.
4. Advance timestep and restart in step 1.

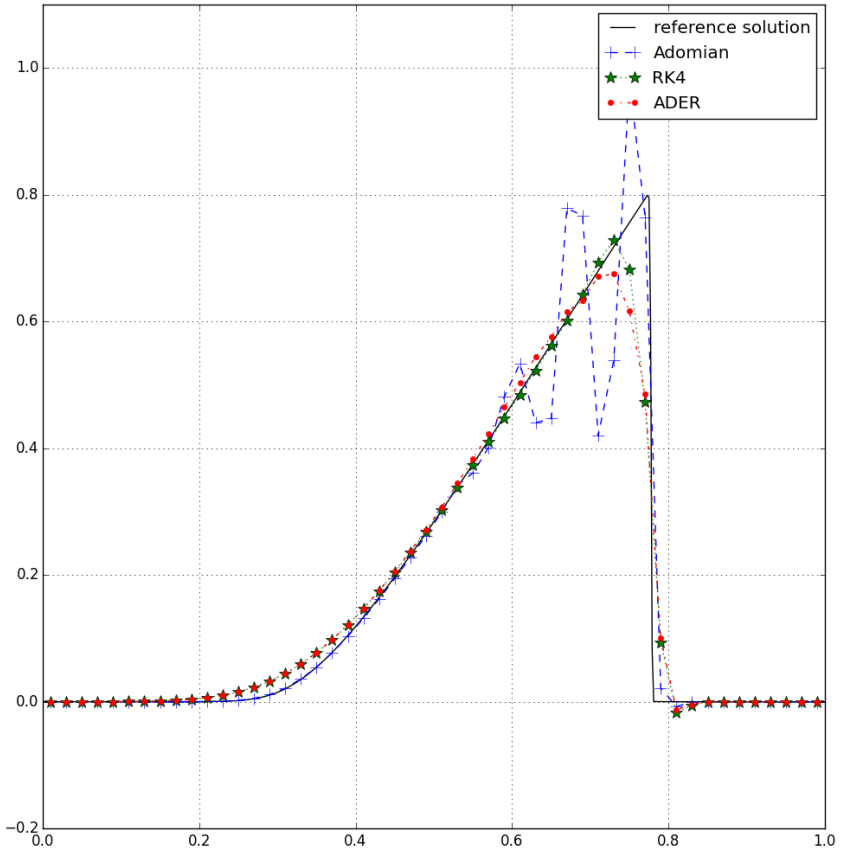

FIGURE 4.8: Adomian (ABS-FV), ADER (ABS-ADER), and RK (RK-FV) shocked results for Burgers' equations with limiters.

Chapter 5

Conclusions and future work

5.1 Conclusions

In this thesis a new multiderivative type explicit time-integration method has been developed, and its performance to solve several fluid dynamics and acoustic related equations has been assessed. Its development is based on the Adomian decomposition method, and we refer to it as ABS standing for Adomian Based Scheme. New solvers have been derived by combination with popular space discretization schemes, such as finite volume (leading to ABS-FV scheme), discontinuous Galerkin (ABS-DG), and more recent ADER method (ABS-ADER).

In chapter 3 a recursive formula for the new approach is proved, rendering an easy to use and implement scheme. A theorem for the time dependency is proved turning the time integration exact. In the linearized Euler equations case the ABS reduces to a particular case of the Runge-Kutta method, with a clear advantage when using ABS. Indeed, the proven recursive formula makes ABS much easier to implement and the time-order selection dynamic (no need to set the order in advance as for RK), changing for each timestep and domain location on demand. These mechanisms are controlled by the Adomian series reminders, hence automatically, becoming a time-adaptive scheme. As a consequence, the accuracy is improved at a minimum cost. A stability result is proved as well.

The ABS-DG and ABS-FV are assessed by comparison to the classical RK-DG and analytical solution of a propagating pulse. The tests showed that ABS-DG is more accurate and up to 20 times faster than the RK-DG method. This is essentially due to the time-adaptive property of ABS. Indeed, the method time order is given by the number of computed Adomian terms, which is different for each timestep and space location.

In chapter 4 the well-known fractional-step method for incompressible Navier-Stokes equations is modified, where the intermediate velocity field in the prediction step is obtained using the ABS scheme developed in chapter 3, ABS-FV. In this work Kim and Moin's approach is adopted, and an explicit method with no pressure terms is considered in the velocity prediction step. Therefore, a two-dimensional viscous Burgers' equation is obtained, also known as the convection-diffusion equation. Discretization is performed on a MAC type grid.

The obtained ABS-FV scheme is validated for the Taylor-Green vortex case and a square cylinder vortex shedding by comparison to an exact solution and a forward Euler in time finite volume method. For the Taylor-Green case, the proposed method shows better accuracy in coarse grids compared to classical fraction-step methods. In fine grids equivalent results are obtained. For the vortex shedding, the proposed method was up to three times faster than forward Euler thanks to its time-adaptive capability.

In the same chapter, an ADER scheme is constructed based on the ABS algorithm (ABS-ADER) as a higher-order alternative to the previous fractional-method method ABS-FV. Precisely, the Taylor series in HEOC-ADER is substituted by an Adomian series. New ABS-ADER method is tested on the advection and Burgers' equations, and solutions compared to standard second-order Runge-Kutta and finite volume (RK-FV), and to ABS with finite volume methods (ABS-FV). Results show ABS-FV is the fastest and the most accurate method for smooth conditions, but becomes unstable for the shocked Burgers' equation. Fortunately, the ADER-ABS method gives stable solutions equivalent to RK-FV.

To sum up, the proposed ABS method is demonstrated to be a potential strategy to build time-adaptive solvers. It can be used together with DG, FV, and ADER methods among others. The adaptive property and the recursive formulation makes obtained schemes highly accurate and easy to implement.

5.2 Future work

Further studies and deeper analysis are necessary to fully understand ABS properties. In the following some of them are listed:

- The effect of boundaries in Adomian iterations should be better understood. Especially in nonlinear equations.
- Numerical flux methods for higher-order time derivatives of conservation laws need to be studied in order to stabilize Adomian methods in the presence of shocks.
- Application of limiters to Adomian formulation.
- In ABS time discretization is converted to space-type operations. Its relation to accuracy and error needs to be carefully analyzed.

Bibliography

[1] URL: http://cordis.europa.eu/home_en.html.

[2] R. Abgrall and S. Karni. "A comment on the computation of non-conservative products". In: *Journal of Computational Physics* 229.8 (2010), pp. 2759 –2763.

[3] G. Adomian. "A Review of the Decomposition in Applied Mathematics". In: *Journal of Mathematical Analysis and Applications* 135.2 (1988), pp. 501–544.

[4] G. Adomian and R. Rach. "Modified decomposition solution of linear and nonlinear boundary-value problems". In: *Nonlinear Analysis* 23.5 (1994), pp. 615–619.

[5] A. Agarwal, P. J. Morris, and R. Mani. "The calculation of sound propagation in nonuniform flows: suppression of instability waves". In: *AIAA Journal* 42.1 (2004), pp. 80–88.

[6] Y. Allaneau and A. Jameson. "Connections between the filtered discontinuous Galerkin method and the flux reconstruction approach to high order discretizations". In: *Computer Methods in Applied Mechanics and Engineering* 200 (2011), pp. 3626–3636.

[7] R. Arina, R. Della Ratta Rinaldi, and A. Iob. "A Discontinuous Galerkin Method for Long-Time Simulations in Aeroacoustics". In: *16th AIAA/CEAS Aeroacoustics Conference* (2010).

[8] D. N. Arnold et al. "Discontinuous Galerkin methods for elliptic problems". In: *Lecture Notes in Computational Science and Engineering* 11 (2000), pp. 89–102.

[9] D. N. Arnold et al. "Unified Analysis of Discontinuous Galerkin Methods for Elliptic Problems". In: *SIAM J. Numer. Anal.* 39 (2001), pp. 1749–1779.

[10] C. Bailly and D. Juve. "A Stochastic Approach To Compute Subsonic-Noise Using Linearized Euler's Equations". In: 99-1872 (1999).

[11] C. Bailly and D. Juve. "Numerical solution of acoustic propagation problems using linearized Euler equations". In: *AIAA Journal* 38.1 (2000), pp. 22–29.

[12] P. Batten, U. Goldberg, and S. Chakravarthy. "Interfacing Statistical Turbulence Closures with Large-Eddy Simulation". In: *AIAA Journal* 42.3 (2004), pp. 485–492.

[13] P. Batten et al. “Towards a Generalized Non-Linear Acoustics Solver”. In: *10th AIAA/CEAS Aeroacoustics Conference*. Reston, Virigina: American Institute of Aeronautics and Astronautics, May 2004.

[14] B. Bell and P. Colella. “A second-order projection method for the incompressible Navier-Stokes equations”. In: *Journal of Computational Physics* 85 (1989), pp. 257–283.

[15] V. Bergeaud and V. Lefebvre. “SALOME. A software integration platform for multi-physics, pre-processing and visualisation”. In: (2010).

[16] M. Billson, L.-E. Eriksson, and L. Davidson. “Acoustic Source Terms for the Linearized Euler Equations in Conservative Form”. In: *AIAA Journal* 43 (2005), pp. 752–759.

[17] C. P. A. Blom. “Discontinuous Galerkin method on tetrahedral elements for aeroacoustics”. PhD thesis. 2003.

[18] C. Bogey, C. Bailly, and D. Juve. “Computation of flow noise using source terms in linearized Euler’s equations”. In: *AIAA journal* 40.2 (2002), pp. 235–243.

[19] E. J. Brambley. “The acoustics of curved and lined cylindrical ducts with mean flow”. In: August (2010).

[20] C. Bresten et al. “Strong Stability Preserving Multistep Runge-Kutta Methods”. In: (2013), pp. 1–26. arXiv: 1307.8058.

[21] D. L. Brown, R. Cortez, and M. L. Minion. “Accurate projection methods for the incompressible Navier–Stokes equations”. In: *Journal of computational physics* 168.2 (2001), pp. 464–499.

[22] J.C. Butcher. *Numerical Methods for Ordinary Differential Equations*. 2008, p. 463.

[23] D. Casalino, M. Barbarino, and A. Visingardi. “Simulation of Helicopter Community Noise in Complex Urban Geometry”. In: *AIAA Journal* 49.8 (2011), pp. 1614–1624.

[24] C. E. Castro. “High order ADER FV/DG numerical methods for hyperbolic equations”. PhD thesis. 2007.

[25] C. E. Castro and E. F. Toro. *Alternative Solvers for the Derivative Riemann Problem for Hyperbolic Balance Laws The Derivative Riemann Problem*. Tech. rep.

[26] C. E. Castro and E. F. Toro. “Solvers for the high-order Riemann problem for hyperbolic balance laws”. In: *Journal of Computational Physics* 227.4 (Feb. 2008), pp. 2481–2513.

[27] C. Chalons and F. Coquel. "A new comment on the computation of non-conservative products using Roe-type path conservative schemes". In: *Journal of Computational Physics* 335 (2017), pp. 592–604.

[28] Y. Cherruault, G. Saccomandi, and B. Some. "New results for convergence of Adomian's method applied to integral equations". In: *Mathematical and Computer Modelling* 16.2 (1992), pp. 85–93.

[29] H. Choi and P. Moin. "Effects of the computational time step on numerical solutions of turbulent flow". In: *Journal of Computational Physics* 113.1 (1994), pp. 1–4.

[30] A. J. Chorin. "Numerical solution of incompressible flow problems". In: *Studies in Numerical Analysis* 2 (1968), pp. 64–71.

[31] A. J. Chorin. *Numerical solutions of the Navier-Stokes equations*. 1968.

[32] B.-T. Chu and L. S. G. Kovásznay. *Non-linear interactions in a viscous heat-conducting compressible gas*. 1958.

[33] B. Cockburn. *Discontinuous Galerkin Methods*. Tech. rep. Institute for Mathematics and its Applications, University of Minnesota, 2003, pp. 731–754.

[34] B. Cockburn, S. Hou, and C-W. Shu. *The Runge-Kutta local projection discontinuous Galerkin finite element method for conservation laws. IV. The multidimensional case*. 1990.

[35] B. Cockburn, G. E. Karniadakis, and C-W. Shu. "The development of discontinuous Galerkin methods". In: *IMA Preprint Series No. 1662* 0 (1999).

[36] B. Cockburn, S.-Y. Lin, and C-W. Shu. "TVB Runge-Kutta local projection discontinuous Galerkin finite element method for conservation laws III: One-dimensional systems". In: *Journal of Computational Physics* 84 (1989), pp. 90–113.

[37] B. Cockburn and C-W. Shu. "The Runge-Kutta Discontinuous Galerkin Method for Conservation Laws V". In: *Journal of Computational Physics* 141 (1998), pp. 199–224.

[38] B. Cockburn and C-W. Shu. *TVB Runge-Kutta local projection discontinuous Galerkin finite element method for conservation laws. II. General framework*. 1989.

[39] G. C. Cohen. *Higher-Order Numerical Methods for Transient Wave Equations*. Springer Berlin Heidelberg, 2002.

[40] P. Colella. "A direct Eulerian MUSCL scheme for gas dynamics". In: *SIAM Journal on Scientific and Statistical Computing* 6.1 (1985), pp. 104–117.

[41] P. Colella and P. R. Woodward. "The Piecewise Parabolic Method (PPM) for gas-dynamical simulations". In: *Journal of Computational Physics* 54.1 (1984), pp. 174 –201.

[42] T. Colonius and Sanjiva K. Lele. "Computational aeroacoustics: Progress on nonlinear problems of sound generation". In: *Progress in Aerospace Sciences* 40.6 (2004), pp. 345–416.

[43] N. Curle. "The Influence of Solid Boundaries upon Aerodynamic Sound". In: *Proceedings of the Royal Society of London. Series A* 231.1187 (1955), pp. 505–514. arXiv: arXiv:1011.1669v3.

[44] M. A. Dablain. "The application of high-order differencing to the scalar wave equation". In: *Geophysics* 51.1 (1986), pp. 54–66.

[45] G. Dal Maso, P. G. Lefloch, and F. Murat. "Definition and weak stability of nonconservative products". In: *Journal de mathématiques pures et appliquées* 74.6 (1995), pp. 483–548.

[46] W. De Roeck. "Hybrid methodologies for the computational aeroacoustics analysis of confined subsonic flows". PhD thesis. 2007.

[47] M. Dieste and G. Gabard. "Random particle methods applied to broadband fan interaction noise". In: *Journal of Computational Physics* 231.24 (2012), pp. 8133–8151.

[48] D. Drikakis and W. Rider. *High-Resolution Methods for Incompressible and Low-Speed Flows*. Computational Fluid and Solid Mechanics. Springer Berlin Heidelberg, 2006.

[49] J. S. Duan. "New recurrence algorithms for the nonclassic Adomian polynomials". In: *Computers and Mathematics with Applications* 62.8 (2011), pp. 2961–2977.

[50] J. S. Duan et al. "A review of the Adomian decomposition method and its applications to fractional differential equations". In: *Communications in Fractional Calculus* 3.2 (2012), pp. 73–99.

[51] M. Dumbser, A. Hidalgo, and O. Zanotti. "High order space time adaptive ADER-WENO finite volume schemes for non-conservative hyperbolic systems". In: *Computer Methods in Applied Mechanics and Engineering* 268 (2014), pp. 359–387.

[52] M. Dumbser and E. F. Toro. "A Simple Extension of the Osher Riemann Solver to Non-conservative Hyperbolic Systems". In: *Journal of Scientific Computing* 48.1 (2011), pp. 70–88.

[53] M. Dumbser et al. "ADER schemes on unstructured meshes for nonconservative hyperbolic systems: Applications to geophysical flows". In: *Computers & Fluids* 38.9 (2009), pp. 1731 –1748.

[54] M. Dumbser et al. “FORCE schemes on unstructured meshes II: Non-conservative hyperbolic systems”. In: *Computer Methods in Applied Mechanics and Engineering* 199.9 (2010), pp. 625 –647.

[55] A. Ebaid. “A new analytical and numerical treatment for singular two-point boundary value problems via the Adomian decomposition method”. In: *Journal of Computational and Applied Mathematics* 235 (2011), pp. 1914–1924.

[56] L. C. Evans. *Partial Differential Equations*. Graduate studies in mathematics. American Mathematical Society, 2010.

[57] R. Ewert and M. Meinke. “Comparison of source term formulations for a hybrid CFD/CAA method”. In: (2001).

[58] R. Ewert, M. Meinke, and W. Schroder. *Computation of Aeroacoustic Sound Via Hybrid CFD/CAA-Methods*. Tech. rep. DTIC Document, 2003.

[59] R. Ewert and W. Schröder. “Acoustic perturbation equations based on flow decomposition via source filtering”. In: *Journal of Computational Physics* 188.2 (2003), pp. 365–398.

[60] F. Farassat. *The Kirchhoff formulas for moving surfaces in aeroacoustics-the subsonic and supersonic cases*. Tech. rep. 1996.

[61] P. di Francescantonio. “A New Boundary Integral Formulation for the Prediction of Sound Radiation”. In: *Journal of Sound and Vibration* 202.4 (1997), pp. 491–509.

[62] F. Frank. *Foundations of Engineering Acoustics*. 2001. arXiv: arXiv:1011.1669v3.

[63] J. B. Freund. “Noise sources in a low-Reynolds-number turbulent jet at Mach 0.9”. In: *Journal of Fluid Mechanics* 438 (2001), pp. 277–305.

[64] J. B. Freund, S. K. Lele, and P. Moin. “Numerical simulation of a Mach 1.92 turbulent jet and its sound field”. In: *AIAA Journal* 38.11 (2000), pp. 2023–2031.

[65] R. Friedrich et al. “Direct numerical simulation of incompressible turbulent flows”. In: *Computers & Fluids* 30.5 (2001), pp. 555–579.

[66] J. Gilbert, L. Menguy, and M. Campbell. “A simulation tool for brassiness studies.” In: *The Journal of the Acoustical Society of America* 123 (2008), pp. 1854–1857.

[67] S. Glegg and W. Devenport. *Aeroacoustics of Low Mach Number Flows: Fundamentals, Analysis, and Measurement*. Elsevier Science, 2017.

[68] S. K. Godunov. “A difference method for numerical calculation of discontinuous solutions of the equations of hydrodynamics”. In: *Matematicheskii Sbornik* 89.3 (1959), pp. 271–306.

[69] S. Gottlieb, D. I. Ketcheson, and C-W. Shu. “High order strong stability preserving time discretizations”. In: *Journal of Scientific Computing* 38 (2009), pp. 251–289.

[70] P. M. Gresho. “On the theory of semi-implicit projection methods for viscous incompressible flow and its implementation via a finite element method that also introduces a nearly consistent mass matrix. Part 1: Theory”. In: *International Journal for Numerical Methods in Fluids* 11.5 (1990), pp. 587–620.

[71] P. M. Gresho and R. L. Sani. “On pressure boundary conditions for the incompressible Navier-Stokes equations”. In: *International Journal for Numerical Methods in Fluids* 7.10 (1987), pp. 1111–1145.

[72] J. L. Guermond, P. Minev, and J. Shen. “An overview of projection methods for incompressible flows”. In: *Computer Methods in Applied Mechanics and Engineering* 195.44-47 (2006), pp. 6011–6045.

[73] H. Guillard and C. Viozat. “On the behaviour of upwind schemes in the low Mach number limit”. In: *Computers & fluids* 28.1 (1999), pp. 63–86.

[74] L. Gutin. “On the sound field of a rotating airscrew”. In: *Zhurnal Tekhnicheskoi Fiziki* 6 (1936), pp. 899–909.

[75] M. M. Hafez. *Numerical Simulations of Incompressible Flows*. World Scientific, 2003.

[76] J. C. Hardin and D. S. Pope. “An Acoustic / Viscous Splitting Technique for Computational Aeroacoustics”. In: *Theoretical and Computational Fluid Dynamics* 6 (1994), pp. 323–340.

[77] F. H. Harlow and J. E. Welch. “Numerical Calculation of Time-Dependent Viscous Incompressible Flow of Fluid with Free Surface”. In: *Physics of Fluids* 8.12 (1965), p. 2182.

[78] A. Harten et al. “Uniformly High Order Accurate Essentially Non-oscillatory Schemes, III”. In: *J. Comput. Phys.* 131.1 (Feb. 1997), pp. 3–47.

[79] A. Hay et al. “hp-Adaptive time integration based on the BDF for viscous flows”. In: *Journal of Computational Physics* 291.Supplement C (2015), pp. 151 –176.

[80] A. Hirschberg et al. “Shock waves in trombones”. In: *The Journal of the Acoustical Society of America* 99.3 (1996), pp. 1754–1758.

[81] M. S. Howe. *Theory of Vortex Sound*. Cambridge Texts in Applied Mathematics. Cambridge University Press, 2003.

[82] F. Q. Hu. "On absorbing boundary conditions for linearized Euler equations by a perfectly matched layer". In: *Journal of Computational Physics* 129 (1995), pp. 201–219.

[83] F. Q. Hu and H. L. Atkins. "Eigensolution analysis of the discontinuous Galerkin method with nonuniform grids: I. one space dimension". In: *Journal of Computational Physics* 182.2 (2002), pp. 516–545.

[84] H. H. Hubbard and K. P. Shepherd. "Aeroacoustics of large wind turbines". In: *The Journal of the Acoustical Society of America* 89.6 (1991), pp. 2495–2508.

[85] M. A. Hulsen. *The discontinuous Galerkin method with explicit Runge-Kutta time integration for hyperbolic and parabolic systems with source terms*. Tech. rep. 1991.

[86] H. T. Huynh. "Accurate Upwind Methods for the Euler Equations". en. In: *SIAM Journal on Numerical Analysis* 32.5 (Oct. 1995), pp. 1565–1619.

[87] J. Kim and P. Moin. "Application of a fractional step method to incompressible Navier-Stokes equations". In: *Journal of Computational Physics* 59.2 (1985), pp. 308–323.

[88] S. Klainerman and A. Majda. "Compressible and incompressible fluids". In: *Communications on Pure and Applied Mathematics* 35.5 (1982), pp. 629–651.

[89] L. Kleiser and U. Schumann. "Treatment of incompressibility and boundary conditions in 3-D numerical spectral simulations of plane channel flows". In: *Proceedings of the Third GAMM—Conference on Numerical Methods in Fluid Mechanics*. Springer. 1980, pp. 165–173.

[90] D. B. Kothe and R. C. Mjolsness. "RIPPLE-A new model for incompressible flows with free surfaces". In: *AIAA journal* 30.11 (1992), pp. 2694–2700.

[91] W. Kress and P. Lötstedt. "Time step restrictions using semi-explicit methods for the incompressible Navier-Stokes equations". In: *Computer Methods in Applied Mechanics and Engineering* 195 (2006), pp. 4433–4447.

[92] N. Kroll et al. *IDIHOM-Industrialization of High-Order Methods–A Top Down Approach, Notes on Numerical Fluid Mechanics and Multidisciplinary Design, vol. 128*. Springer International Publishing Switzerland, 2015.

[93] K. A. Kurbatskii and R. R. Mankbadi. "Review of Computational Aeroacoustics Algorithms". In: *International Journal of Computational Fluid Dynamics* 18.6 (2004), pp. 533–546.

[94] S. Laizet and E. Lamballais. "High-order compact schemes for incompressible flows: A simple and efficient method with quasi-spectral accuracy". In: *Journal of Computational Physics* 228.16 (2009), pp. 5989–6015.

[95] P. Lax and B. Wendroff. "Systems of conservation laws". In: *Communications on Pure and Applied mathematics* 13.2 (1960), pp. 217–237.

[96] M. J. Lighthill. "On sound generated aerodynamically. I. General theory". In: *Proceedings of the Royal Society of London A: Mathematical, Physical and Engineering Sciences*. Vol. 211. 1107. The Royal Society. 1952, pp. 564–587.

[97] M. J. Lighthill. "On sound generated aerodynamically. II. Turbulence as a source of sound". In: *Proceedings of the Royal Society of London A: Mathematical, Physical and Engineering Sciences*. Vol. 222. 1148. The Royal Society. 1954, pp. 1–32.

[98] G. M. Lilley. "On the Noise Radiated from a Turbulent High Speed Jet". In: Springer New York, 1993, pp. 85–115.

[99] W. Y. Liu. "A review on wind turbine noise mechanism and de-noising techniques". In: *Renewable Energy* 108.Supplement C (2017), pp. 311 – 320.

[100] E. Longatte. "Modélisation de la propagation et de la génération du bruit au sein des écoulements turbulents internes". PhD thesis. Châtenay-Malabry, Ecole Centrale de Paris, 1998.

[101] T. S. Lund. "The use of explicit filters in large eddy simulation". In: *Computers & Mathematics with Applications* 46.4 (2003), pp. 603–616.

[102] A. Majda and J. Sethian. "The derivation and numerical solution of the equations for zero Mach number combustion". In: *Combustion science and technology* 42.3-4 (1985), pp. 185–205.

[103] T. A. Manning. "A numerical investigation of sound generation in supersonic jet screech". In: *Ph D*. 1999.

[104] K. Masatsuka. *I do like CFD, VOL.1, Second Edition*. v. 1. Masatsuka, K., 2013.

[105] A. McAdams, E. Sifakis, and J. Teran. "A parallel multigrid Poisson solver for fluids simulation on large grids". In: *Eurographics/ ACM SIGGRAPH Symposium on Computer Animation* (2010), p. 10.

[106] A. Meister and J. Struckmeier. *Hyperbolic partial differential equations: theory, numerics and applications*. Springer Science & Business Media, 2012.

[107] S. Mendez et al. "On the use of the Ffowcs Williams-Hawkings equation to predict far-field jet noise from large-eddy simulations". In: *International Journal of Aeroacoustics* 12.1-2 (June 2013), pp. 1–20.

[108] I. S. Men'Shov. "Increasing the order of approximation of Godunov's scheme using solutions of the generalized Riemann problem". In: *USSR Computational Mathematics and Mathematical Physics* 30.5 (1990), pp. 54–65.

[109] G. H. Miller and P. Colella. "A Conservative Three-Dimensional Eulerian Method for Coupled Solid–Fluid Shock Capturing". In: *Journal of Computational Physics* 183.1 (2002), pp. 26 –82.

[110] R. C. Millington, V. A. Titarev, and E. F. Toro. "ADER: Arbitrary-Order Non-Oscillatory Advection Schemes". In: *Hyperbolic Problems: Theory, Numerics, Applications*. Birkhäuser Basel, 2001, pp. 723–732.

[111] S. Momani and Z. Odibat. "Analytical solution of a time-fractional Navier-Stokes equation by Adomian decomposition method". In: *Applied Mathematics and Computation* 177 (2006), pp. 488–494.

[112] G. Montecinos et al. "Comparison of solvers for the generalized Riemann problem for hyperbolic systems with source terms". In: *Journal of Computational Physics* 231.19 (Aug. 2012), pp. 6472–6494.

[113] P. Morris et al. "Numerical predictions of high speed jet noise". In: *3rd AIAA/CEAS Aeroacoustics Conference*. Reston, Virigina: American Institute of Aeronautics and Astronautics, May 1997.

[114] A. Nigro et al. "Modified extended BDF scheme for the discontinuous Galerkin solution of unsteady compressible flows". In: *International Journal for Numerical Methods in Fluids* 76.9 (2014), pp. 549–574.

[115] R.L. Panton. *Incompressible Flow*. Wiley, 2013.

[116] R. Peyret. *Spectral Methods for Incompressible Viscous Flow*. Applied Mathematical Sciences. Springer New York, 2013.

[117] R. Peyret and T. D. Taylor. *Computational methods for fluid flow*. Springer Science & Business Media, 2012.

[118] L. Quartapelle. *Numerical Solution of the Incompressible Navier-Stokes Equations*. International Series of Numerical Mathematics. Birkhäuser Basel, 1993.

[119] P. Quéméré and P. Sagaut. "Zonal multi-domain RANS/LES simulations of turbulent flows". In: *International journal for numerical methods in fluids* 40.7 (2002), pp. 903–925.

[120] G. Raman, R. C. Ramachandran, and M. R. Aldeman. "A review of wind turbine noise measurements and regulations". In: *Wind Engineering* 40.4 (2016), pp. 319–342. eprint: https://doi.org/10.1177/0309524X16649080.

[121] H. Ran and T. Colonius. "Numerical simulation of the sound radiated by a turbulent vortex ring". In: *International Journal of Aeroacoustics* 8.4 (2009), pp. 317–336.

[122] B. D. Reddy. *Introductory Functional Analysis: With Applications to Boundary Value Problems and Finite Elements*. Introductory Functional Analysis Series. Springer, 1998.

[123] S. Redonnet and G. Cunha. "An advanced hybrid method for the acoustic prediction". In: *Advances in Engineering Software* 88 (2015), pp. 30–52.

[124] S. Rhebergen. "Discontinuous Galerkin finite element methods for (non) conservative partial differential equations". PhD thesis. University of Twente, 2010.

[125] B. Rider. *The benefits of using "primitive variables" | The Regularized Singularity*. https://wjrider.wordpress.com/2016/08/08/the-benefits-of-using-primitive-variables/. (Accessed on 10/15/2017).

[126] W. J. Rider and R. B. Lowrie. *The use of classical Lax-Friedrichs Riemann solvers with discontinuous Galerkin methods*. Tech. rep. Los Alamos National Lab., NM (US), 2001.

[127] C. W. Rowley, T. Colonius, and A. J. Basu. "On self-sustained oscillations in two-dimensional compressible flow over rectangular cavities". In: *Journal of Fluid Mechanics* 455 (2002), pp. 315–346.

[128] J. Saltzman. "An Unsplit 3D Upwind Method for Hyperbolic Conservation Laws". In: *Journal of Computational Physics* 115.1 (1994), pp. 153–168.

[129] R. L. Sani et al. "Pressure boundary condition for the time-dependent incompressible Navier–Stokes equations". In: *International Journal for Numerical Methods in Fluids* 50.6 (2006), pp. 673–682.

[130] M. R. Sari, M. Kezzar, and R. Adjabi. "A Comparison of Adomian and Generalized Adomian Methods in Solving the Nonlinear Problem of Flow in Convergent-Divergent Channels". In: 8.7 (2014), pp. 321–336.

[131] D. C. Seal, Y. Güçlü, and A. J. Christlieb. "High-order multiderivative time integrators for hyperbolic conservation laws". In: *Journal of Scientific Computing* 60.1 (2014), pp. 101–140.

[132] J. H. Seo and Y. J. Moon. "Linearized perturbed compressible equations for low Mach number aeroacoustics". In: *Journal of Computational Physics* 218 (2006), pp. 702–719.

[133] C-W. Shu and H. L. Atkins. "Quadrature-Free Implementation of Discontinuous Galerkin Method for Hyperbolic Equations". In: *AIAA Journal* 36.5 (May 1998), pp. 775–782.

[134] C. K. W. Tam. *Computational Aeroacoustics: A wave number approach*. Vol. 33. Cambridge University Press, 2012.

[135] C. K. W. Tam. "Computational aeroacoustics-Issues and methods". In: *AIAA journal* 33.10 (1995), pp. 1788–1796.

[136] C. K. W. Tam and J. C. Webb. *Dispersion-relation-preserving finite difference schemes for computational acoustics*. 1993.

[137] R. Témam. "Sur l'approximation de la solution des équations de Navier-Stokes par la méthode des pas fractionnaires (I)". In: *Archive for Rational Mechanics and Analysis* 32.2 (1969), pp. 135–153.

[138] R. Témam. "Sur l'approximation de la solution des équations de Navier-Stokes par la méthode des pas fractionnaires (II)". In: *Archive for Rational Mechanics and Analysis* 33.5 (1969), pp. 377–385.

[139] L. J. P. Timmermans, P. D. Minev, and F. N. Van De Vosse. "An approximate projection scheme for incompressible flow using spectral elements". In: *International journal for numerical methods in fluids* 22.7 (1996), pp. 673–688.

[140] E. F. Toro, ed. *Godunov Methods*. Springer Nature, 2001.

[141] E. F. Toro. *Riemann Solvers and Numerical Methods for Fluid Dynamics: A Practical Introduction*. Springer Berlin Heidelberg, 2009.

[142] E. F. Toro and V. A. Titarev. "Derivative Riemann solvers for systems of conservation laws and ADER methods". In: *Journal of Computational Physics* 212.1 (Feb. 2006), pp. 150–165.

[143] P. Tucker. *Unsteady Computational Fluid Dynamics in Aeronautics*. Fluid Mechanics and Its Applications. Springer Netherlands, 2013.

[144] C. Wagner, T. Hüttl, and P. Sagaut. *Large-Eddy Simulation for Acoustics*. Cambridge Aerospace Series. Cambridge University Press, 2007.

[145] Z. J. Wang. *Adaptive High-order Methods in Computational Fluid Dynamics*. Advances in computational fluid dynamics. World Scientific, 2011.

[146] E. Weinan and J.-G. Liu. "Projection Method I: Convergence and Numerical Boundary Layers". In: *SIAM Journal on Numerical Analysis* 32.4 (1995), pp. 1017–1057.

[147] V. L. Wells and R. A. Renaut. "Computing Aerodynamically Generated Noise". In: *Annual Review of Fluid Mechanics* 29.1 (1997), pp. 161–199.

[148] J. E. F. Williams and D. L. Hawkings. "sound generation by turbulence and surfaces in arbitfrary motion". In: *Philosophical Transactions of the Royal Society of London. Serie A, Mathematical and Physical Sciences* 264.1151 (1969), pp. 321–342.

[149] J. E. F. Williams and D. L. Hawkings. "Sound generation by turbulence and surfaces in arbitrary motion". In: *Philosophical Transactions of the Royal Society of London A: Mathematical, Physical and Engineering Sciences* 264.1151 (1969), pp. 321–342.

[150] O. Zanotti et al. "Space – time adaptive ADER discontinuous Galerkin finite element schemes with a posteriori sub-cell finite volume limiting". In: *Computers & Fluids* 118 (2015), pp. 204–224.

[151] D. Zhou. "High-order numerical methods for pressure Poisson equation reformulations of the incompressible Navier-Stokes equations". PhD thesis. Massachusetts Institute of Technology, 2014.